Fully Polarimetric Analysis of Weather Radar Signatures

Vollpolarimetrische Analyse von Wetterradar-Signaturen

Dissertation

zur Erlangung des akademischen Grades

Dr.-Ing.

vorgelegt

der Fakultaet fuer Elektrotechnik und Informationstechnik

der Technischen Universitaet Chemnitz

von Dipl. Phys. Michele Galletti

geboren am 13-11-1978 in Bologna

Chemnitz, den 26 Januar 2009

ABSTRACT

The present doctoral thesis deals with radar polarimetry, namely with the investigation of properties of polarimetric variables potentially useful in radar meteorology.
For use with dual-polarization radars, the degree of polarization is analyzed. This variable is available to planned operational radars. The degree of polarization is dependent on transmit polarization state and, consequently, it is dependent on the radar system operating mode. The primary operating mode of operational radars consists in simultaneous transmission and simultaneous receive of both horizontal and vertical components. The secondary operating mode consists of horizontal transmission and simultaneous receive. Both degrees of polarization are investigated in this thesis.
Also, as operational systems are being updated to dual-polarization, research should start investigating the capabilities of fully polarimetric weather radar systems. Among the numerous variables available from this operating mode, the target entropy was chosen for investigation, also because of its close relation to the degree of polarization.

ZUSAMMENFASSUNG

Diese (Doktor)arbeit beschäftigt sich mit Radar-Polarimetrie, insbesondere mit der Untersuchung der Eigenschaften von polarimetrischen Variablen, die potenziellen Nutzen für die Radar-Meteorologie haben.
Für den Einsatz in Dual-Polarisations-Radargeräten wird der Polarisationsgrad analysiert. Diese Variable wird in künftigen operationellen Radargeräten verfügbar sein. Der Polarisationsgrad hängt vom transmittierten Polarisationszustand und in weiterer Folge auch vom Betriebsmodus des Radargeräts ab. Der Hauptbetriebsmodus von operationellen Radargeräten sendet und empfängt gleichzeitig sowohl die horizontale als auch die vertikale Komponente. Der sekundäre Betriebsmodus sendet und empfängt simultan die horizontal polarisierte Komponente. In dieser Arbeit werden beide Polarisationsgrade untersucht.
Da operationelle Systeme derzeit auf den Dual-Polarisationsmodus aufgerüstet werden, sollte künftig die Anwendungsmöglichkeiten von vollpolarimetrischen Wetterradarsystemen untersucht werden. Aus allen Variablen, die in diesem Betriebsmodus zur Verfügung stehen, wurde die Entropie (des gemessen Objektes) ausgewählt und wegen seiner engen Beziehung zum Polarisationsgrad näher untersucht.

CONTENTS

List of Symbols

ALD	Alignment Direction
B_0	Huynen Generator of target structure
CDR	circular depolarization ratio
CP	canting parameter
δco	backscatter differential phase
H	target entropy
H_w	wave entropy
KDP	Specific Differential phase
LDR	linear depolarization ratio (transmit polarization not specified)
LDR_H	linear depolarization ratio at horizontal polarization transmit
LDR_V	linear depolarization ratio at vertical polarization transmit
ORTT	Orientation parameter
ρ_{hv}	copolar correlation coefficient
ρ_{hv}^{hy}	copolar correlation coefficient measured at hybrid mode
ρ_{xh}	cross-polar correlation coefficient at horizontal polarization transmit
ρ_{xv}	cross-polar correlation coefficient at vertical polarization transmit
p_H	degree of polarization at horizontal polarization transmit
p_V	degree of polarization at vertical polarization transmit
p_{RHC}	degree of polarization at right-hand circular polarization transmit
p_{LHC}	degree of polarization at left-hand circular polarization transmit
p_C	degree of polarization at circular transmit (with no further specification)
p_{+45}	degree of polarization at +45° linear polarization transmit
p_{-45}	degree of polarization at -45° linear polarization transmit
p_{45}	degree of polarization at slant linear transmit (with no further specification)
Rx	receive
Tx	transmit
Z_{DR}	Differential Reflectivity
Z_H	Reflectivity at horizontal polarization transmit
Z_V	Reflectivity at vertical polarization transmit

List of Acronyms

ADC	Analog-to-Digital Converter
AME	Antenna Mounted Electronics
CW	Continuous Wave
DARR	Delft Atmospheric Research Radar
DC	Direct Current
DFT	Digital Fourier Transform
DLR	Deutsches Zentrum fuer Luft- und Raumfahrt (German Aerospace Center)
DLR-IPA	DLR-Institut fuer Physik der Atmosphaere
DLR-HR	DLR-Institut fuer Hochfrequenztechnik und Radarsysteme
DLR-HR-RK	DLR-HR-Radarkonzepte Abteilung
DSP	Digital Signal Processor
EEC	Enterprise Electronics Corporation
IF	Intermediate Frequency
ISM	Instantaneous Scattering Matrix
OMT	Ortho-Mode Transducer
POLDIRAD	Polarization Diversity Radar
PPI	Plane Position Indicator
PRF	Pulse Repetition Frequency
PRI	Pulse Repetition Interval
RF	Radio Frequency
RHI	Range Height Indicator
SAR	Synthetic Aperture Radar
STC	Sensitivity Time Control
WCM	Wave Covariance Matrix

List of Figures

List of Tables

Author's publications

[1] M. Galletti, D. H. O. Bebbington, M. Chandra, T. Boerner, "Measurement and Characterization of Entropy and Degree of Polarization of Weather Radar Targets" *Transactions on Geoscience and Remote Sensing*, Vol. 46, n.10, October 2008

[2] M. Galletti, D. H. O. Bebbington, M. Chandra, T. Boerner, "Fully polarimetric analysis of weather radar signatures" Proc. 2008 IEEE Radar Conference, Rome, Italy, May 2008

Curriculum Vitae

Michele Galletti was born in Bologna on November the 13th, 1978. He received the Laurea degree in Physics (110/110 e lode) from the Alma Mater Studiorum Universita di Bologna, Bologna, Italy, in 2003. In 2004 and 2005, he was a Scientist with the European Union-funded Project Application of Multi-parameter Polarimetry in Environmental Remote Sensing, working on the applications of radar polarimetry. Since 2006, he has been with the Microwaves and Radar Institute, German Aerospace Center, Wessling, Germany.

Acknowledgments

My mother, my father, my sisters Gaia and Giulia.

Also, my mother's partner Gerardo, and his children, Danilo, Nicola and Floriana,

Well, my best friends, Lorenzo Neri, Giulio Giangaspero, Fabio Pisano and Matteo Vettore. There s another thousand friends I should quote though. Two of them are Massimo Gallo and Riccardo Fini.

My ex-girlfriend, Tjasa. Also, some of my roommates who have shared with me these last five years: Susann Buchheim, Jonathan Spiller, Julius Pflug, Ralf Mueller, Thomas Baersch, Ming Xi Li.

One person I am especially indebted to is Prof. Madhu Chandra. Without him I wouldn't be here writing this page. Another person who deserves a special mention is Dr. David Bebbington. Thanks David.

People I met in my professional life that I would like to thank are: Pier Paolo Alberoni, Laura Carrea, Tobias Otto, Patrick Tracksdorf, Gerhard Krieger, Manfred Zink, Alberto Moreira, Gerd Wanielik, Thomas Boerner, David Hounam, Dirk Schrank, Andreas Danklmayer, Maria Donata Polimeni, Bjoern Doering, Nico Gebert, Helmut Schoen, Koichi Iribe, Jordi Figueras, Federica Bordoni, Alessandro Parizzi, Matteo Soccorsi, Eric Pottier, Marco Schwerdt, Esra Erten, Carolina Gonzalez, Benjamin Braeutigam, Jaime Hueso Gonzalez, Nuria, Ortega, Stefan Sauer, Clemens, and.. well… almost everybody I got to know at DLR.
A special thank goes to Carlos Lopez-Martinez, for having understood me when no one else did. I still remember I owe an e-mail to you, but this page is probably more meaningful in this regard.

Among my late twenties acquaintances, some have become definitely good friends: Juan Jose Caliz-Rodriguez, Raphael Zandona Schneider, Adriano Meta and Francesco de Zan.

Ultimately, Michael Stipe, Mike Mills, Peter Buck, Billy Corgan, Chris Martin, Anthony Kiedis, David Gilmour, Roger Waters, Richard Wright and Nicolas Mason.

1. Introduction

Polarimetry has now become an operational feature of weather radar systems.
Such a choice has been motivated by the capability of polarimetric variables to distinguish different hydrometeor types and to improve the accuracy of quantitative precipitation estimation. These technologies have attained a degree of maturity such that major investments were undertaken by national governments for the implementation of polarimetric upgrades of weather radar networks. Examples are the US and German national networks, whose polarimetric upgrade contracts have already been signed. In Italy, some operational radars do already have dual-polarization capabilities.
Normally, five polarimetric variables are considered in radar meteorology: reflectivity (Z_H), differential reflectivity (Z_{DR}), linear depolarization ratio (LDR), specific differential phase (K_{DP}) and copolar correlation coefficient (ρ_{hv}). All of them are used for classification purposes, three of them are also used for quantitative rain rate estimation. These variables are introduced in Chapter 3. Table 1.1 lists symbols, names and operational use.

Symbol	Name	Used for classification	Used for quantitative estimation
$\mathbf{Z_H}$	Reflectivity	Yes	Yes
$\mathbf{Z_{DR}}$	Differential Reflectivity	Yes	Yes
LDR	Linear Depolarization Ratio	Yes	No
$\mathbf{K_{DP}}$	Specific Differential phase	Yes	Yes
$\boldsymbol{\rho_{hv}}$	Copolar correlation coefficient	Yes	No
$\boldsymbol{\rho_{xh}}$	Cross-polar correlation coefficient (H transmit)	No	No
$\boldsymbol{\rho_{xv}}$	Cross-polar correlation coefficient (V transmit)	No	No

Table 1.1 Polarimetric variables used in radar meteorology.

Active research topics in radar meteorology concern classification algorithms, in order to distinguish a larger number of target classes, as well as quantitative precipitation estimation, in order to invert models to obtain important geophysical parameters from radar observations. The polarimetric variables available to a weather radar system are dictated by the pulsing scheme in use and, consequently, by the radar architecture. Indeed, a given radar architecture is chosen to yield a definite set of variables. The present doctoral thesis investigates new polarimetric variables. The definition of new quantities is highly needed since the existing variables do not generally capture all the degrees of freedom contained in the radar measurements. Also, new variables might highlight physical properties of the target in a unique way, thus rendering classification and/or model inversion more effective. In this thesis, we consider polarimetric variables

for both dual-polarization and fully-polarimetric architectures. For dual-polarization architectures, three variables are considered: degree of polarization at horizontal transmit, degree of polarization at slant linear transmit and degree of polarization at circular transmit. For fully polarimetric architectures, scattering entropy is investigated and compared to the degree of polarization. A fully polarimetric radar system measures the covariance matrix, that is, a matrix with 9 degrees of freedom. A dual-polarization radar (single polarization transmit, 2-channel receive) measures the wave covariance matrix (WCM), that is, a matrix with 4 degrees of freedom.

Symbol	Name	Required Radar Architecture
$\mathbf{p_H}$	Degree of polarization at horizontal transmit	Dual-polarization: H Tx, 2-channel Rx
$\mathbf{p_V}$	Degree of polarization at vertical transmit	Dual-polarization: V Tx, 2-channel Rx
$\mathbf{p_{45}}$	Degree of polarization at slant linear transmit	Dual-polarization: 45° Tx, 2-channel Rx
$\mathbf{p_C}$	Degree of polarization at circular transmit	Dual-polarization: Circular Tx, 2-channel Rx
H	Entropy	Fully polarimetric
CP	Canting parameter	Fully polarimetric

Table 1.2 Polarimetric variables investigated in the present work.

For optimal hydrometeor classification and quantitative precipitation estimation, it is important to provide the optimal set of variables. Radar polarimetry has the task to provide radar meteorology with the most meaningful quantities. The variables in use should have, ideally, rich physical meaning, that is, it should be possible to relate their values, as precisely and linearly as possible, to some geophysical feature of the illuminated target. The process of searching the optimal set of polarimetric variables has not ended yet. For example, the cross-polar correlation coefficients appearing in the covariance matrix (or in the wave covariance matrix at horizontal or vertical transmit) are not operationally exploited. Further, polarimetric variables are not limited to the quantities appearing explicitly as entries of the covariance matrix. More complex signal processing procedures should be envisioned if the evaluation of physically meaningful polarimetric variables is achieved. The application of target decomposition theorems or of unitary transformations, as well as the evaluation of the depolarization response (defined in the present work), rank among these possibilities.

This work is a contribution to radar polarimetry, with applications to polarimetric classification of weather radar targets. Together with the design of classification algorithms, it is important to understand how many and which variables are needed for the optimal performance of a given radar architecture and its corresponding pulsing scheme. Ultimately, the operational real-time evaluation of useful additional variables can simply be achieved through inexpensive digital signal processing. These issues have theoretical and practical relevance, since they might improve the performance of hydrometeor classifiers, the latter already being a part of the product portfolio of major weather radar companies.

1.1 Dual-polarization operational weather radars

The dual-polarization architecture chosen by weather radar manufacturers allows the implementation of two polarimetric modes. The primary mode consists of transmitting simultaneous horizontal and vertical polarizations and coherently receiving the backscattered signal in the horizontal and vertical polarimetric channels (hybrid mode, or Z_{DR} mode). Since this mode does not allow for the measurement of the linear depolarization ratio, a secondary polarimetric mode is available, and consists of transmitting horizontal polarization and receiving the backscattered signal in the horizontal and vertical polarimetric channels (LDR mode).

Operational systems allow for dual-polarization receivers, but do not allow for polarization agility on transmit, and a choice can be made between circular/slant or horizontal transmit. Besides the measurement of V and W (velocity and spectral width), the primary mode allows for the measurement of Z_H, Z_{DR}, K_{DP} and $|\rho_{hv}|$, while the secondary allows for the measurement of Z_H and LDR. The choice of the hybrid mode as the default, is justified by the fact that weather targets most often show mirror reflection symmetry and low cross-talk on backscattering. The complementary horizontal transmit /dual-polarization receive mode is conceived for the measurement of LDR, for the cases when relevant 'depolarization' on backscattering might render this variable useful for the understanding of the underlying microphysics.

Pictorially, we can represent the default hybrid mode (simultaneous transmission, 2-channel receive) and the horizontal transmit mode (horizontal send, 2-channel receive) as in Fig. 1.1 and 1.2.

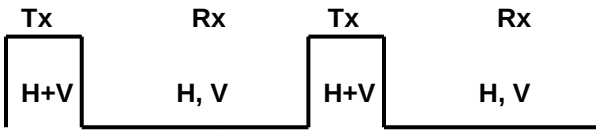

Figure 1.1 **Pulsing scheme for simultaneous transmission, simultaneous receive mode (hybrid mode or Z_{DR} mode). Measured variables are Z_H, Z_{DR}, K_{DP}, $|\rho_{hv}|$, p_C or p_{45}.**

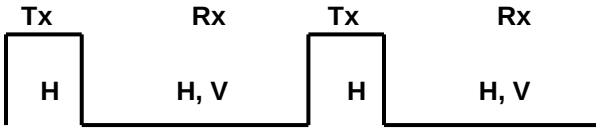

Figure 1.2 **Pulsing scheme for horizontal transmission, simultaneous receive mode (LDR mode). Measured variables are Z_H, LDR, p_H, $|\rho_{xh}|$.**

Operational radars implementing the hybrid scheme do not necessarily transmit slant linear polarization. Indeed, they simultaneously transmit horizontal and vertical polarizations without measuring the phase between these two components. So, the polarization state that is actually transmitted lies somewhere on the circular/slant circle of the Poincare sphere (the great circle going through the poles and the slant linear polarization states).
For completeness, we also mention another dual-polarization pulsing scheme used in the past: polarization agility on transmit, single polarization receiver.

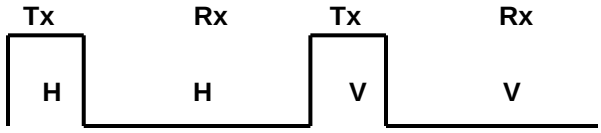

Figure 1.3 Measured variables: Z_H, Z_{DR}, K_{DP}, $|\rho_{hv}|$.

This architecture allows the measurement of Z_H, Z_{DR}, K_{DP} and $|\rho_{hv}|$, just like the hybrid scheme presented above. However, from an operational perspective, dual-polarization on receive gained momentum with respect to single polarization on receive combined with polarization agility on transmit.

From a theoretical perspective, a dual-polarization coherent receiver measures the wave covariance matrix, which has 4 degrees of freedom. When horizontal polarization is transmitted, only two variables are evaluated (Z_H and LDR) from a matrix with 4 degrees of freedom, leaving half of the information unprocessed.
The present work investigates the properties of the degree of polarization, a parameter available whenever a dual-polarization coherent receiver is used (2-channel receiver). From a mathematical viewpoint, this choice is not fanciful, but rather most straightforward, since the degree of polarization is one of the two invariants of the wave covariance matrix. The term invariant refers to the fact that this quantity does not change under a polarization basis transformation.
Adhering to the basic definition of degree of polarization, this variable is available in either polarimetric mode (hybrid and horizontal transmit) but, as will be seen in the following, its properties are crucially dependent on transmit polarization state.

In the case of horizontal transmit, it will be shown that p_H (degree of polarization at horizontal transmit) is extremely robust against propagation and enhances the contrast between rain and non-rain targets in a way that is unique. The phenomenon can be qualitatively explained as follows. When rain is illuminated (let us imagine non-canted rain) the value of the copolar correlation coefficient is affected by: axis ratio dispersion (equilibrium Drop Size Distribution + axisymmetric drop oscillations), finite width of the 0°-mean canting angle distribution, backscatter differential phase (especially at C-band). If the degree of polarization is measured with simultaneous transmission, it is sensitive to the same set of geophysical features. However, if transmission is horizontal or vertical, the degree of polarization is affected only by the finite width of the 0°-mean canting

angle distribution, but not by axis ratio dispersion (due to dispersion in raindrop size and axisymmetric drop oscillations) or backscatter differential phase (relevant at C-band but not at S-band when rain is illuminated).
The copolar correlation coefficient is generally used for classification purposes, namely to distinguish between rain and non-rain scatterers. It takes on lower values when non-rain is illuminated, since rain is characterized by values close to 1 (0.997-0.998 at S-band). However, the factors listed above are such that the copolar correlation coefficient values for rain can be sensibly lower than 1, thus decreasing the polarimetric contrast needed for classification. At C-band this effect is by no means negligible (because of Mie scattering) and the copolar correlation coefficient performance for classification is questionable. S-band is not affected by Mie scattering and indeed the copolar correlation coefficient performs definitely better than at C-band. At C-band (and, to a lesser extent, at S-band), the degree of polarization at horizontal transmit has, with respect to the copolar correlation coefficient, the advantage of optimizing the polarimetric contrast, since its values for rain are closer to 1 than the copolar correlation coefficient.
Ultimately, the backscattering properties from rain of the degree of polarization at horizontal (vertical) send are identical to those of the linear depolarization ratio. The distinctive advantage of the degree of polarization at horizontal send with respect to the linear depolarization ratio is that, contrary to the first, the latter is badly affected by antenna cross-channel coupling. This circumstance will be substantiated by experimental evidence in Chapter 5.

In the case of simultaneous transmission, the degree of polarization has different properties than at horizontal transmit. If non-canted rain is illuminated, its behavior is identical to the copolar correlation coefficient and indeed, its evaluation does not appear to bring additional information. However, if more depolarizing weather targets are illuminated (graupel, hail), it will be theoretically and experimentally shown that this variable can in general differ from the copolar correlation coefficient, and might therefore help in classification and, perhaps, inversion.

1.2 Fully polarimetric weather radars

Besides the exploitation of variables derived from the wave covariance matrix, research should also be addressed at the investigation of fully polarimetric signal processing procedures.
As operational radars make their way into dual-polarization, research radars should take advantage of their fully polarimetric capabilities and investigate whether knowledge of the complete covariance matrix adds valuable information.
Two pulsing schemes yielding the full covariance matrix are illustrated in Fig. 1.4 and Fig. 1.5.

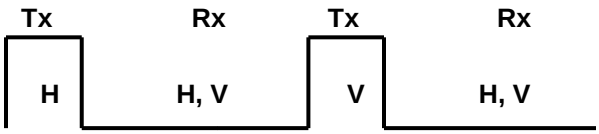

Figure 1.4 Pulsing scheme for fully polarimetric measurements.

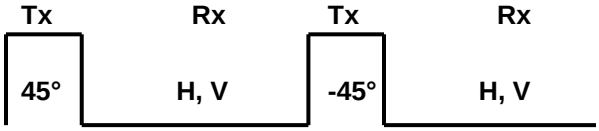

Figure 1.5 Another pulsing scheme for fully polarimetric measurements.

It consists of a dual-polarization coherent receiver (2-channel receiver) combined with polarization agility on transmit, namely sending out orthogonal polarization states on a pulse to pulse basis. The choice of orthogonal states can be either horizontal and vertical, or +45°/-45°. This allows for the measurement of the full covariance matrix and the implementation of fully polarimetric signal processing procedures like the application of Target Decomposition Theorems, rotations to other polarization bases or the evaluation of the depolarization response of radar targets.
Target decomposition (TD) theorems can be divided into coherent and incoherent theorems. Among the first group rank Cameron, Pauli and Krogager, whereas among the second we find the Huynen-Barnes and the Cloude-Pottier decompositions. Every TD theorem is rather application-dependent and its use is subject to a careful analysis of the observed scene. Given the highly incoherent nature of hydrometeors, our investigation is directed towards variables developed for the study of incoherent targets. In the frame of radar meteorology, the term incoherent refers to the short decorrelation time of weather targets. At microwave wavelengths such a time is of the order of milliseconds, with a dependence on wavelength, hydrometeor type and turbulence in the resolution volume. As far as TD theorems are concerned, the present work investigates entropy, a fully polarimetric variable derived from the Cloude-Pottier decomposition. Further, the depolarization response, a newly introduced concept, gives an interesting representation of the depolarization from volume targets. In particular, from the depolarization response, a new variable, named canting parameter (CP) and representing the mean canting angle of the illuminated target, will be defined.

The data used in this work are from POLDIRAD, DLR C-band fully polarimetric research weather radar. POLDIRAD capabilities are not limited to polarization agility, namely the capability to switch on a pulse to pulse basis between a fixed pair of orthogonal polarimetric channels, but can implement an especially flexible form of polarization diversity, namely the capability to fast switch on transmit between any pair of orthogonal polarimetric channels. An exhaustive description of the system will be provided in Chapter 3.

It is important to start investigating the classification capabilities of fully polarimetric systems, to check if they can discriminate a larger number of classes than their dual-polarization counterparts. Indeed, the scan time of fully polarimetric weather radars is generally considered too long to match the requirements of operational needs. However, the advent of polarimetric phased array weather radars allows to dramatically reduce the scan time by sending pairs of pulses into different rays and then acquiring independent samples (beam multiplexing). As an example, a pulsing scheme that sends 3 pulses into each ray (say H – H - V) would allow to implement a fully polarimetric mode with fast scan times and no trade-off on the Doppler velocity (velocity would be estimated from the first 2 samples, the full scattering matrix would be evaluated from the last two).

Michele Galletti
DLR-HR-RK

German Aerospace Center,
(DLR Deutsches Zentrum fuer Luft und Raumfahrt)

Microwaves and Radar Institute
(HR Institut fuer Hochfrequenztechnik und Radarsysteme, Director Prof. Dr. A. Moreira)

Radar Concepts Department
(RK Radarkonzepte, Director Dr. G. Krieger)

July 2008

2. Fundamentals of Radar Polarimetry

Radar polarimetry deals with the use of multiple polarimetric channels (generally 2 or 4) for the qualitative and quantitative characterization of targets. Notable fields of application are weather radar and synthetic aperture radar (SAR). In the first case, polarimetry is used to distinguish different hydrometeor classes as well as biological (birds, insects) or other kinds of targets (wildfire smoke, volcanic ashes). Further, use of polarimetric variables enhances the accuracy of quantitative precipitation estimates. In radar meteorology, polarimetry has attained a degree of maturity that it is being operationally implemented in National Weather radar networks. Polarimetric synthetic aperture radars mainly have military applications, for target recognition, concealed target detection and change detection. Civilian applications for polarimetric SAR are also emerging, mainly dealing with segmentation and classification of SAR images. Research topics are also the characterization of sea and land ice (age, thickness, structure) and classification of agricultural crops for use by governmental agencies.
Polarimetry is useful for the characterization of targets since it is capable to account for geometric properties like shape, symmetries or rotation angle around the radar line of sight.
In this chapter we introduce the mathematical concepts normally used in radar polarimetry like the Jones vector, used to describe a fully polarized wave, and the Sinclair matrix, used to describe the interaction of a coherent target with a fully polarized wave. The description of incoherent processes makes use of second order statistics. A partially polarized wave is represented by the wave covariance matrix, equivalent to a Stokes vector. The interaction of a fully (or partially) polarized wave with a coherent (or incoherent) target is represented by means of the Kennaugh matrix, generally regarded as a linear map between two wave states. Ultimately, incoherent targets can also be represented by the more modern covariance or coherency matrix [20]. Special emphasis will be given to the group theory interpretation of these operators, and to the role that SU(2), SU(3) and SO(1,3) play in polarimetry [11]. Group theory is well known to high energy physicists but less known to engineers working on electromagnetic scattering. SO(1,3), the so-called Lorentz group, enters the picture as the transformation group for Minkowski space-time in special relativity. SU(2) plays a role in the description of global internal symmetries of 2-state systems and, for example, underpins the concepts of spin and isotopic spin. An example for the concept of spin is an atom in a state with orbital angular momentum l subjected to a magnetic field. If all the effects of the electrons' spins are neglected (including degeneracies caused by them) then the energy eigenvalue of a state with angular momentum l is (2l+1)-fold degenerate in the absence of the field, but splits into (2l+1) different values when the field is applied.

In polarimetry, group theory enters naturally when polarization basis transformations are considered: SU(2) is related to polarization basis transformations for the scattering matrix, SU(3) is related to polarization basis transformations for the covariance (coherency) matrix, SO(1,3) is related to polarization basis transformations for the Kennaugh matrix. How the set of polarization basis transformations relates to the

structure of the corresponding Lie group is of central importance to solve the problem of optimal polarizations and to assign a physical meaning to invariant parameters [8]. The search for invariant parameters as a way to characterize the target for practical applications has seen a number of relevant developments in polarimetry, from the Huynen fork for coherent targets [14] to the Cloude-Pottier decomposition for incoherent targets [9]. The study of invariants of the Kennaugh matrix has been pursued to a lesser extent. Also, invariance is a principle often invoked when dealing with target decomposition theorems. The use of invariant parameters can be envisioned if interesting physics is highlighted. We should not however lose sight of the fact that most often parameters simply derived from the covariance matrix (namely, directly related to the radar measurements) are extremely meaningful, and more complex procedures, even though possessing nice mathematical properties, should be adopted only if the system performance is improved. In Chapters 4 and 5, where the scientific results of the present doctoral thesis are presented, this point of view permanently accompanies the exposition of concepts, and the properties of new variables are always compared with standard variables with similar physical meaning, in order to objectively assess if any improvement is achieved.

This chapter is meant to be more a review rather than an analytical exposition of concepts, since the latter can be found on many classical textbooks [19, 20, 34]. If, on one side, many practical applications of radar polarimetry have made their way well into the commercial market, the development of the formal theory of polarimetry has been somehow unusual, and has gone through a number of controversies. One of the most notable is the apparent difficulty in establishing a convention for generally oriented reference frames. In the last two paragraphs of this introductory chapter we expose some concepts of geometric polarimetry [1, 2], a mathematical framework providing a rigorous description of fundamental principles encompassing, for example, a consistent formulation for transformations to different reference frames or propagation through dissipative media. Geometric polarimetry draws on spinor theory [1, 2] and Clifford algebras [6] for the description of coherent as well as incoherent scattering. The material of the last two paragraphs is taken from [1, 2], that contain an exhaustive exposition of the theory.

2.1 Wave Polarimetry: Jones vector

The tip of the electric field intensity vector of a single-frequency electromagnetic wave traces the so-called polarization ellipse at a fixed position in space as time increases. Mathematically, the polarization ellipse can be expressed by the Jones vector, obtained by complexifying the electric field on the wave-plane by means of two phasors. Boldface indicates non-scalar quantities like vectors, tensors or spinors, non-boldface indicates scalar quantities, namely real or complex numbers. The imaginary unit is indicated with i.

$$\underline{\mathbf{E}} = \begin{bmatrix} E_1 \\ E_2 \end{bmatrix} = \begin{bmatrix} |E_1| e^{i\varphi_1} \\ |E_2| e^{i\varphi_2} \end{bmatrix} \tag{2.1}$$

The form of this ellipse and the sense of rotation with respect to the propagation direction characterize the state of polarization. The latter, obtained by eliminating from the Jones vector the size of the ellipse as well as the position of the tip of the electric vector on the ellipse, can be described by the complex polarization ratio.

$$\rho = \frac{E_2}{E_1} \tag{2.2}$$

It should be highlighted that the Jones vector contains the helicity of the wave but is unable to relate it to the direction of propagation of the plane wave. In the case of Back Scatter Alignment convention, (BSA), in order to distinguish between incoming and outgoing waves, classical polarimetry introduces the concepts of directional Jones vector and the Time Reversal operator in order to transform between the vector spaces corresponding to the incoming and outgoing waves.

As outlined in [1], the commonly accepted definition of Jones vector is at the origin of the problems encountered in theoretical polarimetry. For example, the concept of Jones vector exists only in the wave-plane of a given propagation direction. When the propagation direction changes, there is no consistent way of defining a reference frame transformation. The solution that is generally envisioned is the introduction of conventions (BSA and FSA are examples) that, unfortunately, undermine the general validity of the subsequent mathematical apparatus. Indeed, a long-standing problem of classical polarimetry has been the identification and labeling of states of polarization in differently oriented frames. This is particularly important in bistatic scattering, a topic of growing importance in radar applications. The source of many of the problems encountered in the theoretical formulation of polarimetry stems from the unrecognized spinorial nature of the state of polarization. The algebraic derivation of the polarization spinor [1] explicitly indicates that an additional spinor must be inserted alongside the state of polarization descriptor to make spatial rotations generally consistent. This additional element, named in the literature ‘phase flag’ [2], specifies the orientation of the phase reference direction in the wave-plane. When changes of the orientation of the reference frame are effected, via unitary transformations, the phase flag keeps track of the phase reference direction. Such direction is indeed path-dependent, that is, equivalent polarization states transform in a way that also depends on the path followed to transform the reference frame from the initial to the final state. The arousal of this additional phase is known to physicists under the name of Berry phase or geometrical phase and occurs in quantum-mechanical as well as classical systems (for example, Foucault pendulum precession around a general path).

In the last paragraph of the present chapter we report from [1, 2] the rigorous derivation of the polarization state spinor and of the phase flag spinor. We defer to the last paragraph further discussions on geometric polarimetry.

2.2 Wave Polarimetry: Wave Covariance Matrix

In practical radar polarimetry problems, one has to deal with partially polarized waves. For a partially polarized field, there is an associated stochastic process that in many cases is either theoretically or assumed to be Gaussian. Under this assumption, the probability density function of the field is completely described by second order moments. The second order descriptor of a partially polarized electromagnetic wave is the Wave Covariance Matrix, constructed as the ensemble average of Jones vector outer products (2.3).

$$\mathbf{J} = \begin{bmatrix} J_{11} & J_{12} \\ J_{21} & J_{22} \end{bmatrix} = \langle \underline{\mathbf{E}} \otimes \underline{\mathbf{E}}^{+} \rangle = \begin{bmatrix} \langle |E_1|^2 \rangle & \langle E_1 E_2^* \rangle \\ \langle E_2 E_1^* \rangle & \langle |E_2|^2 \rangle \end{bmatrix} = \frac{1}{2} \begin{bmatrix} g_0 + g_1 & g_2 - ig_3 \\ g_2 + ig_3 & g_0 - g_1 \end{bmatrix} \tag{2.3}$$

In (2.3), the symbol $\otimes$ indicates outer product, the superscript asterisk indicates complex conjugation, the superscript cross indicates adjoint and i indicates the imaginary unit.
The entries of the last matrix in (2.3) are the Stokes' parameters, namely the components of the Stokes vector, an alternative choice for the representation of fully as well as partially polarized waves.

$$\underline{\mathbf{g}} = \begin{bmatrix} g_0 \\ g_1 \\ g_2 \\ g_3 \end{bmatrix} = \begin{bmatrix} |E_1|^2 + |E_2|^2 \\ |E_1|^2 - |E_2|^2 \\ E_1 E_2^* + E_2 E_1^* \\ i(E_1 E_2^* - E_2 E_1^*) \end{bmatrix} \tag{2.4}$$

The Stokes vector can be decomposed into an unpolarized and a polarized part (in 2.5, superscript p stands for polarized, superscript u stands for unpolarized).

$$\underline{\mathbf{g}} = \underline{\mathbf{g}}^{p} + \underline{\mathbf{g}}^{u} = (1 - p) \begin{bmatrix} g_0 \\ 0 \\ 0 \\ 0 \end{bmatrix} + \begin{bmatrix} p g_0 \\ g_1 \\ g_2 \\ g_3 \end{bmatrix} \tag{2.5}$$

The degree of polarization is defined and expressed by the Stokes parameters as

$$p = \frac{I_{pol}}{I_{tot}} = \frac{\sqrt{g_1^2 + g_2^2 + g_3^2}}{g_0} \qquad 0 \le p \le 1 \tag{2.6}$$

In (2.6) I_{tot} indicates the total intensity of the propagating wave, I_{pol} indicates the intensity of the fully polarized component of the wave.

Simple algebra yields the degree of polarization as a function of invariants of the wave covariance matrix (det indicates the determinant, trace indicates the trace of the matrix):

$$\det(\mathbf{J}) = \det(\mathbf{U}^{-1}\mathbf{J}\mathbf{U}) = \lambda_1 \cdot \lambda_2$$
$$\mathrm{trace}(\mathbf{J}) = \mathrm{trace}(\mathbf{U}^{-1}\mathbf{J}\mathbf{U}) = \lambda_1 + \lambda_2 \tag{2.7}$$

$$p = \sqrt{1 - \frac{4\det\mathbf{J}}{(\mathrm{trace}\mathbf{J})^2}} = \frac{\lambda_1 - \lambda_2}{\lambda_1 + \lambda_2} \tag{2.8}$$

Here, the lambdas are the wave covariance matrix eigenvalues.
Since the eigenvalues are basis independent, the degree of polarization is a polarimetric invariant that does not depend on the polarimetric basis used to describe (detect) the backscattered wave.

A concept analog to the degree of polarization is the wave entropy, defined as

$$H_w = -\frac{\lambda_1}{\lambda_1 + \lambda_2}\log_2\left(\frac{\lambda_1}{\lambda_1 + \lambda_2}\right) - \frac{\lambda_2}{\lambda_1 + \lambda_2}\log_2\left(\frac{\lambda_2}{\lambda_1 + \lambda_2}\right) \tag{2.9}$$

The wave entropy is one-to-one related to the degree of polarization [1].

$$H_w(p) = -\left(\frac{1+p}{2}\right)\log_2\left(\frac{1+p}{2}\right) - \left(\frac{1-p}{2}\right)\log_2\left(\frac{1-p}{2}\right) \tag{2.10}$$

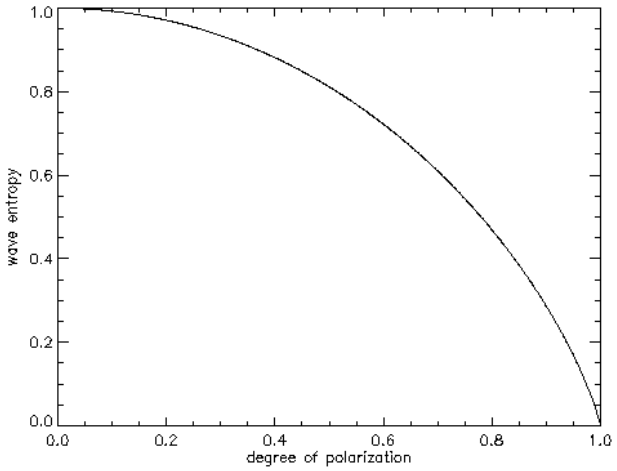

Figure 2.1 Plot of (2.10) - Degree of Polarization vs. Wave Entropy

2.3 Target Polarimetry: Scattering matrix

After introducing the Back Scatter Alignment convention (BSA), the polarimetric behavior of a coherent target can be described by a scattering matrix **S** operating on the outgoing Jones vector and yielding the incoming (backscattered) fully polarized wave. It is important to note that the entries of the scattering matrix are dependent on the conventions chosen at the beginning. Generally, the Forward Scattering Alignment (FSA) and Back Scattering Alignment (BSA) conventions are known to polarimetrists, and the Back Scatter Alignment convention is the choice for monostatic radar problems.

$$\underline{\mathbf{E}}^{s} = \mathbf{S}\,\underline{\mathbf{E}}^{i} \tag{2.11}$$

In the monostatic case, the scattering matrix is symmetric, with 5+1 degrees of freedom.

$$\mathbf{S} = \begin{bmatrix} S_{11} & S_{12} \\ S_{21} & S_{22} \end{bmatrix}_{\mathrm{BSA}} \tag{2.12}$$

Even though a fully polarimetric monostatic radar measurement yields six degrees of freedom, only five are actually meaningful parameters (when considering incoherent targets), since the absolute phase of the scattering matrix is dependent on the individual positions of the scatterers in the radar resolution volume. Since averages are needed to estimate the variables of interest, its value is discarded in the averaging process. Even though the absolute phase is bundled with the propagation phase (and, indeed, its one-shot numerical value might be of little importance), we remind that phase differences are important both for weather radar (wind velocity estimation, Doppler polarimetry) and

SAR (interferometry, permanent scatterers). Also, interesting enough, these phase differences are dependent on the polarization state used. The absolute phase of the scattering matrix is intrinsically a property of the radar target, relating to the polarization basis invariant phase center of the illuminated volume.

The scattering matrix polarization basis change can be expressed as a congruence transformation [2].

$$\mathbf{S}' = \mathbf{U}\mathbf{S}\mathbf{U}^{\mathrm{t}} \tag{2.13}$$

In (2.13) the superscript t indicates transpose. The unitary matrices involved in polarization basis transformations are elements of SU(2), namely, 2 by 2 unitary matrices with determinant equal to +1. SU(2) is a Lie group, a differentiable manifold obeying the group properties and that satisfies the additional condition that the group operations are differentiable. The tangent space at the identity of a Lie group always has the structure of a Lie algebra, and this Lie algebra determines the local structure of the Lie group via the exponential map. The Lie algebra can be represented by a number of infinitesimal generators (matrices) that generate the Lie group. The Lie algebra is generally indicated with the same name as the group, but with lower case letters, so, for example, the Lie algebra associated with the Lie group SU(2) is indicated with su(2).
Given the Pauli matrices,

$$\boldsymbol{\sigma}_1 = \begin{bmatrix} 0 & 1 \\ 1 & 0 \end{bmatrix}$$

$$\boldsymbol{\sigma}_2 = \begin{bmatrix} 0 & -\mathrm{i} \\ \mathrm{i} & 0 \end{bmatrix}$$

$$\boldsymbol{\sigma}_3 = \begin{bmatrix} 1 & 0 \\ 0 & -1 \end{bmatrix} \tag{2.14}$$

The matrices $\{\mathrm{i}\boldsymbol{\sigma}_\mathrm{j}\}$ constitute the infinitesimal generators of SU(2). Expressions for elements of SU(2) can be found via the exponential map:

$$\exp(\tau \cdot \mathrm{i}\boldsymbol{\sigma}_1) = \begin{bmatrix} \cos(\tau) & \mathrm{i} \cdot \sin(\tau) \\ \mathrm{i} \cdot \sin(\tau) & \cos(\tau) \end{bmatrix}$$

$$\exp(\varphi \cdot \mathrm{i}\boldsymbol{\sigma}_2) = \begin{bmatrix} \cos(\varphi) & \sin(\varphi) \\ -\sin(\varphi) & \cos(\varphi) \end{bmatrix}$$

$$\exp(\delta \cdot \mathrm{i}\boldsymbol{\sigma}_3) = \begin{bmatrix} \mathrm{e}^{\mathrm{i}\delta} & 0 \\ 0 & \mathrm{e}^{-\mathrm{i}\delta} \end{bmatrix} \tag{2.15}$$

A general element of SU(2) can then be written as

$$[\mathbf{U}] = \exp[\mathrm{i} \cdot (\tau\boldsymbol{\sigma}_1 + \varphi\boldsymbol{\sigma}_2 + \delta\boldsymbol{\sigma}_3)] = \begin{bmatrix} \cos(\tau) & \mathrm{i} \cdot \sin(\tau) \\ \mathrm{i} \cdot \sin(\tau) & \cos(\tau) \end{bmatrix} \begin{bmatrix} \cos(\varphi) & \sin(\varphi) \\ -\sin(\varphi) & \cos(\varphi) \end{bmatrix} \begin{bmatrix} \mathrm{e}^{\mathrm{i}\delta} & 0 \\ 0 & \mathrm{e}^{-\mathrm{i}\delta} \end{bmatrix} \tag{2.16}$$

Before proceeding to the illustration of scattering descriptors for incoherent targets, we retain important to highlight some properties of SU(2), especially to appreciate the richer mathematical structure it underpins. Indeed, its appearance as the transformation group for polarization basis change is a strong clue for redefining the concept of polarization state as a spinor.

If we indicate with SO(n) the special orthogonal group in N dimensions (associated with standard rotations in N-dimensional space), its universal covering group is indicated with Spin(n). The double cover provided by the spin group is essential for the exact description of rotations in space. Geometrically, it permits a precise description of rotation-entanglement, a feature not captured by the rotation group transformations that do not distinguish between a 2π and a 4π rotation. The elements of a representation of a spin group are the spinors. Ultimately, Spin(n) can be constructed as a subgroup of the invertible elements in the Clifford algebra Cl(n).
In the case of low dimensions, some accidental isomorphisms occur:

$$\begin{aligned} &\mathrm{Spin}(3) = \mathrm{SU}(2) \\ &\mathrm{Spin}(4) = \mathrm{SU}(2) \otimes \mathrm{SU}(2) \\ &\mathrm{Spin}(6) = \mathrm{SU}(4) \end{aligned} \tag{2.17}$$

The first relation is of primary importance in physics since the whole theory of spin for electrons and other elementary particles is based on the fact that there exist a two-to-one homomorphic mapping of the group SU(2) onto the group SO(3).
This fact is also important for electromagnetic wave scattering, since the proper description of the absolute phase in polarization measurements requires the additional structure provided by the spin group.

2.4 Target Polarimetry: Kennaugh matrix

If an incoherent target is illuminated, the scattering matrix is a realization of a stochastic process and, therefore, a whole set of scattering matrices is needed to characterize the target. Under the assumption of a Gaussian stochastic process, a second order descriptor fully characterizes the target.

One such second order descriptor is the Kennaugh matrix, generated by averaged outer products of single scattering matrices.

$$\mathbf{K} = \mathbf{Q}^{*}\langle \mathbf{S} \otimes \mathbf{S}^{*} \rangle \mathbf{Q}^{+} \tag{2.18}$$

where the unitary matrix **Q** is

$$\mathbf{Q} = \frac{1}{\sqrt{2}}\begin{bmatrix} 1 & 0 & 0 & 1 \\ 1 & 0 & 0 & -1 \\ 0 & 1 & 1 & 0 \\ 0 & \mathrm{i} & -\mathrm{i} & 0 \end{bmatrix} \qquad \mathbf{Q}^{+} = \frac{1}{\sqrt{2}}\begin{bmatrix} 1 & 1 & 0 & 1 \\ 0 & 0 & 1 & -\mathrm{i} \\ 0 & 0 & 1 & \mathrm{i} \\ 1 & -1 & 0 & 0 \end{bmatrix}$$

$$\mathbf{Q}\mathbf{Q}^{+} = \mathbf{I} \qquad \mathbf{Q}\mathbf{Q}^{\mathrm{t}} = \mathrm{diag}[1 \quad 1 \quad 1 \quad -1] \tag{2.19}$$

Superscript cross indicates adjoint, superscript t indicates transpose, superscript asterisk indicates complex conjugation. In terms of Huynen parameters, the Kennaugh matrix can be parameterized as (monostatic backscattering case)

$$\mathbf{K} = \begin{bmatrix} A_0 + B_0 & C & H & F \\ C & A_0 + B & E & G \\ H & E & A_0 - B & D \\ F & G & D & -A_0 + B \end{bmatrix} \tag{2.20}$$

where Huynen parameters are defined as:

A_0 = Generator of Target Symmetry
B_0 = Generator of Target Structure (Hamiltonian)

$B_0 - B$ = Generator of Target Non-Symmetry
$B_0 + B$ = Generator of Target Irregularity

H = Coupling due to Target Orientation (Tilt angle)
G = Coupling between Symmetric and Non-symmetric parts (Glue)
C = Shape Factor (Maximum for Line Target)
D = Measure of Local Curvature Difference
E = Surface Torsion
F = Target Helicity

The Kennaugh matrix can be considered either as a transformation operator from wave-state to wave-state, or as a quadratic power form. The latter viewpoint can be interpreted as a quadric surface in Stokes space, namely the analytical surface of antenna states (not necessarily physically realizable) for which the copolar power vanishes [1].

From the point of view of the Kennaugh matrix, there is always a Lorentz transformation that will diagonalize it.

Lorentz transformations present a group algebraic structure and form the Lorentz group, indicated with SO(1,3). The Lorentz group is a 6-dimensional real Lie group, and the subgroup containing the identity is referred to as the proper orthochronous Lorentz group, indicated with $SO^{+}(1,3)$.
In the previous section we hinted at the homomorphic mapping between SU(2) and SO(3). We remind the reader that SU(2) is a subgroup of SL(2,C) and SO(3) is a subgroup of $SO^{+}(1,3)$. SL(2,C) is the group of 2×2 complex matrices with determinant equal to +1, SU(2) is the group of 2×2 unitary matrices with determinant equal to +1.
A generalization of the result presented in the previous section is that there exist a two-to-one homomorphic mapping of the group SL(2,C) onto the proper orthochronous homogeneous Lorentz group $SO^{+}(1,3)$.
If $\mathbf{a} \in \mathrm{SL}(2,\mathbb{C})$ maps onto $\Lambda(\mathbf{a}) \in \mathrm{SO}^{+}(3,1)$, then $\Lambda(\mathbf{a}) = \Lambda(-\mathbf{a})$ and the mapping may be chosen so that

$$\Lambda(\mathbf{a})_{\mathrm{jk}} = \frac{1}{2}\mathrm{trace}\{\boldsymbol{\sigma}_{\mathrm{j}}\mathbf{a}\boldsymbol{\sigma}_{\mathrm{k}}\mathbf{a}^{+}\} \qquad \mathrm{j,k} = 1,2,3,4 \tag{2.21}$$

SL(2,C), namely the group formed by 2×2 complex matrices with determinant equal to 1, is a double cover of PSL(2,C), the projective special linear group or, the group of Moebius transformations. The Moebius group is a 3-dimensional complex Lie group (or a 6 dimensional real Lie group). Also, PSL(2,C) is isomorphic to $SO^{+}(1,3)$.
Moebius transformations can be generated as one-parameter subgroups of SL(2,C) by exponentiating $\frac{\theta}{2}$ (for the three boosts) and $\frac{\mathrm{i}\theta}{2}$ (for the three rotations) times the three Pauli matrices. Each of these six generators of Moebius transformations can be mapped onto a one-parameter subgroup of $SO^{+}(1,3)$ representing Lorentz transformations.

For the three rotations we have

$$\exp\left(\mathrm{i}\frac{\theta_1}{2}\cdot\boldsymbol{\sigma}_1\right) = \begin{bmatrix} \cos\left(\frac{\theta_1}{2}\right) & \mathrm{i}\sin\left(\frac{\theta_1}{2}\right) \\ \mathrm{i}\sin\left(\frac{\theta_1}{2}\right) & \cos\left(\frac{\theta_1}{2}\right) \end{bmatrix} \rightarrow \begin{bmatrix} 1 & 0 & 0 & 0 \\ 0 & 1 & 0 & 0 \\ 0 & 0 & \cos\theta_1 & -\sin\theta_1 \\ 0 & 0 & \sin\theta_1 & \cos\theta_1 \end{bmatrix} = \mathbf{R}_1$$

$$\exp\left(\mathrm{i}\frac{\theta_2}{2}\cdot\boldsymbol{\sigma}_2\right) = \begin{bmatrix} \cos\left(\frac{\theta_2}{2}\right) & \sin\left(\frac{\theta_2}{2}\right) \\ -\sin\left(\frac{\theta_2}{2}\right) & \cos\left(\frac{\theta_2}{2}\right) \end{bmatrix} \rightarrow \begin{bmatrix} 1 & 0 & 0 & 0 \\ 0 & \cos\theta_2 & 0 & \sin\theta_2 \\ 0 & 0 & 1 & 0 \\ 0 & -\sin\theta_2 & 0 & \cos\theta_2 \end{bmatrix} = \mathbf{R}_2$$

$$\exp\left(\mathrm{i}\frac{\theta_3}{2}\cdot\boldsymbol{\sigma}_3\right)=\begin{bmatrix} e^{\mathrm{i}\frac{\theta_3}{2}} & 0 \\ 0 & e^{-\mathrm{i}\frac{\theta_3}{2}} \end{bmatrix} \rightarrow \begin{bmatrix} 1 & 0 & 0 & 0 \\ 0 & \cos\theta_3 & -\sin\theta_3 & 0 \\ 0 & \sin\theta_3 & \cos\theta_3 & 0 \\ 0 & 0 & 0 & 1 \end{bmatrix} = \mathbf{R}_3 \tag{2.22}$$

The most general rotation is then given by the combination of the three matrices above

$$\mathbf{R}=\mathbf{R}_1\mathbf{R}_2\mathbf{R}_3 \tag{2.23}$$

The most general rotation represents also the general polarization basis transformation that can be effected on the Kennaugh matrix

$$\mathbf{K}'=\mathbf{R}\mathbf{K}\mathbf{R}^{-1} \tag{2.24}$$

There are 6 independent infinitesimal generators for $SO^{+}(1,3)$, namely 3 rotations and 3 boosts. Consequently, the degrees of freedom associated with the Kennaugh matrix are 6+4-1 (6 infinitesimal generators, + 4 diagonal elements, -1, that corresponds to the constraint for the Kennaugh matrix to be traceless), which is 9 in total, and this is an isomorphic map with the covariance (or coherency) matrix.
Ultimately, the analogy between the Lorentz group and the Kennaugh matrix is not complete. If the three rotations correspond to polarization basis transformations and the three boosts provide the additional 3 degrees of freedom needed for the description of general radar targets, it has to be noted that the Lorentz group spans a larger set of transformations than those associated with the Kennaugh scattering matrix for radar targets.
This is a consequence of the physical fact that an electromagnetic wave has degree of polarization between 0 and 1 (positive):

$$1-\mathrm{p}^2=\frac{\underline{\mathbf{g}}_\mu\underline{\mathbf{g}}^\mu}{g_0^2} \tag{2.25}$$

In (2.25), the upper and lower μ indices indicate contravariant and covariant components of two vectors (a vector and a covector) contracting into a scalar. So, 4-vectors associated with electromagnetic waves must always be either lightlike (fully polarized waves) or timelike (partially polarized waves) and the domain and range of transformations associated to Kennaugh matrices is the time-like cone of Minkowski space (lateral surface included and representing fully polarized waves) [35]. The consequence of the fact that Lorentz transformations span a larger set than the possible existing Kennaugh matrices is that it is difficult to associate a physical meaning to its eigenvalues.

2.5 Target Polarimetry: Covariance (coherency) matrix

Other second order descriptors for incoherent targets are the covariance or coherency matrices. These matrices are constructed by first forming a target feature vector. The latter can be formed either by using the lexicographic basis or the Pauli spin matrices plus the identity.

$$\underline{\boldsymbol{\Psi}}_{\mathrm{L}} = \left\{ \begin{bmatrix} 1 & 0 \\ 0 & 0 \end{bmatrix}, \begin{bmatrix} 0 & 0 \\ 1 & 0 \end{bmatrix}, \begin{bmatrix} 0 & 1 \\ 0 & 0 \end{bmatrix}, \begin{bmatrix} 0 & 0 \\ 0 & 1 \end{bmatrix} \right\}$$

$$\underline{\boldsymbol{\Psi}}_{\mathrm{P}} = \left\{ \begin{bmatrix} 1 & 0 \\ 0 & 1 \end{bmatrix}, \begin{bmatrix} 0 & 1 \\ 1 & 0 \end{bmatrix}, \begin{bmatrix} 0 & -\mathrm{i} \\ \mathrm{i} & 0 \end{bmatrix}, \begin{bmatrix} 1 & 0 \\ 0 & -1 \end{bmatrix} \right\} \tag{2.26}$$

In the monostatic case, the corresponding target vectors are:

$$\underline{\mathbf{k}}_{\mathrm{L}} = \begin{bmatrix} S_{xx} \\ \sqrt{2}S_{xy} \\ S_{yy} \end{bmatrix}$$

$$\underline{\mathbf{k}}_{\mathrm{p}} = \frac{1}{\sqrt{2}} \begin{bmatrix} S_{xx} + S_{yy} \\ S_{xx} - S_{yy} \\ 2S_{xy} \end{bmatrix} \tag{2.27}$$

Averaged products yield the covariance and coherency matrices.

$$\langle [\mathbf{C}] \rangle = \langle \underline{\mathbf{k}}_{\mathrm{L}} \cdot \underline{\mathbf{k}}_{\mathrm{L}}^{+} \rangle = \frac{1}{\mathrm{N}} \sum_{\mathrm{i}=1}^{\mathrm{N}} [\mathbf{C}_{\mathrm{i}}]$$

$$\langle [\mathbf{T}] \rangle = \langle \underline{\mathbf{k}}_{\mathrm{p}} \cdot \underline{\mathbf{k}}_{\mathrm{p}}^{+} \rangle = \frac{1}{\mathrm{N}} \sum_{\mathrm{i}=1}^{\mathrm{N}} [\mathbf{T}_{\mathrm{i}}] \tag{2.28}$$

For clarity, we write the entries of a rank-1 covariance matrix.

$$[\mathbf{C}] = \underline{\mathbf{k}}_{\mathrm{L}} \cdot \underline{\mathbf{k}}_{\mathrm{L}}^{+} = \begin{bmatrix} |S_{xx}|^2 & \sqrt{2}S_{xx}S_{xy}^{*} & S_{xx}S_{yy}^{*} \\ \sqrt{2}S_{xy}S_{xx}^{*} & 2|S_{xy}|^2 & \sqrt{2}S_{xy}S_{yy}^{*} \\ S_{yy}S_{xx}^{*} & \sqrt{2}S_{yy}S_{xy}^{*} & |S_{yy}|^2 \end{bmatrix} \tag{2.29}$$

With respect to the Kennaugh matrix, the covariance (coherency) matrix has two advantages. The first is that, under the assumption of a multivariate Gaussian distribution of the coherent signals, the covariance (coherency) matrix is Wishart distributed. This provides the developer of classification algorithms with a distance between matrices and an analytical form for its statistical distribution. This fact is of primary importance if classification algorithms for fully polarimetric weather radar data are to be developed. The second advantage is that its entries are directly related to the radar system measurables. Indeed, elements of the covariance matrix are also rich in physical meaning, and all standard radar meteorological variables are rather simply derived from covariance matrix elements. The covariance (coherency) matrix can be constructed as an object equivalent to the Kennaugh matrix, with a linear mapping between the two. However, since the degree of polarization for different transmit polarizations is more easily evaluated from the Kennaugh matrix, both representations will be used in this work.

Change of polarization basis for the covariance (coherency) matrix are effected by using unitary matrices, according to the formula

$$[\mathbf{C}]' = \mathbf{U}[\mathbf{C}]\mathbf{U}^{-1}$$

$$[\mathbf{T}]' = \mathbf{U}[\mathbf{T}]\mathbf{U}^{-1} \tag{2.30}$$

The matrix **U** is an element of a representation of SU(3), namely the Lie group of 3×3 special unitary matrices. In this case, the associated Lie algebra is represented by 8 infinitesimal generators, the Gell-Mann matrices:

$$\boldsymbol{\lambda}_1 = \begin{bmatrix} 0 & 1 & 0 \\ 1 & 0 & 0 \\ 0 & 0 & 0 \end{bmatrix} \quad \boldsymbol{\lambda}_2 = \begin{bmatrix} 0 & -\mathrm{i} & 0 \\ \mathrm{i} & 0 & 0 \\ 0 & 0 & 0 \end{bmatrix} \quad \boldsymbol{\lambda}_3 = \begin{bmatrix} 1 & 0 & 0 \\ 0 & -1 & 0 \\ 0 & 0 & 0 \end{bmatrix} \quad \boldsymbol{\lambda}_4 = \begin{bmatrix} 0 & 0 & 1 \\ 0 & 0 & 0 \\ 1 & 0 & 0 \end{bmatrix}$$

$$\boldsymbol{\lambda}_5 = \begin{bmatrix} 0 & 0 & -\mathrm{i} \\ 0 & 0 & 0 \\ \mathrm{i} & 0 & 0 \end{bmatrix} \quad \boldsymbol{\lambda}_6 = \begin{bmatrix} 0 & 0 & 0 \\ 0 & 0 & 1 \\ 0 & 1 & 0 \end{bmatrix} \quad \boldsymbol{\lambda}_7 = \begin{bmatrix} 0 & 0 & 0 \\ 0 & 0 & -\mathrm{i} \\ 0 & \mathrm{i} & 0 \end{bmatrix} \quad \boldsymbol{\lambda}_8 = \frac{1}{\sqrt{3}} \begin{bmatrix} 1 & 0 & 0 \\ 0 & 1 & 0 \\ 0 & 0 & -2 \end{bmatrix} \tag{2.31}$$

Elements of a representation of SU(3) can then be obtained with the exponential map:

$$\exp(\mathrm{i} \cdot \alpha_1 \boldsymbol{\lambda}_1) = \begin{bmatrix} \cos\alpha_1 & \mathrm{i} \cdot \sin\alpha_1 & 0 \\ \mathrm{i} \cdot \sin\alpha_1 & \cos\alpha_1 & 0 \\ 0 & 0 & 1 \end{bmatrix}$$

$$\exp(\mathrm{i}\cdot\alpha_2\boldsymbol{\lambda}_2)=\begin{bmatrix}\cos\alpha_2 & \sin\alpha_2 & 0\\ -\sin\alpha_2 & \cos\alpha_2 & 0\\ 0 & 0 & 1\end{bmatrix}$$

$$\exp(\mathrm{i}\cdot\alpha_3\boldsymbol{\lambda}_3)=\begin{bmatrix}e^{\mathrm{i}\alpha_3} & 0 & 0\\ 0 & e^{-\mathrm{i}\alpha_3} & 0\\ 0 & 0 & 1\end{bmatrix}$$

$$\exp(\mathrm{i}\cdot\alpha_4\boldsymbol{\lambda}_4)=\begin{bmatrix}\cos\alpha_4 & 0 & \mathrm{i}\cdot\sin\alpha_4\\ 0 & 1 & 0\\ \mathrm{i}\cdot\sin\alpha_4 & 0 & \cos\alpha_4\end{bmatrix}$$

$$\exp(\mathrm{i}\cdot\alpha_5\boldsymbol{\lambda}_5)=\begin{bmatrix}\cos\alpha_5 & 0 & \sin\alpha_5\\ 0 & 1 & 0\\ -\sin\alpha_5 & 0 & \cos\alpha_5\end{bmatrix}$$

$$\exp(\mathrm{i}\cdot\alpha_6\boldsymbol{\lambda}_6)=\begin{bmatrix}1 & 0 & 0\\ 0 & \cos\alpha_6 & \mathrm{i}\cdot\sin\alpha_6\\ 0 & \mathrm{i}\cdot\sin\alpha_6 & \cos\alpha_6\end{bmatrix}$$

$$\exp(\mathrm{i}\cdot\alpha_7\boldsymbol{\lambda}_7)=\begin{bmatrix}1 & 0 & 0\\ 0 & \cos\alpha_7 & \sin\alpha_7\\ 0 & -\sin\alpha_7 & \cos\alpha_7\end{bmatrix}$$

$$\exp(\mathrm{i}\cdot\alpha_8\boldsymbol{\lambda}_8)=\begin{bmatrix}e^{\mathrm{i}\frac{\alpha_8}{\sqrt{3}}} & 0 & 0\\ 0 & e^{\mathrm{i}\frac{\alpha_8}{\sqrt{3}}} & 0\\ 0 & 0 & e^{-2\mathrm{i}\frac{\alpha_8}{\sqrt{3}}}\end{bmatrix} \tag{2.32}$$

The most general element of SU(3) can be written as

$$\mathbf{U}=\exp\left(\mathrm{i}\cdot\alpha_{\mathrm{i}}\boldsymbol{\lambda}_{\mathrm{i}}\right) \tag{2.33}$$

where the Einstein summation convention is used.

Two observations need be made.
An SU(3) matrix has 8 parameters, so the degrees of freedom of the diagonalized matrix should be 8+3, namely, the 8 parameters of the unitary transformation plus the 3 eigenvalues. The coherency (covariance) matrix has 9 degrees of freedom so it appears

that two degrees of freedom are lost somewhere. A look at the above matrices clearly tells us that the problem is associated with matrices $\boldsymbol{\lambda}_3$ and $\boldsymbol{\lambda}_8$. These degrees of freedom are unobservable since the coherency (covariance) matrix is obtained from the outer product of a target vector with itself (conjugate), thus leading to real diagonal terms. Indeed, the intrinsic significance of SU(3) is the description of the physics of the interaction of two different 3-state vectors. The first application example was Gell-Mann eightfold way, where 3 degrees of freedom (up, down and strange flavours) particles (quarks) combined into 8 new particles (mesons), each made up of two quarks. Nowadays, even though other flavors have been discovered and it was understood that the initial up/down/strange symmetry was accidental, SU(3) still has a primary role in the standard model (U(1)×SU(2) ×SU(3)), since interactions in quantum chromodynamics (QCD) manifest themselves through the color charge, which has 3 degrees of freedom (red, green, blue) giving rise to eight bosons (gluons) each characterized by two colors.
From another perspective, the problem is that the covariance (coherency) matrix does not describe an interaction, namely, does not transform one target vector into another. On the other hand, the scattering matrix and the Kennaugh matrix do actually map one wave state into another and the corresponding degrees of freedom are precisely expressed by SU(2) and SO(1,3) respectively.

The second problem concerning the use of SU(3) for the description of polarimetric scattering is that the unitary matrix describing a general polarimetric basis change is associated only with matrices $\boldsymbol{\lambda}_1$, $\boldsymbol{\lambda}_4$ and $\boldsymbol{\lambda}_7$. So, when a coherency/covariance matrix is diagonalized by means of a general SU(3) element, the ratio of the maximum-to-minimum eigenvalue is larger than or equal to the ratio of maximum-to-minimum backscattered power.
This circumstance also holds for the Kennaugh matrix, where the eigenvalues are only loosely related to the physics of scattering.

Despite the above-outlined drawbacks, the analysis of the covariance (coherency) matrix eigenvalues still allows the extraction of parameters that are rich in physical meaning. In particular, the decomposition of the covariance (coherency) matrix into three rank-one matrices suggests the possibility to measure the degree of randomness of the polarimetric scattering process, as captured by the target entropy.

2.6 Target Decomposition Theorems

Target decomposition theorems can be divided into coherent and incoherent theorems. Among the first group rank Cameron, Pauli and Krogager [13, 15], whereas among the second we find the Huynen-Barnes and the Cloude-Pottier decompositions [14, 18, 9]. Every target decomposition theorem is rather application dependent, and its use is subject to a careful analysis of the observed scene. Given the highly incoherent nature of hydrometeors, our investigation is directed toward variables developed for the study of

incoherent targets. In the frame of radar meteorology, the term incoherent refers to the short decorrelation time of weather targets. At microwave wavelengths, such time is on the order of milliseconds, with a dependence on wavelength, hydrometeor type, and turbulence in the resolution volume. The Cloude-Pottier approach to target decomposition involves an eigen-analysis of the coherency matrix. The covariance and the coherency matrices have the same eigenvalues, so, the use of the Pauli basis can be avoided if eigen-vector derived variables are not needed.

The coherency matrix is Hermitian and positive semi-definite, yielding three non-negative eigenvalues

$$\langle[\mathbf{T}]\rangle = [\mathbf{U}_3][\mathbf{\Sigma}][\mathbf{U}_3]^{-1} = \begin{bmatrix} \underline{\mathbf{u}}_1 & \underline{\mathbf{u}}_2 & \underline{\mathbf{u}}_3 \end{bmatrix} \begin{bmatrix} \lambda_1 & 0 & 0 \\ 0 & \lambda_2 & 0 \\ 0 & 0 & \lambda_3 \end{bmatrix} \begin{bmatrix} \underline{\mathbf{u}}_1 & \underline{\mathbf{u}}_2 & \underline{\mathbf{u}}_3 \end{bmatrix}^{*t}$$

$$\lambda_1 \geq \lambda_2 \geq \lambda_3 \geq 0 \tag{2.34}$$

The relative probabilities for each eigenvalue are defined as

$$p_i = \frac{\lambda_i}{\sum_{k=1}^{3} \lambda_k} \tag{2.35}$$

Ultimately, we arrive at the definition of three eigenvalue-derived variables, namely Entropy, Anisotropy and Span.

$$H = -\sum_{i=1}^{3} p_i \log_3(p_i)$$

$$A = \frac{\lambda_2 - \lambda_3}{\lambda_2 + \lambda_3}$$

$$\text{Span}[\mathbf{T}] = \sum_{i=1}^{3} \lambda_i \tag{2.36}$$

Target entropy is a measure of the heterogeneity of the scattering matrices that come in the formation of the covariance matrix and can be regarded as the most general indicator of the "depolarizing" properties of the target. If entropy equals 0, then a set of identical scattering matrices are contributing to the covariance matrix that, even after averaging, keeps being rank-1. If entropy equals 1, then the scattering process is random, namely, the scattering matrices contributing to the covariance matrix are significantly different.

Anisotropy is a measure of the departure from azimuthal symmetry of the illuminated target. Span is related to the total backscattered power.
As pointed out above, the eigenvalues of these two matrices are the same and, indeed, the three eigenvalue-derived variables can be equally evaluated from both matrices. Ultimately, the reason for the introduction of the Pauli basis is the evaluation of eigenvector derived variables. The unitary matrix that diagonalizes the coherency matrix can be parameterized as follows

$$[\mathbf{U}_3] = \begin{bmatrix} \cos\alpha_1 & \cos\alpha_2 & \cos\alpha_3 \\ \sin\alpha_1\cos\beta_1 e^{i\delta_1} & \sin\alpha_2\cos\beta_2 e^{i\delta_2} & \sin\alpha_3\cos\beta_3 e^{i\delta_3} \\ \sin\alpha_1\sin\beta_1 e^{i\gamma_1} & \sin\alpha_2\sin\beta_2 e^{i\gamma_2} & \sin\alpha_3\sin\beta_3 e^{i\gamma_3} \end{bmatrix} \tag{2.37}$$

The three column eigenvectors appearing in the unitary matrix are to be considered as statistically independent degrees of freedom of the coherency matrix, and not as physical scattering mechanisms existing in the resolution volume. In the Cloude-Pottier decomposition, these principal components are averaged into a single column vector by means of averaged parameters

$$\begin{aligned} \underline{\alpha} &= p_1\alpha_1 + p_2\alpha_2 + p_3\alpha_3 \\ \underline{\beta} &= p_1\beta_1 + p_2\beta_2 + p_3\beta_3 \\ \underline{\gamma} &= p_1\gamma_1 + p_2\gamma_2 + p_3\gamma_3 \\ \underline{\delta} &= p_1\delta_1 + p_2\delta_2 + p_3\delta_3 \end{aligned} \tag{2.38}$$

A unitary target vector $\underline{\mathbf{u}}_0$ can then be defined

$$\underline{\mathbf{u}}_0 = \begin{bmatrix} \cos\underline{\alpha} \\ \sin\underline{\alpha} \cdot \cos\underline{\beta} e^{i\underline{\delta}} \\ \sin\underline{\alpha} \cdot \sin\underline{\beta} e^{i\underline{\gamma}} \end{bmatrix} \tag{2.39}$$

that, together with the target magnitude

$$\underline{\lambda} = p_1\lambda_1 + p_2\lambda_2 + p_3\lambda_3 \tag{2.40}$$

yields the target vector corresponding to the whole coherency matrix

$$\underline{\mathbf{k}}_0 = \sqrt{\underline{\lambda}} \begin{bmatrix} \cos\underline{\alpha} \\ \sin\underline{\alpha} \cdot \cos\underline{\beta} e^{i\underline{\delta}} \\ \sin\underline{\alpha} \cdot \sin\underline{\beta} e^{i\underline{\gamma}} \end{bmatrix} \tag{2.41}$$

A physical meaning has been associated to the alpha and beta angles. Alpha is regarded as a roll-invariant indicator of the main scattering mechanism present in the resolution volume, namely, single (or odd) bounce scattering is responsible for values of alpha between 0° and 40°, double (or even) bounce scattering is responsible for values of alpha between 50° and 90°. Values between 40° and 50° might be generated by scattering from dipoles. Beta can be related to the orientation angle of the illuminated target.

2.7 Problems in theoretical polarimetry

The scattering matrix **S** can be interpreted either as a linear form or as a transform operator. These two viewpoints are known in radar polarimetry as the network interpretation and the field interpretation. The antenna height vector $\underline{\mathbf{h}}$ can be defined in terms of the radiated far-field from the antenna

$$\underline{\mathbf{E}} = e^{-i\frac{2\pi}{\lambda}R} \frac{IZ_0}{2\lambda R} \underline{\mathbf{h}} \tag{2.42}$$

where I is the antenna current (with a time signature $e^{i\omega t}$), Z_0 the impedance of free space, λ the wavelength, and R ($>> \lambda$) is the distance from the antenna. In the network interpretation, the scattering matrix is seen as a symmetric form yielding the copolar voltage.

$$V(\underline{\mathbf{h}}) = \underline{\mathbf{h}}^t \mathbf{S}\, \underline{\mathbf{h}} = \begin{bmatrix} h^1 \\ h^2 \end{bmatrix}^t \begin{bmatrix} S_{11} & S_{12} \\ S_{21} & S_{22} \end{bmatrix} \begin{bmatrix} h^1 \\ h^2 \end{bmatrix} \tag{2.43}$$

In this formulation, the electric field vector does not appear directly and, as a consequence, the field interpretation (2.44) is generally preferred and adopted for the illustration of the scattering process. In this case, the scattering matrix is seen as an operator mapping the outgoing (with respect to the antenna) to the incoming (with respect to the antenna) electric fields.

$$\underline{\mathbf{E}}_s = \mathbf{S}\, \underline{\mathbf{E}}_i \tag{2.44}$$

For these two representations, we now consider a polarization basis transformation.

The antenna height, complex in general, can be written as

$$\underline{\mathbf{h}} = h^1 \hat{\mathbf{e}}_1 + h^2 \hat{\mathbf{e}}_2 \tag{2.45}$$

where $\hat{\mathbf{e}}_1$ and $\hat{\mathbf{e}}_2$ are unit vectors and constitute an orthonormal basis. The elements of an orthonormal basis are regarded as covariant, whereas the components are contravariant. When the first undergo a unitary transformation **U** (basis change) the second transform inversely, $\mathbf{U}^{-1}$. Since the voltage is a constant, regardless of the polarization basis we use to express our relations, the following relation follows for the basis transformation for the scattering matrix.

$$\begin{bmatrix} S'_{11} & S'_{12} \\ S'_{21} & S'_{22} \end{bmatrix} = \mathbf{U} \begin{bmatrix} S_{11} & S_{12} \\ S_{21} & S_{22} \end{bmatrix} \mathbf{U}^t \tag{2.46}$$

This transformation is known as a congruence transformation and shows that the scattering matrix is a rank-2 covariant object, namely, it obeys the same transformation rules as the basis vectors. This is to be expected, since bilinear forms (covariant) act to contract the contravariant components of two vectors into a scalar. When the scattering matrix is regarded as a matrix operator, this transformation law (congruence) highlights that a mapping between different mathematical entities occurs, namely a vector is mapped into a covector.

We remind that vectors are the elements of a vector space, with contravariant components and covariant basis vectors, on which linear transformations act (2.47).

$$\mathbf{v} = \hat{\mathbf{e}}_i \, v^i \tag{2.47}$$

Covectors are the elements of the dual space associated with every vector space, that is, they are linear transformations acting on vectors to yield a scalar, with covariant components and contravariant basis vectors (2.48).

$$\mathbf{v} = \hat{\mathbf{e}}^i \, v_i \tag{2.48}$$

When the transformation rule worked out above is applied to the field representation, the outcome is that the incoming and outgoing fields have different transformation laws.

$$\mathbf{U}\underline{\mathbf{E}}_s = \mathbf{U}\mathbf{S}\mathbf{U}^t\mathbf{U}^{t-1}\underline{\mathbf{E}}_i \qquad \Rightarrow \qquad \underline{\mathbf{E}}'_1 = \mathbf{U}^{t-1}\underline{\mathbf{E}}_i \qquad \underline{\mathbf{E}}'_s = \mathbf{U}\underline{\mathbf{E}}_s \tag{2.49}$$

The reason for this is that in the network representation the antenna height vectors are expressed in the same reference frame, whereas in the field representation the

backscattered field propagates in the opposite direction as the radiated field. Classical polarimetry goes around the problem by introducing directional Jones vectors and the time reversal operator, the latter being antilinear.

A linear transformation is defined as

$$L(\alpha_1 \mathbf{x}_1 + \ ... \ + \alpha_n \mathbf{x}_n) = \alpha_1 L(\mathbf{x}_1) + \ ... + \ \alpha_n L(\mathbf{x}_n) \tag{2.50}$$

In particular, basis-change transformations for linear operators are expressed by similarity transformations.

An antilinear transformation is defined as (superscript asterisk denotes complex conjugation)

$$L(\alpha_1 \mathbf{x}_1 + \ ... \ + \alpha_n \mathbf{x}_n) = \alpha_1^* L(\mathbf{x}_1) + \ ... + \ \alpha_n^* L(\mathbf{x}_n) \tag{2.51}$$

In particular, basis-change transformations for antilinear operators are expressed by conjugate similarity (consimilarity) transformations.

$$\mathbf{S}' = \mathbf{U}\mathbf{S}\mathbf{U}^{*-1} \tag{2.52}$$

Now, when a change of polarization basis is considered and unitary matrices are involved, a consimilarity transformation reduces to a congruence transformation that, as shown above, is a correct result.

$$\mathbf{S}' = \mathbf{U}\mathbf{S}\mathbf{U}^{*-1} \qquad \rightarrow \qquad \mathbf{S}' = \mathbf{U}\mathbf{S}\mathbf{U}^{t} \tag{2.53}$$

If one tries to generalize the transformation rule for the antilinear interpretation (consimilarity) to non-unitary transformations, the identity between consimilarity and congruence transformations does not hold anymore, and one is forced to use the following relation.

$$\mathbf{S}' = \mathbf{T}\mathbf{S}\mathbf{T}^{*-1} \tag{2.54}$$

A case of practical importance is the problem of propagation through dissipative media, where non-unitary matrices are involved. In this case consimilarity does not preserve the symmetry of the scattering matrix.
Another problem rising from the theory of polarimetry as outlined in the previous paragraphs is the inability to properly describe bistatic scattering geometries in a consistent way. This problem is not the subject of the present work; it is however useful to remind how the description of bistatic scattering automatically involves the introduction of a convention in order to orient the axes of the polarization plane along the

new propagation direction. In geometric polarimetry, the concept of phase flag is introduced to keep track of the orientation of the reference frame when the direction of propagation changes.

2.8 Spinorial Concepts

In this paragraph we report the derivation of the spinorial wave state from the electromagnetic field tensor [2]. The advantage point of this approach is that a constant spinor (the phase flag) allows the contraction of a 2-spinor into a 1-spinor, the latter being representative of the wave state. The constant spinor used for the contraction (the phase flag) is the tool that makes a difference in this mathematical construction: since it can be transformed independently, it can be used to keep track of the reference in the polarization plane when new propagation directions are to be described. There are two other advantage points descending from this simple approach: the first is that spinor algebra can be used to pinpoint the matrix to be used for transformations to circular polarization basis, the second is that the antilinear time reversal operator and the subsequent conjugate similarity transformations need not be invoked, allowing for a neater description of propagation through lossy media. Only in this section, (due to the presence of upper and lower indices for spinors with contravariant and covariant components) complex conjugation will be indicated not by a superscript asterisk but by overbars and primed indices.

Maxwell's equations can be formulated in tensor form with the help of the electromagnetic field tensor,

$$\mathbf{F}_{ab} = \begin{bmatrix} 0 & E_x & E_y & E_z \\ -E_x & 0 & -cB_z & cB_y \\ -E_y & cB_z & 0 & -cB_z \\ -E_z & -cB_y & cB_x & 0 \end{bmatrix} \tag{2.55}$$

its Hodge dual

$${}^{*}\mathbf{F}_{ab} = \begin{bmatrix} 0 & -cB_x & -cB_y & -cB_z \\ cB_x & 0 & -E_z & E_y \\ cB_y & E_z & 0 & -E_x \\ cB_z & -E_y & E_x & 0 \end{bmatrix} \tag{2.56}$$

and another tensor encapsulating the electric displacement $\vec{\mathbf{D}}$ and the magnetic field $\vec{\mathbf{H}}$ for linear media (arrows indicate 3D vectors, including time-space propagators)

$$\mathbf{G}_{ab} = \begin{bmatrix} 0 & cD_x & cD_y & cD_z \\ -cD_x & 0 & -H_z & H_y \\ -cD_y & H_z & 0 & -H_x \\ -cD_z & -H_y & H_x & 0 \end{bmatrix} \tag{2.57}$$

In SI units, Maxwell equations can be written as

$$\begin{aligned} \boldsymbol{\partial}_a \, {}^*\mathbf{F}^{ab} &= 0 \\ \boldsymbol{\partial}_a \mathbf{G}^{ab} &= \mathbf{J}^b \end{aligned} \tag{2.58}$$

where **J** is the current density, and ρ is the charge density.

$$\begin{aligned} \mathbf{J} &= (c\rho \quad J_x \quad J_y \quad J_z) \\ \boldsymbol{\partial}_a &= \frac{\partial}{\partial \mathbf{x}^a} = \left(\frac{1}{c}\frac{\partial}{\partial t} \quad \frac{\partial}{\partial x} \quad \frac{\partial}{\partial y} \quad \frac{\partial}{\partial z}\right) \end{aligned} \tag{2.59}$$

In spinor form, a real electromagnetic field may be represented by a mixed spinor,

$$\mathbf{F}_{ABA'B'} = \boldsymbol{\varphi}_{AB}\boldsymbol{\varepsilon}_{A'B'} + \boldsymbol{\varepsilon}_{AB}\overline{\boldsymbol{\varphi}}_{A'B'} \tag{2.60}$$

(overbar and primed indices indicate complex conjugation here) where

$$\boldsymbol{\varepsilon}_{AB} = \begin{bmatrix} 0 & 1 \\ -1 & 0 \end{bmatrix} \tag{2.61}$$

is the metric spinor and $\boldsymbol{\varphi}_{AB}$ is the electromagnetic spinor, encoding all the information contained in the electromagnetic field. As expected, the spinor has two indices, as prescribed by quantum theory for fields with spin-1 carriers (photons). However, since for practical purposes we are interested in the derivation of a 1-index spinor, we are led to consider the electromagnetic potential, a 4-vector whose components are the electrostatic potential ϕ and the magnetic vector potential $\vec{\mathbf{A}}$:

$$\boldsymbol{\Phi}^a \equiv \left(\phi, \quad \vec{\mathbf{A}}\right) \tag{2.62}$$

The electromagnetic tensor $\mathbf{F}_{ab}$ can be expressed in terms of $\mathbf{\Phi}^a$ as:

$$\mathbf{F}_{ab} = \boldsymbol{\partial}_a \mathbf{\Phi}_b - \boldsymbol{\partial}_b \mathbf{\Phi}_a \quad \rightarrow \quad \begin{cases} \vec{\mathbf{E}} = -\frac{1}{c}\frac{\partial \vec{\mathbf{A}}}{\partial t} - \vec{\nabla}\phi \\ \vec{\mathbf{B}} = \vec{\nabla} \times \vec{\mathbf{A}} \end{cases} \tag{2.63}$$

where $\mathbf{\Phi}_a \equiv \left(\phi, \quad -\vec{\mathbf{A}}\right)$.

In the Fourier domain the derivative becomes

$$\boldsymbol{\partial}_a \quad \rightarrow \quad i\mathbf{k}_a$$

$$\mathbf{k}_a = \left[\frac{\omega}{c} \quad -k_x \quad -k_y \quad -k_z\right] \tag{2.64}$$

where $\mathbf{k}_a$ is the wavevector

Thus yielding

$$\mathbf{F}_{ab} = i[\mathbf{k}_a \mathbf{\Phi}_b - \mathbf{k}_b \mathbf{\Phi}_a] \tag{2.65}$$

Given the potential, it is necessary to assume the propagation direction in order to derive the field. In spinor form, the vector potential $\mathbf{\Phi}_a$ is a 4-vector isomorphic to a hermitian matrix, $\mathbf{\Phi}_{AB'}$

$$\mathbf{\Phi}_{AB'} \equiv \begin{bmatrix} \phi - A_z & -A_x + iA_y \\ -A_x - iA_y & \phi + A_z \end{bmatrix} \tag{2.66}$$

Further, a choice has to be made for the gauge freedom of the vector potential since:

$$\widetilde{\mathbf{\Phi}}_a = \mathbf{\Phi}_a - \boldsymbol{\partial}_a \chi \quad \Rightarrow \quad \begin{cases} \widetilde{\phi} = \phi - \frac{\partial \chi}{\partial t} \\ \widetilde{\vec{\mathbf{A}}} = \vec{\mathbf{A}} + \vec{\nabla}\chi \end{cases} \tag{2.67}$$

The Lorenz gauge is generally chosen for it is relativistic invariant. Other choices are however possible, like the radiation gauge:

$$\mathbf{k}^a \mathbf{F}_{ab} = 0 \tag{2.68}$$

and the Coulomb gauge

$$\boldsymbol{\omega}_a \mathbf{\Phi}^a = 0$$

(2.69)

with $\boldsymbol{\omega}_a \equiv [1 \quad 0 \quad 0 \quad 0]$ and implies $\phi = 0$.

These choices are not mutually exclusive and can be simultaneously satisfied for a radiating plane wave. For a wave propagating in the z-direction, the radiation gauge implies that $A_z = 0$ and together with the Coulomb gauge we obtain

$$\boldsymbol{\Phi}_a \equiv [0 \quad -A_x \quad -A_y \quad 0] \quad \rightarrow \quad \boldsymbol{\Phi}_{AB'} = \begin{bmatrix} 0 & \Phi_{01'} \\ \Phi_{10'} & 0 \end{bmatrix} = \begin{bmatrix} 0 & -A_x + iA_y \\ -A_x - iA_y & 0 \end{bmatrix} \tag{2.70}$$

Now, the above expression contains conjugate components representative of the opposite helicity polarizations (right-hand circular and left-hand circular). To arrive at a 1-index representation (analogous to the Jones vector), it is necessary to project $\boldsymbol{\Phi}_{AB'}$ onto a spinor with one index. The polarization information contained in (2.70) can be amalgamated into a 1-index spinor by contracting with a constant spinor $\overline{\boldsymbol{\theta}}^{B'}$:

$$\boldsymbol{\psi}_A = ik_0 \boldsymbol{\Phi}_{AB'} \overline{\boldsymbol{\theta}}^{B'} = ik_0 \begin{bmatrix} 0 & \Phi_{01'} \\ \Phi_{10'} & 0 \end{bmatrix} \begin{bmatrix} 1 \\ 1 \end{bmatrix} = \begin{bmatrix} ik_0 \Phi_{01'} \\ ik_0 \Phi_{10'} \end{bmatrix} \tag{2.71}$$

The entries in the right-hand column vector of (2.71) are the circular polarization components of the wave. The first outstanding novelty of this formulation is that (2.71) is valid in every rotated reference frame, provided all elements are transformed according to the appropriate rule:

$$\widetilde{\boldsymbol{\psi}}_A = \mathbf{U}_A{}^B \boldsymbol{\psi}_B$$

$$\widetilde{\boldsymbol{\Phi}}_{AB'} = \mathbf{U}_A{}^C \overline{\mathbf{U}}_{B'}{}^{D'} \boldsymbol{\Phi}_{CD'}$$

$$\widetilde{\overline{\boldsymbol{\theta}}}_{A'} = \overline{\mathbf{U}}_{A'}{}^{B'} \overline{\boldsymbol{\theta}}_{B'} \tag{2.72}$$

with $\mathbf{U}_A{}^B$ the unitary spinor describing the rotation of the frame.
Geometric polarimetry provides an approach for handling polarization in every reference frame.

As a final remark, we highlight the consequences of recognizing the spinorial nature of the Jones vector in terms of the definition of the scalar product.

If $\boldsymbol{\psi}$ and $\boldsymbol{\varphi}$ are spinors with complex entries,

$$\boldsymbol{\psi} = \begin{bmatrix} \psi_1 \\ \psi_2 \end{bmatrix} \qquad \boldsymbol{\varphi} = \begin{bmatrix} \varphi_1 \\ \varphi_2 \end{bmatrix} \tag{2.73}$$

then two kinds of scalar products are possible:

$$\boldsymbol{\psi}^{*\mathrm{t}}\boldsymbol{\varphi} = \psi_1^*\varphi_1 + \psi_2^*\varphi_2$$

$$\boldsymbol{\psi}^{\mathrm{t}}\mathrm{i}\boldsymbol{\sigma_2}\boldsymbol{\varphi} = \psi_1\varphi_2 - \psi_2\varphi_1 \tag{2.74}$$

which have automorphism groups U(2) and Sp(2,C)=SL(2,C), respectively. Here, Sp(2,C) is the group of 2 by 2 symplectic matrices with complex entries, and superscript asterisk denotes complex conjugation.

The corresponding conditions for orthogonality are

$$\langle\boldsymbol{\psi}|\boldsymbol{\varphi}\rangle_{\mathrm{U}(2)} = \psi_1^*\varphi_1 + \psi_2^*\varphi_2 = 0$$

$$\langle\boldsymbol{\psi}|\boldsymbol{\varphi}\rangle_{\mathrm{Sp}(2,\mathbb{C})} = \psi_1\varphi_2 - \psi_2\varphi_1 = 1 \tag{2.75}$$

Now, given the spinor

$$\boldsymbol{\psi}_{\mathrm{A}} = \frac{1}{\sqrt{2}}\begin{bmatrix} 1 \\ \mathrm{i} \end{bmatrix} \tag{2.76}$$

It is easy to check that, according to the first definition of scalar product, the spinors

$$\boldsymbol{\psi}_1 = \frac{1}{\sqrt{2}}\begin{bmatrix} 1 \\ -\mathrm{i} \end{bmatrix} \qquad \boldsymbol{\psi}_2 = \frac{1}{\sqrt{2}}\begin{bmatrix} \mathrm{i} \\ 1 \end{bmatrix} \tag{2.77}$$

are both orthogonal to $\boldsymbol{\psi}_{\mathrm{A}}$.
However, if the second scalar product is used, only $\boldsymbol{\psi}_2$ is orthogonal to $\boldsymbol{\psi}_{\mathrm{A}}$. These observations lead to a choice for the transformation matrix to circular polarization basis that preserves the absolute phase of the scattering matrix.

References Chapter 2

[1] Bebbington, D. "Fundamentals of Radar Polarimetry using Complex Spinor Formalism" A monograph under BAA #99-025 for long range scientific projects, 30 August 1999.

[2] Bebbington, D., Carrea L., Krogager E. "Geometric Polarimetry Part 1: Spinors and Wave States", April 2008, available at http://arxiv.org/abs/0804.0745

[3] Bebbington, D. H. O., E. Krogager and M. Hellmann, "Vectorial Generalization of Target Helicity", *3rd European Conference on Synthetic Aperture Radar, EUSAR 2000*, pp 531-534, Munich, May 2000.

[4] Barakat R.,"Bilinear constraints between the elements of the 4x4 Mueller-Jones matrix of polarization theory", Optical communications, Vol. 38, pp159-161, Aug. 1981.

[5] Boerner, W-M., L-L Liu and X. Zhang, "Comparison of optimization procedures for 2x2 Sinclair, 2x2 Graves, 3x2 covariance and 4x4 Mueller (Kennaugh) matrices in coherent radar polarimetry and its application to target versus background clutter discrimination in microwave remote sensing and imaging", *EARSel, Advances in Remote Sensing* Vol. 2 (1) pp 55-82.

[6] Carrea L. Ph.D thesis, available from +44 7831784094 (mobile uk), +39 3477956637 (mobile it).

[7] S. R. Cloude and E. Pottier, "Concept of polarization entropy in optical scattering," Opt. Eng. 34, 1599–1610 (1995).

[8] S. R. Cloude and E. Pottier, "A Review of Target Decomposition Theorems in Radar Polarimetry," IEEE Transactions on Geoscience and Remote Sensing, vol. 34, no. 2, pp. 498-518, March 1996.

[9] S. R. Cloude and E. Pottier, "An Entropy Based Classification Scheme for Land Applications of Polarimetric SAR," IEEE Transactions on Geoscience and Remote Sensing, vol. 35, no. 1, pp. 68-78, January 1997.

[10] S. R. Cloude, J. Fortuny, J. M. Lopez and A. J. Sieber, "Wide Band Polarimetric Radar Inversion Studies for Vegetation Layers," IEEE Transactions on Geoscience and Remote Sensing, Vol. 37/2, No. 5, pp. 2430-2442, September 1999.

[11] S. R. Cloude, "Group theory and polarisation algebra," Optik 75, 26–36 (1986).

[12] S. R. Cloude and K. P. Papathanassiou, "Coherence optimization in polarimetric SAR interferometry," IGARSS '97 Proc., Singapore, pp. 1932-1934, 1997.

[13] W. L. Cameron and L.K. Leung, "Feature motivated polarization scattering matrix decomposition," Proc. IEEE Int. Radar Conf., Arlington, VA, May 7-10, pp.549-557, 1990.

[14] J. R. Huynen, "Phenomenological theory of radar targets," Ph. D. dissertation, Technical Univ., Delft, The Netherlands, 1970.

[15] E. Krogager, "Aspects of polarimetric radar imaging" in Ph.D. dissertation, Tech. Univ. Denmark, published Danish Defence Res. Establishment, May 1993.

[16] E. Krogager and Z. H. Czyz, "Properties of the sphere, diplane, helix decomposition," in Proc. 3rd Int. Workshop Radar Polarimetry, JIPR Nantes, France, Mar. 1995, pp 106-114.

[17] E. Krogager, "A new decomposition of the radar target scattering matrix," Electron.Lett., vol. 26, no. 18, pp. 1525-1526, 1990.

[18] R. M. Barnes, "Roll-invariant decompositions of the polarization covariance matrix" Lincoln Lab., M.I.T., Lexington, Internal Rep., 1988.

[19] M. Born and E. Wolf, Principles of Optics: Electromagnetic Theory of Propagation, Interference and Diffraction of Light, 7th ed. Cambridge University Press, 1999.

[20] H. Mott, Remote Sensing with Polarimetric Radar, John Wiley & Sons, IEEE press, 2007.

[21] Fry, E.S. and G. W. Kattawar, "Relationship between elements of the Stokes matrix", Applied Optics Vol. 20 (16) pp 2811-2814, 1981.

[22] Graves, C. D. , "Radar polarization power scattering matrix", Proceedings of the I.R.E., Vol. 44, pp248-242, 1956.

[23] Hubbert, J. C., and V. N. Bringi, "Specular Null Polarization Theory: Applications to Radar Meteorology", IEEE Transactions on Geoscience and Remote Sensing T-GRS 34 (4) pp 859-873, July 1996.

[24] Kostinski, A.B., B.D. James and W-M. Boerner, "Optimal reception of partially polarized waves", Journal of the Optical Society of America A, Vol. 5 (1) pp58-64, Jan. 1988.

[25] Kostinski, A.B., and W-M. Boerner, "On the Polarimetric Contrast Optimization", *IEEE Transactions on Antennas and Propagation* AP-35 (8) pp 988-991 Aug. 1987.

[26] Lee, J.S., M.R. Grunes, and R. Kwok, "Classification of Multilook Polarimetric SAR imagery based on Complex Wishart Distribution", International Journal of Remote Sensing Vol. 15 2299-2311, 1994.

[27] Lueneburg, E., V. Ziegler, A. Schroth, and K. tragl, "Polarimetric Covariance matrix Analysis of Random Radar Targets", *Proc. NATO-AGAARD-EPP Symposium on Target and Clutter Scattering and their Effects on Military Radar Performance*, Ottawa. May, 1991.

[28] Yamaguchi, Y., W-M. Boerner, H. J. Eom and M. Sengoku, S. Motooka and T. Abe, "On characteristic polarization states in the cross-polarized radar channel", *IEEE Transactions on Geoscience and Remote Sensing*, T-GRS 30 (5) pp 1078-1081, 1992.

[29] Yamaguchi, Y., Y. Takayanagi, W-M. Boerner, H.J. Eom and M. Sengoku, "Polarimetric Enhancement in Radar Channel Imagery", *J-IEICE Trans. Communications*, vol. E78-B (1) pp 45-51 Jan. 1996.

[30] Yang, J. "On theoretical aspects of radar polarimetry", Doctoral Thesis, Niigata University, Japan, September 1999.

[31] Yang, J., Yoshio Yamaguchi, Hiroyoshi Yamada, Masakazu Sengoku, "Optimal problem for contrast enhancement in polarimetric radar remote sensing", *J-IEICE Trans. Communications* vol. E82-B (1) pp174-183 Jan. 1999.

[32] van Zyl J. J., C. H. Pappas and C. Elachi, "On the optimum polarizations of incoherently reflected waves", *IEEE Transactions on Antennas and Propagation* T-AP 35 (7) July 1987.

[33] D. H. O. Bebbington, "Target vectors: Spinorial concepts," Proc. 2nd Int. Workshop on Radar Polarimetry, IRESTE, Nantes, France, pp. 26-36, Sept. 1992.

[34] Jong-Sen Lee, Eric Pottier, "Polarimetric Radar Imagiing, from Basics to Applications", CRC Press, 2009

[35] Bebbington, David Henry Oliver, "Geometrical concepts in optimal polarimetry: Stokes formalism in a Minkowski space", Proc. SPIE Vol. 1748, pp. 132-143, Radar Polarimetry, Harold Mott, Wolfgang Martin Boerner Eds.

3 Polarimetric Weather Radar

The data used in this thesis were collected with DLR C-band research weather radar POLDIRAD, the latter being an acronym for POLarization DIversity RADar. The radar was originally manufactured by EEC[1] in1986 and was subsequently modified for fully polarimetric measurements with the main objectives of scientific research in the fields of cloud microphysics, mesoscale meteorology and wave propagation [1]. The system is located on top of the building of the Institute of Atmospheric Physics at DLR campus at Oberpfaffenhofen, Wessling, Bayern, Germany.

http://maps.google.de/maps?hl=de&ie=UTF8&ll=48.086848,11.279097&spn=0.002752,0.004807&t=h&z=18

Figure 3.1 DLR Institute for Atmospheric Physics, Oberpfaffenhofen. On top is visible the radar antenna and the horn feed.

.

[1] Enterprise Electronics Corporation, a US weather radar manufacturer with headquarters in Enterprise, Alabama. More on http://www.eecradar.com/

SYSTEM PERFORMANCE	
Frequency	C-band tunable from 5.48-5.85 GHz
Range	75 m res. unambiguous range 60 km 150m res. unambiguous range 120 km 300m res. unambiguous range 300 km
Reflectivity	< ± 1 dB precision, relative ±0.1 dB
Radial velocity	< ± 1 m s^{-1} precision
Spectral width	< ± 1 m s^{-1} precision
Range bins	452
Number of samples	32, 64, 128

ANTENNA	
Aperture Diameter	approx. 5 m
Azimuth	1° beam width, continuous azimuth scan
Elevation	1° beam width scan -6° to +90°
Focal length	approx. 4 m
Feed	Offset corrugated horn with OMT (Ortho Mode Transducer)
Illumination distribution	$(1-r^2)^3$
Gain	approx. 44.5 dB
Side lobe level	< -32 dB
Cross-polarization isolation (linear pol.)	< -28 dB
Radome	none

TRANSMITTER	
Peak power	400 kW
PRF	variable from 160 to 2400 Hz
Pulse width	2μs 1μs 0.5μs
Loss from transmitter to antenna feed	approx. 2.5 dB
Duty cycle	0.11% (maximum)

RECEIVER	
Number of channels	2
Bandwidth	4.8 MHz
Receiver response	linear, logarithmic (60 dB, 80 dB)
Minimum detectable signal	-108dBm (0.5μs pulse width)

POLARIZATION NETWORK	
Channel isolation	approx. 35 dB, max. 40 dB
Polarizations	variable (linear, circular, elliptic)
Switching time for pol. change	15μs
Switching time between tx and rx	8μs
Switching rate	up to 4800 Hz

Table 3.1 POLDIRAD System parameters.

3.1 Poldirad Architecture

The polarization-agile coherent DLR radar introduced, for the first time, fully polarimetric capabilities. A fully polarimetric radar is able to transmit pulses whose polarization state is switched every pulse repetition interval (henceforth PRT, pulse repetition time, PRF is pulse repetition frequency) and is set to simultaneously receive the copolar and the cross-polar components of the backscattered signal (dual receiver). Such a set up allows quasi-simultaneous measurements of the scattering matrix. The term polarization diversity refers to the system capability of using more than one polarization. The term polarization agility refers to the system capability of using polarization diversity on a pulse to pulse basis.
In the antenna mounted electronics (AME), the high power microwave pulse, generated by a magnetron transmitter, is divided into two components by the polarization network.
These two signals, in general of different amplitudes, say A_1 and A_2, are then phase shifted by amounts δ_1 and δ_2 and fed into the input-ports 1 and 2 (corresponding to linear orthogonal polarization states) of the antenna feed system. This causes the transmission of an elliptically polarized wave $\underline{\mathbf{E}}^+$

$$\underline{\mathbf{E}}^+ = A_1 e^{i\delta_1}\hat{\mathbf{a}}_1 + A_2 e^{i\delta_2}\hat{\mathbf{a}}_2 \tag{3.1}$$

The superscript + denotes an outgoing wave, $\hat{\mathbf{a}}_1$ and $\hat{\mathbf{a}}_2$ are the unit vectors of the orthogonal linear coordinate system. The control signals of the polarization network are generated in the computer and sent to a microprocessor that controls the polarization network. Timing pulses and gates for the polarization network are generated in the digital (Doppler) signal processor (DSP), designed by SIGMET[2] (1986).
The signals received from the two orthogonal ports of the antenna feed are connected to the polarization network in the AME by separate waveguides. The polarization network separates the incoming signals into two parts; the same polarization as that transmitted (co-polarized), and polarization orthogonal to the transmitted signal (cross-polarized). Both the co- and cross-polarized signals are detected simultaneously with coherent and

[2] Sigmet Corporation was merged into Vaisala inc in 2006 and continues operating in Westford, Massachusetts. Sigmet was established in 1980 by experts working at the weather radar laboratory of the Massachusetts Institute of Technology, MIT.

logarithmic receivers in the AME. The outputs of the AME are co- and cross-polarized log video signals and co and cross polarized linear signals (I-Q, in-phase and quadrature signals). These outputs are sent to two DSPs (Digital Signal Processors). The log video signals are corrected in real time for the non ideal receiver transfer function, the linear signals are corrected for the DC offsets. The discrete Fourier transform (DFT) of the linear time series data uses a frequency-domain high-pass filter (software) to provide a clutter correction for the log video. The main task of the DSP is to process signals from the two polarizations, and display a selected set of computed parameters. The DSP offers a number of options for selecting the placement and spacing of range bins, activation of data quality thresholds, linear receiver gain control, scan-timing, PRF, pulse width and time averaging. There are a maximum of 452 range bins available with variable bin spacing of 150 m × N where N = 1, 2, …, 20. There is also a high resolution 75 m bin spacing that is achieved by collecting a ray of data at 150 m resolution, and then shifting each bin by 75 meters in order to complete one-ray of data and repeating this sequence. The 452 range bins can be placed anywhere on the interval from 0 to 900 km, as long as the span from the first to the last bin is less than 300 km. The PRF may be varied from 160 to 2400 Hz, subject to the constraints of maximum transmitter duty cycle (0.11%). The linear receiver gain control can be varied in two ways: sensitivity time control (STC) (a preprogrammed DSP output) and a fixed gain option. The STC option introduces an approximately $1/R^2$ dependence of the linear receiver gain, such that the gain is the same for both co- and cross-polarized channels. The fixed option gives separate control of the gains for both co- and cross-polarized channels. Here 32- 64- or 128- pulse averages of the various quantities can be specified. In the alternating polarization modes, the full number of pulses is sent at each of the two polarizations, and thus a total of 64, 128, or 256 transmitted pulses are averaged to determine the data from any ray location. The signal processor can select a number of data quality checks to assure signal quality with respect to noise and other signal degrading factors. For instance, these are a clutter filter, a speckle remover, a signal-to-clutter threshold and a signal-to-noise ratio threshold. The user operates the whole system with an interactive CRT connected to the minicomputer to select the scanning and signal processing tasks of interest. A color display shows two selected computed parameters simultaneously in an RHI (Range Height Indicator), PPI (Plane Position Indicator) or a special scan display after about 20 s of processing time. A real time monochrome display shows three selected parameters as a function of range. This is a modern analog of the traditional ‘A-scan’.

The antenna is an offset reflector with a dual-polarized corrugated offset feed horn with high polarization purity and very low sidelobes. All critical microwave components are mounted in two temperature and humidity controlled enclosures; one (RF part, Fig. 3.4) is mounted on the boom of the primary feed support to reduce the length of the temperature insulated waveguides from the orthomode transducer to the low noise amplifiers; the second (IF part, Fig. 3.6) is mounted behind the reflector.

Systematic errors in phase and amplitude of the signals are reduced to a minimum by this design. For calibration purposes, a stable RF signal, phase-locked to the transmitted RF pulse, is injected in front of the polarization network in both channels. This CW signal is attenuated by a computer-controlled step-attenuator in 1 dB increments. It is gated on for 30μs just prior to each transmit pulse. Therefore, the calibration data will be in the last range bins of the recorded data

Figure 3.2 POLDIRAD parabolic reflector.

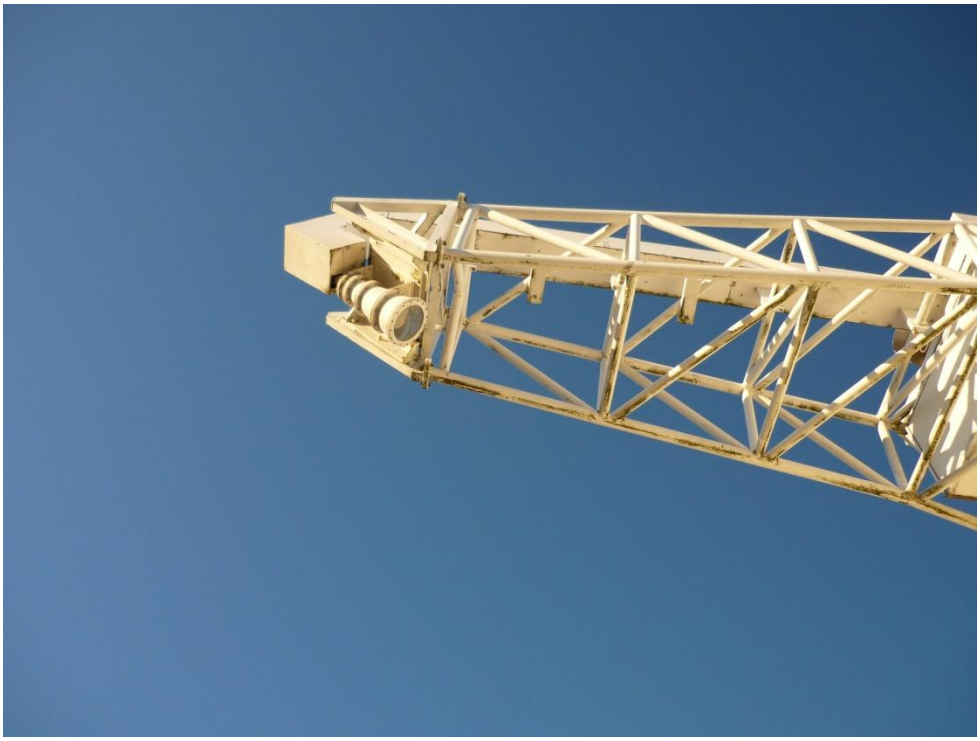

Figure 3.3 Boom of the primary feed support, with the feed horn and OMT on the left. On the right end of the picture, part of the RF enclosure is visible.

Figure 3.4 RF enclosure located at the end of the feed boom.

Figure 3.5 POLDIRAD seen from behind.

Figure 3.6 **Standing right behind the reflector and looking above, the IF enclosure is visible.**

Figure 3.7 **POLDIRAD Magnetron.**

The most peculiar feature of POLDIRAD is its polarimetric measurement capabilities.
The capability of switching from one polarization state to its orthogonal on a pulse to pulse basis is referred to as polarization agility. The term polarization diversity refers to the system capability of using more than one polarization. Indeed, POLDIRAD implements an extremely flexible form of polarization diversity, namely, it is possible to choose among any two orthogonal polarization states present on the Poincare sphere.

Among other modes, POLDIRAD provides transmission of a general elliptical polarization state $\hat{\mathbf{e}}_1$ and reception of in-phase and quadrature voltages of echoes in the corresponding copolar and cross-polar receive channels (I_{c1}, Q_{c1}) and (I_{x1}, Q_{x1}); PRT seconds (=1/PRF) later, the same measurement is conducted, but with a pulse transmitted on polarization $\hat{\mathbf{e}}_2$, orthogonal to $\hat{\mathbf{e}}_1$, yielding the received in-phase and quadrature voltages (I_{c2}, Q_{c2}) and (I_{x2}, Q_{x2}).
This set of measurements is repeated sequentially, yielding a measurement of complex voltages as

$$\left.\begin{aligned} V_{c1}^{n} &= I_{c1}^{n} + iQ_{c1}^{n} \\ V_{x1}^{n} &= I_{x1}^{n} + iQ_{x1}^{n} \end{aligned}\right\} \quad n = 1, 3, \dots, 2M-1$$

$$\left.\begin{aligned} V_{c2}^{m} &= I_{c2}^{m} + iQ_{c2}^{m} \\ V_{x2}^{m} &= I_{x2}^{m} + iQ_{x2}^{m} \end{aligned}\right\} \quad m = 2, 4, \dots, 2M \qquad (3.2)$$

where M, the maximum number of pulses per polarization state is ≤ 128.

3.2 Construction of the Instantaneous Scattering Matrix (ISM)

To collect the data presented in this work, POLDIRAD was operated to switch between horizontal and vertical polarization states on transmit, and was set to receive the copolar and cross-polar components of the backscattered signal. Ideally, all elements of a scattering matrix should be measured simultaneously. However, since the transmit polarizations must be emitted sequentially, the scattering matrix measured by a fully polarimetric weather radar is affected by both mean motion of the target and decorrelation due to random displacements of the single scatterers. Mean motion results in a phase offset between the first and second column of the scattering matrix while random motion manifests itself in amplitude and phase fluctuations of the backscattered signal. If the second effect cannot be corrected, special signal processing procedures must be applied to correct for the Doppler phase shift [2]. In this paragraph we illustrate the signal processing applied to obtain Instantaneous Scattering Matrices.
The first step involves the correction of hardware offset phases. The second step corrects the quasi-instantaneous scattering matrices for Doppler phase shift. We start with the latter.

A. ISM Estimation

In the case of fully polarimetric weather radar like POLDIRAD, the two columns of the scattering matrix **S** are measured at one pulse lag.

$$\mathbf{S} = \begin{bmatrix} S_{hh}(t + PRT) & S_{hv}(t) \\ S_{vh}(t + PRT) & S_{vv}(t) \end{bmatrix} \tag{3.3}$$

At a given time instant, only two terms are actually measured and two others need be estimated. For simplicity, we consider the measurements made at time t and illustrate the procedures to interpolate the two missing terms. As far as the missing cross-polar term is concerned, reciprocity can be invoked and no interpolation is needed. For the missing copolar term the following procedures can be envisioned.

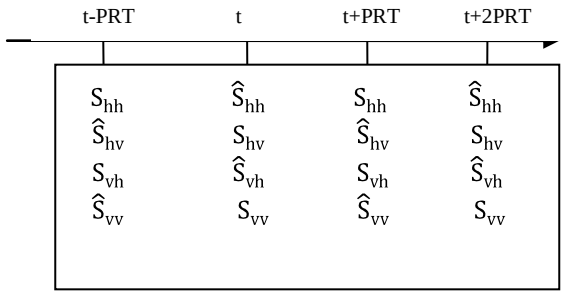

Figure 3.8 Schematic representation of the alternating pulsing scheme for fully polarimetric radar. Circumflex accent indicates the estimated (missing) terms.

As proposed in [2], to estimate the amplitude a simple interpolation can be used, or a full sequence of temporal samples can be considered for a higher order polynomial fit.

$$\left|\hat{S}_{hh}(t)\right| = \frac{1}{2}\left[|S_{hh}(t - PRT)| + |S_{hh}(t + PRT)|\right] \tag{3.4}$$

As far as the phase is concerned, the same technique can be used [2].

$$\arg\left[\hat{S}_{hh}(t)\right] = \frac{1}{2}\left[\arg[S_{hh}(t - PRT)] + \arg[S_{hh}(t + PRT)]\right] \tag{3.5}$$

As pointed out in [2], using only two samples might render the procedure vulnerable to system phase noise and averaging can be considered for phase estimation.
The first approach involves the following quantities, separated by two pulse lags.

$$\widehat{\Phi}_d^{hh} = \frac{1}{2}\arg\left[\sum_{n=1}^{N-1} S_{hh}[2n-1]\cdot S_{hh}[2n+1]^*\right]$$

$$\widehat{\Phi}_d^{vv} = \frac{1}{2}\arg\left[\sum_{n=1}^{N-1} S_{vv}[2n]\cdot S_{vv}[2n+2]^*\right] \tag{3.6}$$

Here, $\widehat{\Phi}_d^{hh}$ and $\widehat{\Phi}_d^{vv}$ are the estimated Doppler phase shift at one pulse lag at horizontal and vertical polarization respectively.

With reference to Fig. 3.8, considering a scattering matrix measured by two successive pulses, the correction to obtain the instantaneous scattering matrix is performed as follows (reciprocity is invoked and amplitude correction is not performed)

$$\begin{bmatrix} S_{hh}(t+PRT) & S_{hv}(t) \\ S_{vh}(t+PRT) & S_{vv}(t) \end{bmatrix} \rightarrow \begin{bmatrix} S_{hh}(t+PRT)e^{+i\widehat{\Phi}_d^{hh}} & S_{hv}(t) \\ S_{hv}(t) & S_{vv}(t) \end{bmatrix}$$

$$\begin{bmatrix} S_{hh}(t+PRT) & S_{hv}(t) \\ S_{vh}(t+PRT) & S_{vv}(t) \end{bmatrix} \rightarrow \begin{bmatrix} S_{hh}(t+PRT) & S_{vh}(t+PRT) \\ S_{vh}(t+PRT) & S_{vv}(t)e^{-i\widehat{\Phi}_d^{vv}} \end{bmatrix} \tag{3.7}$$

We can either tune the first column to the same time instant as the second, or, alternatively, tune the second column to the same time instant as the first (3.7). Another possibility is to shift each by one half pulse lag. The latter approach might have an advantage point since, as the autocorrelation function is quadratic near the origin, decorrelation effects may be proportional to the square of the time interval.

If the two quantities appearing in (3.6) have approximately the same value, some observations can be made. The condition that satisfies this equality is that the phase centre displacement over a pulse lag must be the same at horizontal and vertical polarizations. From a physical viewpoint, this is equivalent to the condition that the target anisotropy and line-of-sight velocity be decoupled. The formulae in (3.6) involve quantities separated by two pulse lags. If the difference between $\widehat{\Phi}_d^{hh}$ and $\widehat{\Phi}_d^{vv}$ is not too large, it is preferable to use estimators relying on quantities separated by just one pulse lag. Such an estimator can be used instead of (3.6) and can be computed as follows [2, 3].

$$\widehat{\Phi}_d^{hv} = \frac{1}{2}\left[\widehat{\Psi}_2 + \widehat{\Psi}_1\right]$$

$$\widehat{\Psi}_1 = \arg\left[\sum_{n=1}^{N-1} S_{hh}[2n+1]\cdot S_{vv}[2n]^*\right]$$

$$\widehat{\Psi}_2 = \arg\left[\sum_{n=1}^{N} S_{vv}[2n] \cdot S_{hh}[2n-1]^*\right] \tag{3.8}$$

The Doppler phase shift corrections here illustrated must be implemented if the scattering matrices have to be used 'as such'. For example, when a unitary rotation is performed to transform scattering matrices to another polarization basis, or when target decomposition theorems are applied. As far as entropy is concerned, a couple of remarks might be helpful. The amplitude correction reported above slightly influences its value. However, tests performed with POLDIRAD data show that these variations hardly ever exceed 0.03-0.04 in the worst cases. Phase corrections do not alter at all its value. This fact will be explained in Chapter 4. Entropy is also insensitive to hardware phase offsets, discussed in the next paragraph. Analyses to evaluate the performance of different Doppler phase shift correction procedures are not discussed here.

B. Hardware relative phase offsets

In the case of POLDIRAD, phase offsets due to hardware configurations are considerable and must be known. One way of calibrating the scattering matrices is to select an area of light rain in the front of the observed event. Such a target is supposed to have no backscatter differential phase shift due to Mie scattering, the cross-polar signals do not fall below the noise level, and propagation effects do not affect the signatures. The two cross-polar hardware offset phases can be estimated directly at zero lag as [2]

$$\widehat{\Phi}_{xh} = \arg\left[\sum_{n=1}^{N} S_{hh}[2n-1] \cdot S_{vh}[2n-1]^*\right]$$

$$\widehat{\Phi}_{xv} = \arg\left[\sum_{n=1}^{N} S_{vv}[2n] \cdot S_{hv}[2n]^*\right] \tag{3.9}$$

For the estimation of the copolar hardware offset phase, first Doppler phase shift correction must be performed with one of the procedures illustrated in the previous paragraph. For the calibration area, it is desirable that the difference between, $\widehat{\Phi}_d^{hh}$ and $\widehat{\Phi}_d^{vv}$ be small, so that the one pulse lag estimator can be used to estimate the copolar hardware phase offset.

$$\widehat{\Psi}_{DP} = \widehat{\Phi}_d^{hv} + \widehat{\Phi}_{co}$$

$$\widehat{\Phi}_{co} = \frac{1}{2}\left[\widehat{\Psi}_2 - \widehat{\Psi}_1\right] \tag{3.10}$$

After estimating the hardware offset phases for every bin, these are averaged over the calibration area.

3.3 Weather Radar Variables

3.3.1 Fully polarimetric measurements at horizontal/vertical polarization

The measurement of a series of scattering matrices allows the evaluation of the full covariance matrix [4, 6, 7]. After averaging over a given number of samples, using the horizontal/vertical polarization basis, we obtain:

$$\langle[\mathbf{C}]\rangle = \begin{bmatrix} \langle|S_{hh}|^2\rangle & \sqrt{2}\langle S_{hh}S_{hv}^*\rangle & \langle S_{hh}S_{vv}^*\rangle \\ \sqrt{2}\langle S_{hv}S_{hh}^*\rangle & 2\langle|S_{hv}|^2\rangle & \sqrt{2}\langle S_{hv}S_{vv}^*\rangle \\ \langle S_{vv}S_{hh}^*\rangle & \sqrt{2}\langle S_{vv}S_{hv}^*\rangle & \langle|S_{vv}|^2\rangle \end{bmatrix} \tag{3.11}$$

It has 9 degrees of freedom, traditionally encapsulated in the following radar meteorological variables:

Reflectivity (Z_H), linear depolarization ratio (LDR) and differential reflectivity (Z_{DR}) for the 3 degrees of freedom on the diagonal (we express these variables in linear units, even though they are most often represented on a logarithmic scale).

Reflectivity (horizontal transmit)

$$Z_H \propto \langle|S_{hh}|^2\rangle \tag{3.12}$$

Linear Depolarization Ratio (horizontal transmit)

$$LDR_H = \frac{\langle|S_{vh}|^2\rangle}{\langle|S_{hh}|^2\rangle} \tag{3.13}$$

Differential Reflectivity

$$Z_{DR} = \frac{\langle|S_{hh}|^2\rangle}{\langle|S_{vv}|^2\rangle} \tag{3.14}$$

Redundantly, from the 3 diagonal elements, the following variables can be defined:

Reflectivity (vertical transmit)

$$Z_v \propto \langle |S_{vv}|^2 \rangle \tag{3.15}$$

Linear Depolarization Ratio (vertical transmit)

$$LDR_V = \frac{\langle |S_{hv}|^2 \rangle}{\langle |S_{vv}|^2 \rangle} \tag{3.16}$$

For the 6 off-diagonal degrees of freedom, 3 complex correlations are defined [5]:

$$|\rho_{hv}| e^{i(\Phi_{DP}+\delta_{co})}$$

$$|\rho_{xh}| e^{i(\Phi_{xh}+\delta_{xh})}$$

$$|\rho_{xv}| e^{i(\Phi_{xv}+\delta_{xv})} \tag{3.17}$$

Copolar correlation coefficient at zero lag

$$|\rho_{hv}(0)| = \frac{|\langle S_{vv} S_{hh}^* \rangle|}{\sqrt{\langle |S_{hh}|^2 \rangle \langle |S_{vv}|^2 \rangle}} \tag{3.18}$$

Cross-polar correlation coefficient at horizontal transmit

$$|\rho_{xh}(0)| = \frac{|\langle S_{hh} S_{vh}^* \rangle|}{\sqrt{\langle |S_{hh}|^2 \rangle \langle |S_{hv}|^2 \rangle}} \tag{3.19}$$

Cross-polar correlation coefficient at vertical transmit

$$|\rho_{xv}(0)| = \frac{|\langle S_{vv} S_{hv}^* \rangle|}{\sqrt{\langle |S_{vv}|^2 \rangle \langle |S_{hv}|^2 \rangle}} \tag{3.20}$$

Copolar propagation phase and copolar backscatter phase

$$\frac{\langle S_{vv}S_{hh}^{*}\rangle}{\sqrt{\langle|S_{hh}|^{2}\rangle\langle|S_{vv}|^{2}\rangle}} = |\rho_{hv}(0)|e^{i(\Phi_{DP}+\delta_{co})} \tag{3.21}$$

Separation of the propagation phase from the backscatter phase is in general difficult. The backscatter phases (copolar, h-cross-polar, v-cross-polar) are potentially attractive polarimetric parameters with

$$\delta_{co} \neq \delta_{xh} \neq \delta_{xv} \tag{3.22}$$

In rain, if Rayleigh scattering is dominant (the probing wavelength is significantly larger than the illuminated spheroids) then the 3 backscatter phases (copolar, h-cross-polar and v-cross-polar) are small and can be assumed to be close to 0.

$$\delta_{co} \sim \delta_{xh} \sim \delta_{xv} \sim 0 \tag{3.23}$$

Further, the following relationship holds for the copolar and cross-polar propagation phases.

$$\frac{1}{2}\Phi_{DP} = \Phi_{xh} = \Phi_{xv} \tag{3.24}$$

Ultimately, from the copolar propagation phase,

$$\Phi_{DP} = \varphi_{hh} - \varphi_{vv} = \arg\langle S_{vv}S_{hh}^{*}\rangle \tag{3.25}$$

the specific differential phase (K_{DP}) is evaluated:

$$K_{DP} = \frac{1}{2}\cdot\frac{\Phi_{DP}(r_2) - \Phi_{DP}(r_1)}{r_2 - r_1} \tag{3.26}$$

For the purpose of quantitative rain rate estimation, Z_H, Z_{DR} and K_{DP} are generally used. For the purpose of hydrometeor classification, besides Z_H, Z_{DR} and K_{DP}, LDR_H and $|\rho_{hv}|$ are also used.

3.3.2 LDR mode

If horizontal polarization is transmitted and the horizontal and vertical channels are coherently received, the wave covariance matrix of the backscattered wave is measured. This matrix constitutes the upper left 2×2 minor of the covariance matrix at horizontal/vertical basis.

$$\mathbf{J}_H = \begin{bmatrix} \langle |S_{hh}|^2 \rangle & \langle S_{hh} S_{vh}^* \rangle \\ \langle S_{vh} S_{hh}^* \rangle & \langle |S_{vh}|^2 \rangle \end{bmatrix} \rightarrow \begin{cases} Z_H \\ LDR_H, |\rho_{xh}|, p_H \\ (\Phi_{xh} + \delta_{xh}) \end{cases} \tag{3.27}$$

From this matrix with 4 degrees of freedom, only 2 variables (reflectivity at horizontal send Z_H and the linear depolarization ratio LDR) are evaluated for operational purposes. For conceptual clarity, we anticipate an important theoretical result, valid for any wave covariance matrix $\mathbf{J}_H$ (that is, valid for any type of illuminated target):

$$(1 - p_H^2) = \frac{4 \cdot LDR_H}{[1 + LDR_H]^2} \cdot (1 - |\rho_{xh}|^2) \tag{3.28}$$

This result tells us that the degree of polarization at horizontal transmit is a function of the cross-polar correlation coefficient and the linear depolarization ratio, and is independent from the h-cross-polar phase $(\Phi_{xh} + \delta_{xh})$.

If vertical polarization is transmitted and the horizontal and vertical channels are coherently received, the following matrix (equivalent to the lower right 2×2 minor of the covariance matrix) is measured:

$$\mathbf{J}_V = \begin{bmatrix} \langle |S_{vv}|^2 \rangle & \langle S_{vv} S_{hv}^* \rangle \\ \langle S_{hv} S_{vv}^* \rangle & \langle |S_{hv}|^2 \rangle \end{bmatrix} \rightarrow \begin{cases} Z_V \\ LDR_V, |\rho_{xv}|, p_V \\ (\Phi_{xv} + \delta_{xv}) \end{cases} \tag{3.29}$$

$$(1 - p_V^2) = \frac{4 \cdot LDR_V}{[1 + LDR_V]^2} \cdot (1 - |\rho_{xv}|^2) \tag{3.30}$$

Again, the degree of polarization at vertical transmit (p_V) is a function of the cross-polar correlation coefficient ($|\rho_{xv}|$) and the linear depolarization ratio (LDR_V), and is independent from the v-cross-polar phase $(\Phi_{xv} + \delta_{xv})$.

For both horizontal and vertical transmission, the linear depolarization ratio, the cross-polar correlation coefficient and the degree of polarization are difficult to measure in rain, due to the 20 dB difference in power between the co and cross polar channels. However,

light rain, drizzle or light drizzle offer an exceptional opportunity for radar calibration control, offering insights in system noise level and antenna cross-polarization isolation.

In general, transmission of vertical polarization is implemented by military radars whose purpose is to detect man-made targets like missiles or aircrafts. Since rain has a larger cross section at horizontal polarization rather than at vertical, transmission of horizontal polarization is generally implemented in weather radars. An exception to the use of horizontal polarization in radar meteorology was sometimes motivated by the need to attenuate reflections from ground clutter. In this case vertical polarization has the capability to better eliminate reflections from the ground and enhance the return from hydrometeors. LDR mode at horizontal transmit is the secondary operating mode of operational weather radars.

3.3.3 Z_{DR} mode

Hybrid mode (also known as Z_{DR} mode) consists in transmitting a polarization state ($\underline{\boldsymbol{\chi}}$), lying on the circular/slant circle of the Poincare sphere (3.31). Note that the phase difference θ_1 between the signals injected in the H and V ports is constant from pulse to pulse and is determined by the radar architecture. This phase difference ultimately establishes the actual radiated polarization state.

$$\underline{\boldsymbol{\chi}} = \frac{1}{\sqrt{2}}\begin{bmatrix} 1 \\ e^{i\theta_1} \end{bmatrix} \tag{3.31}$$

On reception, the signal is simultaneously received in the horizontal and vertical polarization channels to measure the wave covariance matrix $\mathbf{J}_\chi$

$$\mathbf{J}_\chi = \begin{bmatrix} \langle |S_{h\chi}|^2 \rangle & \langle S_{h\chi} S_{v\chi}^* \rangle \\ \langle S_{v\chi} S_{h\chi}^* \rangle & \langle |S_{v\chi}|^2 \rangle \end{bmatrix} \quad \rightarrow \quad \begin{cases} Z_H^{hy} \\ Z_{DR}^{hy}, \left|\rho_{hv}^{hy}\right|, p_\chi \\ \left(\Phi_{hv}^{hy} + \delta_{hv}^{hy}\right) \end{cases} \tag{3.32}$$

where

$$Z_H^{hy} \propto \langle |S_{h\chi}|^2 \rangle \tag{3.33}$$

$$Z_{DR}^{hy} = \frac{\langle |S_{h\chi}|^2 \rangle}{\langle |S_{v\chi}|^2 \rangle} \tag{3.34}$$

$$\left|\rho_{hv}^{hy}\right| = \frac{\left|\langle S_{h\chi} S_{v\chi}^{*}\rangle\right|}{\sqrt{\langle\left|S_{h\chi}\right|^{2}\rangle\,\langle\left|S_{v\chi}\right|^{2}\rangle}} \tag{3.35}$$

$$\left(\Phi_{hv}^{hy} + \delta_{hv}^{hy}\right) = \arg\langle S_{h\chi} S_{v\chi}^{*}\rangle \tag{3.36}$$

The term hybrid refers to the fact that, in this case, the receive polarization channels are not copolar and cross-polar to the transmit polarization.
The hybrid mode (Z_{DR} mode) is the primary operational mode implemented in today's dual-polarization weather radars. This choice was driven by the experimental evidence that, most often, weather targets show low cross-talk upon backscattering as well as mirror reflection symmetry with respect to the vertical axis. Whenever one of these two conditions is not met (canted raindrops, cross-talk upon backscattering due to depolarizing hydrometeors) the measured variables will be biased.
Ultimately, we apply the definition of degree of polarization to the matrix $\mathbf{J}_{\chi}$ to obtain an important theoretical relationship, valid in general.

$$\left(1 - p_{\chi}^{2}\right) = \frac{4 \cdot Z_{DR}^{hy}}{\left[1 + Z_{DR}^{hy}\right]^{2}}\left(1 - \left|\rho_{hv}^{hy}\right|^{2}\right) \tag{3.37}$$

So, when intrinsic scattering from a radar target is considered, the degree of polarization p_{χ} is redundant with respect to differential reflectivity at hybrid Z_{DR}^{hy} and the copolar correlation coefficient at hybrid $\left|\rho_{hv}^{hy}\right|$.

3.3.4 Weather radar variables at circular polarization basis

Weather radars might also operate at circular polarization, namely transmitting alternately right hand circular and left hand circular polarization, and simultaneously receiving these two polarizations (fully polarimetric mode). Also, one single polarization may be transmitted (either right-hand or left-hand circular) and reception may simultaneously occur in the copolar and cross-polar polarimetric channels (dual-polarimetric mode). In this latter mode, considerable research was led in the seventies, and several variables at circular polarization were defined [8, 9].

Considering a target feature vector at circular polarization,

$$\underline{\mathbf{k}}_c = \begin{bmatrix} S_{rr} \\ \sqrt{2}S_{rl} \\ S_{ll} \end{bmatrix} \tag{3.38}$$

the covariance matrix at circular polarization can be obtained with the same procedure as for linear polarization

$$\langle[\mathbf{C}]\rangle_c = \begin{bmatrix} \langle|S_{rr}|^2\rangle & \sqrt{2}\langle S_{rr}S_{rl}^*\rangle & \langle S_{rr}S_{ll}^*\rangle \\ \sqrt{2}\langle S_{rl}S_{rr}^*\rangle & 2\langle|S_{rl}|^2\rangle & \sqrt{2}\langle S_{rl}S_{ll}^*\rangle \\ \langle S_{ll}S_{rr}^*\rangle & \sqrt{2}\langle S_{ll}S_{rl}^*\rangle & \langle|S_{ll}|^2\rangle \end{bmatrix} \tag{3.39}$$

Radar meteorological variables at circular polarization are

Circular Depolarization Ratio

$$\mathrm{CDR} = \frac{\langle|S_{rr}|^2\rangle}{\langle|S_{rl}|^2\rangle} \tag{3.40}$$

Orientation Parameter (cross-polar correlation coefficient at circular polarization)

$$\mathrm{ORTT} = \frac{|\langle S_{rr}S_{rl}^*\rangle|}{\sqrt{\langle|S_{rr}|^2\rangle\langle|S_{rl}|^2\rangle}} \tag{3.41}$$

Also, if the radar system is polarization agile, the alignment direction of the target (ALD) can be evaluated

$$\mathrm{ALD} = \frac{1}{4}[\arg\langle S_{ll}S_{rl}^*\rangle - \arg\langle S_{rr}S_{rl}^*\rangle] \tag{3.42}$$

If only one polarization state is used on transmit, we obtain the wave covariance matrix at circular polarization (we assume right hand polarization transmit, the same holds for left polarization transmit)

$$\mathbf{J}_R = \begin{bmatrix} \langle|S_{rr}|^2\rangle & \langle S_{rr}S_{lr}^*\rangle \\ \langle S_{lr}S_{rr}^*\rangle & \langle|S_{lr}|^2\rangle \end{bmatrix} \quad \rightarrow \quad \mathrm{CDR}, \mathrm{ORTT}, p_C \tag{3.43}$$

The circular depolarization ratio (CDR) is a measure of the target departure from spherical shape, the orientation parameter (ORTT) is a measure of the anisotropy of the

target (indicates the presence of rain, independently from its canting angle). Also, the degree of polarization at circular transmit (p_C) can be evaluated. Applying the definition of degree of polarization to the matrix $\mathbf{J}_R$ we obtain the theoretical relation in (3.44)

$$(1 - p_C^2) = \frac{4 \cdot CDR}{[1 + CDR]^2}(1 - ORTT^2) \tag{3.44}$$

The experimental data used in this work are collected at horizontal/vertical basis. However, since the data are fully polarimetric, the application of unitary transformations to the measured matrices allows the retrieval of scattering matrices in any desired polarization basis. For this reason, knowledge of variables at circular polarization is important. In Chapter 5 for example, ORTT will be used together with Z_{DR} for a preliminary discrimination between rain and non-rain sections of a convective event.
A thorough analysis of the problem of polarization basis transformations on propagation affected scattering matrices goes beyond the scope of the present doctoral thesis. In the following, when unitary transformations are effected on scattering matrices, it will always be assumed that the effects of propagation, even though potentially present, are not so relevant to jeopardize the subsequent scientific results.

3.4 Weather radar variables: phenomenology

The use of polarimetric variables [6, 7] is motivated by the fact that hydrometeors show different shapes in the polarization plane. Raindrops, as they fall, flatten, thus assuming an oblate shape. As a consequence, Z_H is expected to be larger in rain than Z_V, and differential reflectivity assumes positive values in rain.
Non-convective precipitation systems generally show a stratified structure, with rain in the lower kilometers and snow in the upper sections. The layer separating rain from snow is known in radar meteorology as 'melting band', and is clearly detectable by radars since Z_H and Z_{DR} assume larger values, due to water coating of horizontally oriented snowflakes and differential fall speed. Also, the melting band depolarizes the signal relevantly, and accordingly LDR takes on larger values.
Dry snowflakes (aggregates of ice crystals) typically show slightly positive Z_{DR} values, but depolarize the backscattered signal very little, because of their low dielectric constant. Ice crystals, found in the uppermost sections of precipitation systems, present a broad variability of shapes, ranging from plate-like to columnar, depending on the temperature and humidity of the regions in the atmosphere where they form. Ice crystals are generally horizontally oriented, and Z_{DR} can be up to 4 dB. However, in presence of an external electric field, their orientation might depart from the horizontal, and can well be vertical or slant [5, 6].

When precipitation is not stratiform, but rather characterized by intense convection and rapid mixing of air masses, different kinds of hydrometeors may form. These types of hydrometeors are classified with respect to their size, and range from graupel to small hail and hail. Graupel often has a conical shape, hailstones have irregular shapes, sometimes with protuberances. Since frozen hydrometeors tumble as they fall, Z_{DR} is close to zero whereas LDR_H tends to be relevantly larger than in rain. Water-coated hailstones might have unusually high Z_H and LDR_H values. Ultimately, raindrops associated with convective precipitation may have different size distributions than in the stratiform case, and rain dominated by large drops can be identified by larger Z_{DR} values. Winter storms might also generate sleet and freezing rain. Sleet is made of balls of ice, namely frozen raindrops, freezing rain is made of super-cooled raindrops. The latter might also be present in upper sections of the atmosphere, provided convection is strong enough to lift raindrops above the melting band.
Also, weather radars have the capability to detect non-weather targets like insects, birds, volcanic ashes, wildfire smoke, chaff, refractive index variations and other aerosols that might be advected by the wind. Insects, for example, have elongated bodies and can show up with Z_{DR} values up to 6 dB. If swarms of insects move upwards or downwards, differential reflectivity might also become negative, depending on the direction of motion with respect to the radar line-of-sight.
Besides the preliminary discrimination of different classes of scatterers, highly needed in order to know which model has to be used for the inversion and the subsequent extraction of bio-geophysical parameters of interest, polarimetric measurements make available a larger number of variables and more accurate models can be used. For hydrological purposes, quantitative precipitation estimation is of interest, and, in particular, polarimetry can significantly reduce the uncertainty in rain-rate estimates.

Polarimetric signal processing is aimed at the extraction of meaningful variables from the radar measurements. There are several criteria to follow for the evaluation of the performance of a radar variable. Firstly, it should have the capability to highlight some physical property of the target and, possibly, the physical properties of the target should be decoupled as much as possible onto different variables. Also, the illuminated target variability should map onto a large dynamic range of the variable. This renders inversion, if possible, more accurate. Since radar product end-users are interested in the intrinsic properties of the target, a task of the weather radar engineer is to provide approaches to keep control of effects that might degrade the quality of radar variables. These effects can be propagation effects as well as radar system engineering deficiencies like antenna cross-channel coupling.
As far as propagation is concerned, different phenomena can affect polarimetric variables:

1) Attenuation of the horizontal component
2) Attenuation of the vertical component
3) Depolarization
4) Differential phase shift Φ_{DP}

If the attenuation of the vertical component is equal to the attenuation of the horizontal component, the phenomenon is generally referred to as absolute attenuation, if these two components differ, the term differential attenuation is used. Also, depolarization upon

forward scattering can occur. Propagation effects due to different electrical lengths at vertical and horizontal polarizations inducing phase differences between the horizontal and vertical polarimetric channels are referred to as differential propagation phase, and occur because of the presence of oblate or prolate hydrometeors. Even though not relevant for radar meteorology, it is interesting to recall that differential propagation phase effects also occur in the ionosphere, where the right hand circular and the left hand circular components of a polarized electromagnetic wave undergo different phase shifts. This effect is known as Faraday rotation and concerns propagation at somehow longer wavelengths (L-band, P-band).

Different variables might or not be affected by different propagation effects. Differential reflectivity, for example, is affected by differential attenuation but not by absolute attenuation or differential phase shift. The specific differential phase (the range derivative of the differential propagation phase) and the copolar correlation coefficient are not affected by absolute attenuation or differential phase shift (indeed, the effect due to propagation is captured by K_{DP} itself). In table 3.2, some properties of standard radar meteorological variables are listed. For example, only reflectivity is dependent on absolute radar calibration, namely, every term in the radar equation needs to be accurately known in order to relate the retrieved voltages to the radar cross section of the target. For this reason, the evaluation of reflectivity, probably the most important radar meteorological variable, is more delicate than all other variables that do not require absolute radar calibration or absolute attenuation correction.

Ideally, the weather radar community should aim at the acquisition of fully polarimetric datasets. For example, the detection of canted scatterers (insects, raindrops, ice crystals) is possible with fully polarimetric systems. The retrieval of the full scattering matrix has a cost in term of scan time, an important requirement for operational needs. However, the advent of phased-array systems in radar meteorology will dramatically lower the acquisition times. Passive phased arrays are already being used, and, in perspective, the use of active digital beamforming phased arrays will be envisioned. Such systems provide impressively short scan times and, ultimately, the implementation of fast, fully polarimetric acquisitions will be possible. Research in weather radar polarimetry should then be addressed at the exploitation of fully polarimetric techniques as well as at the full exploitation of the potential of today's dual-polarization systems, in every operating mode

	Independent of absolute radar calibration	**Immune to absolute attenuation**	**Immune to differential propagation phase**	**Immune to differential attenuation**	**Used for quantitative estimation**
Z_H	No	No	Yes	Yes	Yes
Z_{DR}	Yes	Yes	Yes	No	Yes
K_{DP}	Yes	Yes	Yes	Yes	Yes
ρ_{hv}	Yes	Yes	Yes	Yes	No
δ_{co}	Yes	Yes	No	Yes	No
LDR	Yes	Yes	Yes	No	No

Table 3.2 Properties of standard weather radar variables

3.4.1 Copolar correlation coefficient

The copolar correlation coefficient and the backscatter differential phase (as well as entropy and the degree of polarization at circular/slant transmit) are crucially affected by probing wavelength. Namely, for spheroids with small sizes compared to the radar wavelength, the Rayleigh approximation applies. This implies that gradual changes in size, axis ratio and dielectric constant produce gradual changes in the polarimetric variables. However, when Mie scattering sets in (namely as the difference between probing wavelength and hydrometeor physical dimension gets small enough) gradual changes in the hydrometeor properties create non-monotonic variations in the polarimetric variables. The backscatter differential phase is the most prominent radar variable indicating that scattering is occurring in the Mie regime: as the hydrometeor size gets larger than about a tenth of the wavelength it undergoes an abrupt increase. At smaller sizes, the backscatter differential phase decreases to zero. The transition is at 10, 5.5, and 3.5 mm for the wavelengths of 10 (S-band), 5 (C-band), and 3 (X-band) cm, respectively.

The backscatter differential phase at S-band (10 cm wavelength) is insensitive to changes in raindrops' sizes (because drops are always smaller than 10 mm) whereas C and X band could be adversely affected by the drops in the range from 3 to 6 mm. Also, mixed phase is often composed of wet aggregates 5-10 mm in size, and, for these hydrometeor types, Mie scattering could occur for all wavelengths traditionally used in ground-based radar meteorology (S, C and X bands). At S band, rain is non resonant whereas mixed-phase or frozen hydrometeors might be resonant. At C and X band both rain and mixed-phase or frozen hydrometeors can be resonant, although to a different degree. As outlined before, S band is less sensitive to resonance than C or X band. However, (and contrary to what might be thought) X band is less sensitive than C band. This fact is due to the nonlinearity that characterizes Mie scattering phenomena.

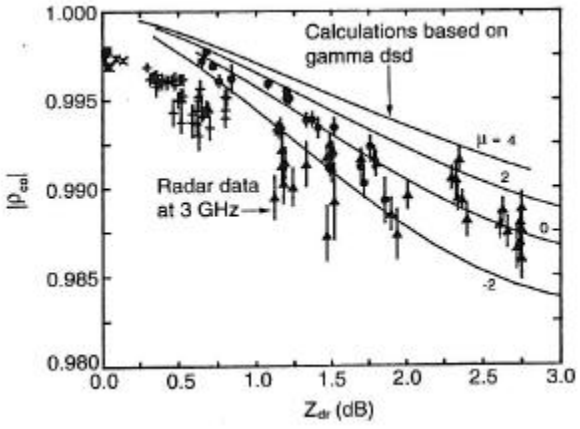

Figure 3.9 Magnitude of the copolar correlation coefficient $|\rho_{hv}(0)|$ versus Z_{DR} in rain using data from the S-band Chilbolton radar, UK. Both mean and standard error are shown. From [6].

With this premise in mind, we now proceed to a review of the properties of the copolar correlation coefficient to see how it is simultaneously affected by raindrop axis-ratio dispersion (equilibrium shape + axisymmetric oscillations), dispersion of backscatter differential phases within the resolution volume as well as hydrometeor shape irregularities and a 0-mean distribution of canting angles. Incidentally, we anticipate also that the degree of polarization at horizontal or vertical send is sensitive only to the latter two phenomena and consequently carries complementary valuable information with respect to entropy, the copolar correlation coefficient or the degree of polarization at circular/slant send. When rain is illuminated, the value of the copolar correlation coefficient mainly depends on the probing wavelength. If S band is used, Rayleigh scattering conditions are generally met and its value is mainly driven by the axis ratio variability of the drop population. The larger the variation in drop eccentricities, the smaller will be the value of the copolar correlation coefficient.

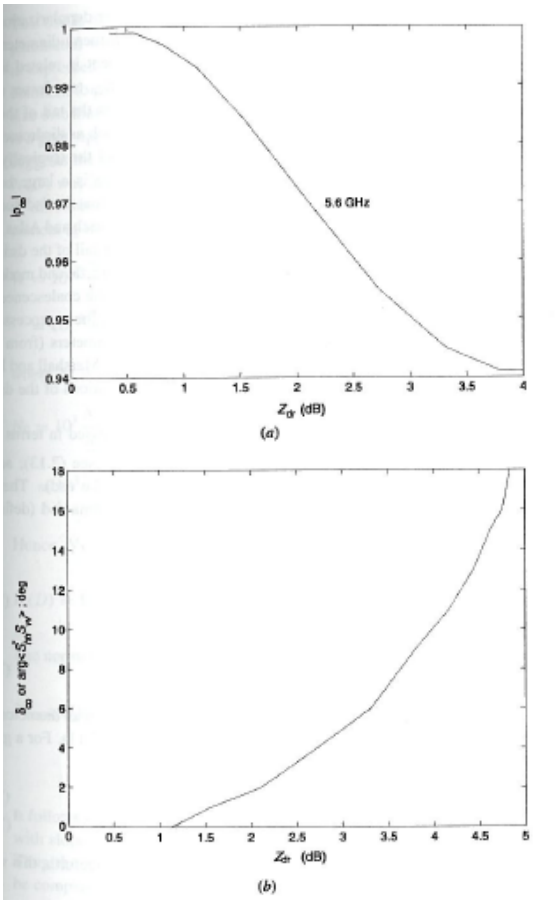

Figure 3.10 Calculations at 5.6 GHz using exponential drop size distributions and the T-matrix method. Beard-Chuang equilibrium shapes are used with Gaussian canting angle distribution with the mean of 0° and standard deviation of 7°. Copolar correlation coefficient (left) and backscatter differential phase (right). From [6].

These axis ratio variations, however, are small in rain and theoretical analysis [10] indicates values larger than 0.99. A simulation for values of the copolar correlation coefficient was carried out in this work and the results are reported in Chapter 4.
S-band measurements (Fig. 3.9) reveal values of 0.98, close to, but less than the theoretical value because canting angle variations, noise, as well as axisymmetric drop oscillations, not accounted for in the theory, act to further decrease the correlation.
When C band is used, differential phase shift upon scattering from raindrops cannot be neglected and causes the composite horizontally and vertically oriented polarized signal to fluctuate differently (the ensemble average in the numerator of 3.17 is less coherent).
The effect of Mie scattering is, in this case, far from negligible. Similar reduction in correlation occurs if canting angles have a probability distribution of finite width [11].
This dependence on canting angles may offer possibilities to discriminate (with a vertically pointed beam) between liquid drops and ice needles if the latter are randomly oriented in the horizontal plane. Irregular shape of hydrometeors is another factor that reduces the correlation. Ultimately, in a mixture of precipitation types the reduction of the correlation coefficient is due to the broader spread in the composite distribution of eccentricities and sizes compared to a distribution of a single precipitation type.

3.4.2 Linear Depolarization Ratio

Before a review of the scattering behavior of the linear depolarization ratio, we anticipate here one of the results of the present doctoral thesis, namely that, at C band, the degree of polarization at horizontal send is not affected by the dispersion in backscatter differential phase induced by the raindrop size distribution. Since raindrop axis-ratio variability does not affect its value either, we can conclude that only irregular hydrometeor shapes, a distribution of raindrop canting angles around a 0-mean, and canted raindrops can indeed increase its value from 0, the value expected for non-canted rain (whatever the rain-rate). These properties are such that the degree of polarization at horizontal send has better discriminating capabilities between rain and non-rain targets with respect to the copolar correlation coefficient, entropy, or the degree of polarization at circular/slant send. The standard radar meteorological variable with the same properties as the degree of polarization at horizontal send (in terms of backscattering from rain), is the linear depolarization ratio. In Chapter 5, the degree of polarization at horizontal send (p_H) will be experimentally compared with the linear depolarization ratio (LDR). The important difference between these two variables is that the linear depolarization ratio is extremely sensitive to antenna cross-channel coupling, whereas the degree of polarization at horizontal send is not.
If isotropic weather targets are considered, LDR values rise as the particles become more oblate or their refractive index increases. Even if snowflakes tumble, they have such a low refractive index that their LDR is about -32 dB. Oblate dry hail or graupel could have values up to -20 dB if the axes ratios were as high as 2.5 or 6. Larger depolarization is expected only for wet, tumbling ice particles. Depolarization by rain is very small, in the range of -30 dB. In the melting band, where ice particles start to melt and become coated with water, LDR_V can reach -16 dB.

References Chapter 3

[1] A. Schroth, M. Chandra and P. F. Meischner, "A C-band coherent polarimetric radar for propagation and cloud physics research," Journal of Oceanic and Atmospheric Technology, Vol. 5, pp. 803-822, December 1988.

[2] V. Chandrasekar, J. Hubbert, V. N. Bringi and P. F. Meischner, "Interpolation procedures to construct complete polarimetric signatures of distributed targets," Proc. SPIE, 1748, pp. 200-212, 1992.

[3] E. A. Mueller, "Calculation procedure for differential propagation phase shift," Preprints, 22nd Conf. on Radar Meteorology, Zuerich, Switzerland, Amer. Meteor. Soc., pp. 397-399, 1984.

[4] J. D. A. G. Kingsbury and Y. M. M. Antar, "Radar partially-polarized backscatter description algorithms and applications," IGARSS'92 Proc., Houston TX, pp. 74-76, 1992.

[5] A. Ryzhkov, D. S. Zrnic, J.C. Hubbert, Bringi V. N., Vivekanandan J., Brandes Edward A., "Polarimetric radar observations and interpretation of co-cross-polar correlation coefficients", Journal of Atmospheric and Oceanic Technology, vol. 19 n.3 pp.340-354, 2002.

[6] V. N. Bringi and V. Chandrasekhar, Polarimetric Doppler Weather Radar. principles and applications, Cambridge University Press, 2001.

[7] R. J. Doviak and D. S. Zrnic, Doppler Radar and Weather Observations, 2nd ed. San Diego, CA: Academic Press, 1993.

[8] A. Hendry, G. C. McCormick and B. L. Barge, "The degree of common orientation of hydrometeors observed by polarization diversity radars," J. Appl. Meteor., 15: pp. 633-640, 1976.

[9] A. Hendry, G. C. McCormick and B. L. Barge, "Ku-Band and S-Band Observations of the Differential Propagation Constant in Snow," IEEE Transactions Antennas and Propagation, AP-24, pp. 521-525, 1976

[10] Sachidananda, M. and Zrnic, D. S. (1985) "Z_{DR} measurement considerations for a fast scan capability radar" Radio Science 20, 907-922.

[11] Balakrishnan, N., and Zrnic, D. S. (1990) "Use of polarization to characterize precipitation and discriminate large hail" J. Atmos. Sci. 47, 565-583.

4. Theoretical Results

4.1 Overview

The present chapter exposes the theoretical results of this doctoral thesis. These results will be substantiated by data presented in Chapter 5.
Throughout the chapter we will introduce the backscattering and propagation properties of the investigated variables, and will compare them with more standard variables that might carry a similar meaning: the copolar correlation coefficient and the linear depolarization ratio. The variables investigated are entropy (H), the degree of polarization at circular transmit (p_C), the degree of polarization at slant transmit (p_{45}) the degree of polarization at horizontal transmit (p_H), the degree of polarization at vertical transmit (p_V).

We itemize the main results of the work:

1. When weather targets are illuminated (with the exception of canted anisotropic hydrometeors), antipodal transmit states on the Poincare sphere yield degrees of polarization with identical properties, namely
    a. The degree of polarization at horizontal send (p_H) behaves like the degree of polarization at vertical send (p_V). In the following we will refer to p_H since horizontal polarization is generally used with weather radars, but every statement on the degree of polarization at horizontal send equally applies to the degree of polarization at vertical send. Exceptions might arise in presence of clutter contaminated cells, because of the different sensitivity of horizontal and vertical polarizations to the presence of clutter. Such differences were not investigated.
    b. The degree of polarization at right hand circular transmit (p_{RHC}) behaves like the degree of polarization at left hand circular transmit (p_{LHC}). In the following we will generally refer to the degree of polarization at circular transmit (p_C), with no further specification.
    c. The degree of polarization at +45° slant polarization transmit (p_{+45}) behaves like the degree of polarization at -45° slant polarization transmit (p_{-45}). In the following we will generally refer to the degree of polarization at slant transmit (p_{45}), with no further specification.

2. When rain is illuminated, the degree of polarization at circular transmit (p_C), the degree of polarization at slant transmit (p_{45}) and the copolar correlation coefficient ($|\rho_{hv}(0)|$) assume very similar numerical values. Also, entropy (H) is sensitive to the same backscattering physics as the above mentioned variables. If rain is illuminated, none of these variables is affected by differential phase shift.

When isotropic weather targets with more relevant depolarizing properties are illuminated (graupel, small hail), the degree of polarization at circular transmit (p_C), the degree of polarization at slant transmit (p_{45}) and the copolar correlation coefficient ($|\rho_{hv}(0)|$) can differ. In this case however, if differential propagation phase affects the electromagnetic pulse before hitting the isotropic weather target (and this might well happen since frozen hydrometeors can be surrounded by volumes of rain), the degree of polarization at circular transmit (p_C) and the degree of polarization at slant transmit (p_{45}) will be affected.

3. From a general theoretical viewpoint, the sensitivity of entropy to the target backscattering physics can be regarded as similar to the minimal degree of polarization (p_{MIN}), defined in the present chapter. It should be remembered that the minima of the depolarization response are obviously target-dependent, and as a consequence it is not in general possible to claim that the entropy behaves like the degree of polarization corresponding to a given transmit state. However, for the two classes of scatterers of interest in radar meteorology (anisotropic and isotropic weather targets) the degree of polarization at circular transmit (p_C) is always minimal. So, if we restrict our observations to weather targets, it is possible to claim that, upon backscattering, entropy approximately behaves like degree of polarization at circular transmit (p_C). The latter is however affected by differential propagation phase, whereas entropy is not. Indeed, entropy is not affected by absolute attenuation either, and is only affected by differential attenuation. Entropy (H) and the degree of polarization at circular transmit (p_C) are the only variables to be strictly canting independent (independent from the mean canting angle of the illuminated anisotropic scatterers).

4. When rain is illuminated, the degree of polarization at horizontal or vertical transmit has completely different properties with respect to the degree of polarization at circular transmit (p_C), the degree of polarization at slant transmit (p_{45}), the copolar correlation coefficient ($|\rho_{hv}(0)|$) and entropy (H). Indeed, the degree of polarization at horizontal (vertical) transmit is always maximal for both isotropic and anisotropic weather targets. In the case of rain (anisotropic target), the backscattering physics of the degree of polarization at horizontal (vertical) transmit is analog to the linear depolarization ratio, and this is the variable the degree of polarization at horizontal send will be compared with. Ultimately, the degree of polarization at horizontal (vertical) send is not affected by any propagation effect.

5. When non-canted rain is illuminated, we have therefore two families of variables sensitive to two different sets of geophysical parameters:

   LDR, p_H, p_V

   $|\rho_{hv}(0)|$, p_C, $p_{45,}$ H

The latter set is affected by 3 factors: finite width of 0-mean canting angle distribution, backscatter differential phase dispersion within the resolution volume, axis-ratio dispersion (due to raindrops equilibrium shape plus axisymmetric drop oscillations). The degree of polarization at horizontal or vertical send and the linear depolarization ratio are affected only by a finite width of a 0-mean canting angle distribution, but not by backscatter differential phase dispersion or raindrop axis-ratio dispersion. These features render the degree of polarization at horizontal or vertical send and the linear depolarization ratio extremely effective for the discrimination between rain and non-rain target classes, since the polarimetric contrast is enhanced.

An important result is that, contrary to the linear depolarization ratio, the degree of polarization at horizontal (vertical) transmit is very robust against cross-channel coupling. This fact is suggested by the theoretical relationship presented in (3.28) and reported in (4.1): since cross-channel coupling causes a simultaneous increase in linear depolarization ratio and cross-polar correlation coefficient, the degree of polarization tends to keep its value unaltered.

$$(1 - \mathrm{p_H^2}) = \frac{4 \cdot \mathrm{LDR_H}}{[1 + \mathrm{LDR_H}]^2} \cdot (1 - |\rho_{\mathrm{xh}}|^2) \tag{4.1}$$

Similarly to (3.29), (3.30) and (3.37), the above relationship is directly obtained by the formula for the degree of polarization.

6. A new polarimetric variable, indicated with CP and named "Canting Parameter", is defined. This new variable can only be evaluated with a fully polarimetric system and is representative of the canting angle of distributed targets. Indeed, besides the definition, no further research is undertaken. Fully polarimetric weather radars can detect canted hydrometeors (electrified raindrops, electrified ice crystals) and can estimate their alignment direction. The canting parameter defined in this thesis (CP) is just one of the variables related to the canting angle of a target. Another example appeared in the literature is ALD, the alignment direction

$$\mathrm{ALD} = \frac{1}{4}[\arg\langle S_{\mathrm{ll}} S_{\mathrm{rl}}^{*}\rangle - \arg\langle S_{\mathrm{rr}} S_{\mathrm{rl}}^{*}\rangle] \tag{4.2}$$

Other variables have appeared in the SAR literature for both coherent and incoherent targets. Further research should be addressed at identifying the optimal indicator of canting effects, since such variables might further help in a more exact classification of targets.

Hydrometeor classifiers have been developed to a mature state and have now entered the commercial market. It is important to keep improving these products by trying to exploit the information contained in the least investigated elements of the covariance matrix or in

variables derived with more complex signal processing. The investigation of the most exotic elements of the covariance matrix has been, not without reason, previously tackled by a number of researchers [11] and it is motivated by the need to improve classification algorithms. For example, target classes should increase in number in order to encompass not only hydrometeors (light rain, moderate rain, heavy rain, large drops rain, graupel/small hail, hail, wet snow, dry snow, horizontally oriented ice crystals, vertically oriented ice crystals) but also non weather targets that might well appear in the signatures of operational weather radars (insects, birds, chaff, volcanic ashes, clutter, other advected aerosols, refractive index discontinuities and many others).
To appreciate the potential operational applications, it is important to note that, even though the present work used fully polarimetric datasets, the degree of polarization can be evaluated also by dual-polarization radars. Namely, the degree of polarization at horizontal send can be evaluated by transmitting horizontal polarization and receiving on the horizontal and vertical channels; the degree of polarization at circular (slant) send can be evaluated by transmitting circular (slant) and receiving on the horizontal and vertical channels. These two pulsing schemes are available to operational weather radars manufactured by major companies like
SELEX-GEMATRONIK http://www.gematronik.com/index2.html,
VAISALA http://www.vaisala.com/weather/products/weatherradar or
EEC http://www.eecradar.com/index.html

4.2 The Depolarization Response: Theory.

Measurements done with a dual polarization coherent receiver can be considered as samples of a random Jones vector of the form [1, 6].

$$\underline{\mathbf{E}}(t) = \begin{bmatrix} E_1(t) \\ E_2(t) \end{bmatrix} = \begin{bmatrix} |E_1(t)|e^{i\varphi_1(t)} \\ |E_2(t)|e^{i\varphi_2(t)} \end{bmatrix} \tag{4.3}$$

The covariance of a random Jones vector (wave covariance matrix **J**) and the degree of polarization p read:

$$\mathbf{J} = \begin{bmatrix} J_{11} & J_{12} \\ J_{21} & J_{22} \end{bmatrix} = \langle \underline{\mathbf{E}} \otimes \underline{\mathbf{E}}^{+} \rangle = \begin{bmatrix} \langle |E_1|^2 \rangle & \langle E_1 E_2^* \rangle \\ \langle E_2 E_1^* \rangle & \langle |E_2|^2 \rangle \end{bmatrix} \tag{4.4}$$

$$p = \sqrt{1 - \frac{4\det\mathbf{J}}{(\mathrm{trace}\mathbf{J})^2}} = \frac{\lambda_1 - \lambda_2}{\lambda_1 + \lambda_2} \tag{4.5}$$

The symbol $\otimes$ indicates external product. As λ_1 and λ_2 are wave covariance matrix eigenvalues, the degree of polarization p is a basis invariant quantity and as such does not

depend on the orthogonal pair of polarimetric channels chosen to sample the backscattered wave. This fact is implicit in the unitary transformation **U** corresponding to a polarization basis transformation for wave covariance matrix.

$$\mathbf{J}' = \mathbf{U}\mathbf{J}\mathbf{U}^{-1} \tag{4.6}$$

For a coherent target, the backscattered wave is totally polarized, regardless of the transmit polarization state. For an incoherent target, the degree of polarization of the backscattered wave does in general depend on the polarization state of the transmitted wave. Such a function, that may be named **depolarization response**, can be plotted either on the Poincaré sphere or with the help of surface plots, and can be indicated with $p(\chi,\psi)$, where χ and ψ are the ellipticity and orientation angles of the transmitted polarization state. Even though straightforward, it is helpful to observe that the depolarization response of a coherent target is constant and equal to 1. Further, it is useful to define the minimal (maximal) degree of polarization as the degree of polarization corresponding to the minima (maxima) of the depolarization response function and to indicate it with p_{MIN} (p_{MAX}). Other subscripts can be used to refer to the degree of polarization corresponding to a given transmit state: p_{RHC}, p_{LHC} and p_C can be used to refer to right-hand circular, left-hand circular or circular (with no further specification) polarization transmit respectively; p_{+45}, p_{-45} and p_{45} can be used to refer to +45° linear, -45° linear, or slant (with no further specification) polarization transmit respectively; p_H and p_V can be used to refer to horizontal and vertical polarization transmit respectively.

In order to get a first understanding of the variability of the degree of polarization as a function of transmitted polarization state, we introduce the concept of canonical incoherent target.

A canonical incoherent target is constructed as a weighted sum of clouds of canonical coherent scatterers. Canonical coherent scatterers are the sphere, the spheroid, the horizontal dipole, the vertical dipole, the canted dipole, the right-handed helix, the left-handed helix and so on. Given the scattering matrix corresponding to a canonical coherent scatterer, a cloud of such scatterers can be constructed by forming the corresponding Kennaugh matrix (equivalent to a rank-1 covariance matrix) as described in Chapter 2:

$$\mathbf{K}_i = \mathbf{Q}^* \langle \mathbf{S}_i \otimes \mathbf{S}_i^* \rangle \mathbf{Q}^+ \tag{4.7}$$

A canonical incoherent scatterer can then be constructed as a weighted sum of such Kennaugh matrices.

$$\mathbf{K} = \sum_i w_i \mathbf{K}_i \tag{4.8}$$

Such a theoretical framework can be used to synthesize Kennaugh matrices corresponding to different admixtures of clouds of scatterers.

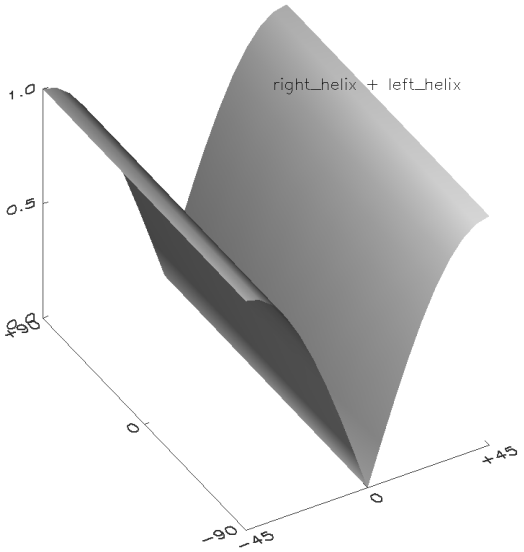
right_helix + left_helix
1.0
0.5
R/R
0
−90
−45
0
+45

A

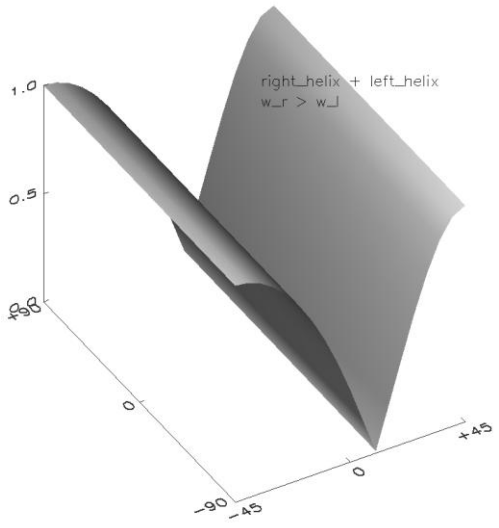
right_helix + left_helix
w_r > w_l
1.0
0.5
R/R
0
−90
−45
0
+45

B

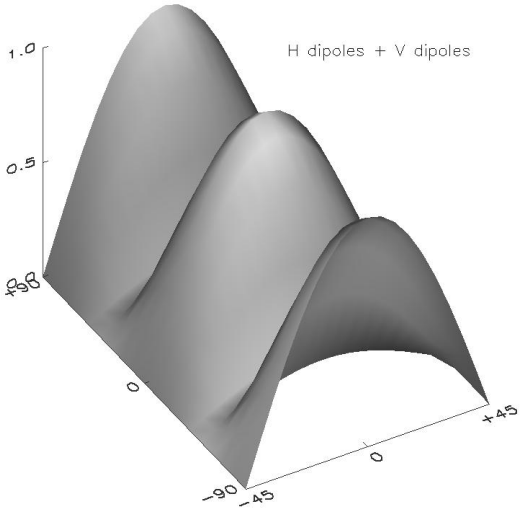
H dipoles + V dipoles
1.0
0.5
R/R
0
−90
−45
0
+45

C

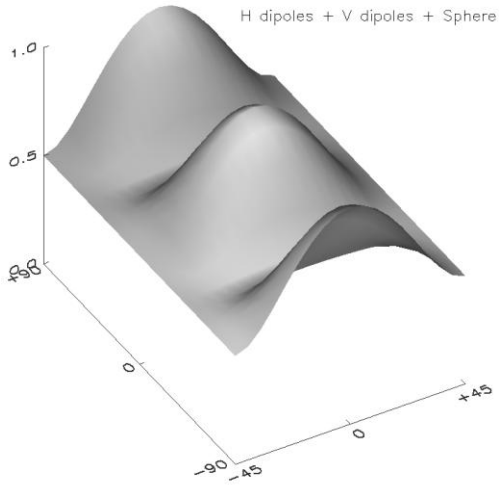
H dipoles + V dipoles + Sphere
1.0
0.5
R/R
0
−90
−45
0
+45

D

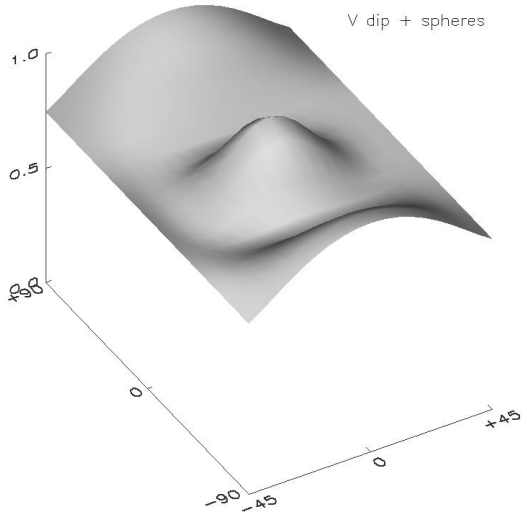

E

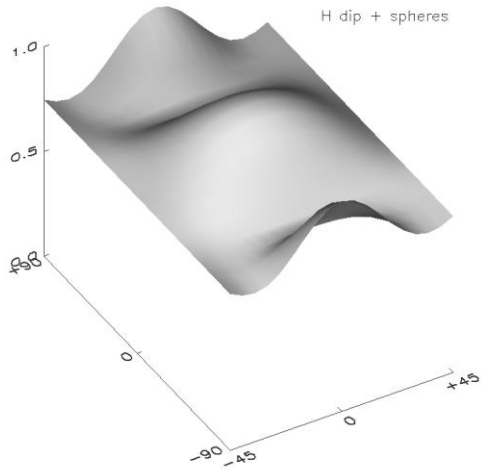

F

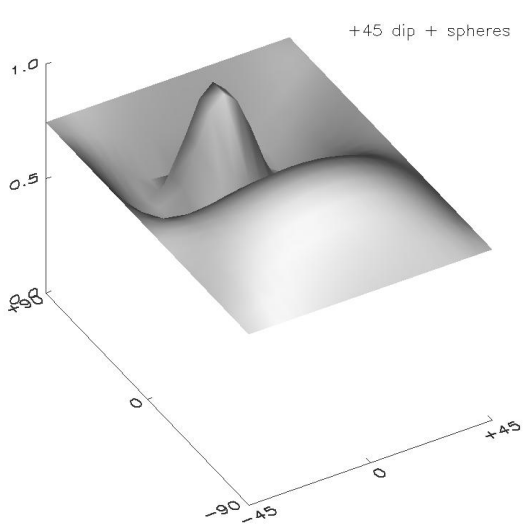

G

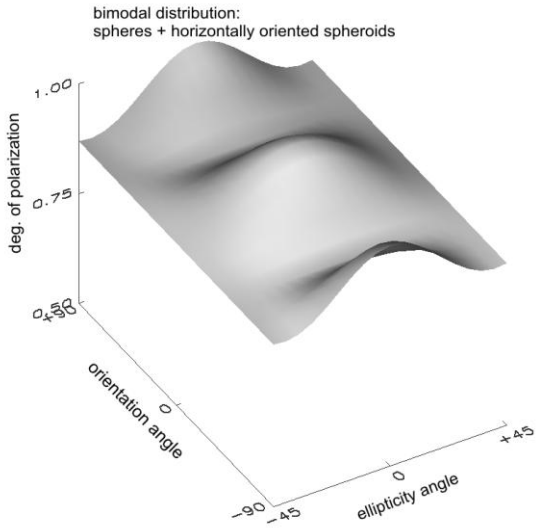

H

Figure 4.1 **Depolarization response plots for a) a cloud of right-hand plus a cloud of left-hand helices, b) a cloud of right-hand plus a cloud of left-hand helices, summed with different weights, c) a cloud of horizontally oriented dipoles plus a cloud of vertically oriented dipoles, d) a cloud of horizontally oriented dipoles plus a cloud of vertically oriented dipoles plus a cloud of spheres, e) a cloud of vertically oriented dipoles plus a cloud of spheres, f) a cloud of horizontally oriented dipoles plus a cloud of spheres, g) a cloud of 45°degree oriented dipoles plus a cloud of spheres, h) a cloud of spheres plus a cloud of slightly oblate, horizontally oriented spheroids.**

In Fig. 4.1 A, B, depolarization response plots for different admixtures of right and left helices are reported. It has to be noted how an unbalanced mixture of right-hand and left-hand helices is capable of breaking the depolarization response symmetry about the equatorial plane.

Plots in Fig. 4.1 C, D, E, F, H show us that, if the target is constituted by anisotropic scatterers (dipoles, oblate spheroids) either horizontally or vertically aligned, the depolarization response plots present a peculiar pattern made up of a minimal circle along the circular/slant circle of the Poincare sphere and a maximal axis going through the horizontal and vertical polarization states. As far as the maximal axis is concerned, the amplitudes of the lobes on the horizontal and vertical polarization states is dependent on the scattering amplitude of the scatterers aligned in that same direction. This effect is particularly evident by comparing Fig. 4.1 E and F.

Ultimately, Fig. 4.1 G shows that a cloud of canted scatterers displaces the maximal axis of the depolarization response along the equator of the Poincare sphere. A consequence of this fact is that the evaluation and analysis of the depolarization response plot is capable of indicating the presence of canted scatterers and of estimating their alignment direction. This observation leads to the definition of the canting parameter:

$$-90° < \mathrm{CP} \leq +90°$$

$$\mathrm{CP} \equiv \psi_{\mathrm{maxlobe}} \tag{4.9}$$

where ψ_{maxlobe} indicates the angle between the horizontal polarization state and the maximum amplitude lobe of the maximal axis of the depolarization response. The canting parameter is representative of the mean canting angle of incoherent targets.
A couple of cautionary notes are however due. In the case of a cloud of uniformly canted scatterers with the same axis ratio, the depolarization response would be constant and equal to 1 and, therefore, the above-outlined procedure is not doable. The condition for its implementation is that the observed incoherent scatterer must have either an axis ratio distribution or a canting angle distribution (around a zero or non-zero mean), condition that, in the case of weather observations, is generally met.

From the depolarization response plots of Fig. 4.1, we note how, for certain types of incoherent targets, the degree of polarization can span the whole dynamic range, from 0 to 1. For example, a cloud of right-hand helices plus a cloud of left hand helices produces no depolarization when circular polarization is transmitted but produces a totally depolarized wave if linear polarization is transmitted. The same happens, for example, for a cloud of horizontally oriented plus a cloud of vertically oriented dipoles: when horizontal or vertical polarization is sent no depolarization occurs, but when circular polarization is sent the return is completely depolarized.
These examples show that one single degree of polarization cannot actually tell much about the variability of the scatterers present in the radar resolution volume. The optimal indicator for the heterogeneity of the illuminated target is therefore the target entropy,

obtainable, like the complete depolarization response, only from fully polarimetric measurements.
A general theory relating the value of target entropy (quad-pol) to the values of the degree of polarization (or wave entropy, the same as the degree of polarization, see chapter 2) is not yet developed. It was stated that, since the minimal degree of polarization is obtained when the target is illuminated with the most depolarization sensitive polarization state, its behavior should approximately mirror the target entropy's. This is however only a loose similarity, since the minimal degree of polarization (maximum wave entropy) "saturates more quickly than the target entropy".
For instance, in the case of a cloud of randomly oriented dipoles the maximum wave entropy, like the target entropy, is equal to 1. However, for the cloud of horizontally plus vertically oriented dipoles, the maximal wave entropy (for circular polarization transmit) is 1, whereas the target entropy is only 0.63. So, there can be targets with target entropy <1 whose maximal wave entropy equals 1.
This is due to the fact that the depolarization response is evaluated by means of polarization basis transformations, namely, SU(2) transformations. Target Entropy is evaluated by means of a diagonalization of the covariance matrix, corresponding to SU(3) transformations. Since SU(2) is a subgroup of SU(3), the variability that can be achieved with SU(2) transformations is more restricted than that associated with SU(3) transformations.

Besides the theoretical problem of precisely relating the target entropy to values of the degree of polarization (or wave entropy), there is the problem of identifying the degrees of freedom of the depolarization response plot.
The degree of polarization as a function of the transmit polarization state and target Kennaugh matrix can be expressed as [6]

$$1 - \mathrm{p}^2 = 2 \cdot \frac{\underline{\mathbf{g}}\mathbf{K}\mathbf{G}\mathbf{K}\underline{\mathbf{g}}}{\underline{\mathbf{g}}\mathbf{K}\mathbf{I}\mathbf{K}\underline{\mathbf{g}}} \tag{4.10}$$

where $\underline{\mathbf{g}}$ is the transmit Stokes vector,

$$\mathbf{I} = \begin{bmatrix} 1 & 0 & 0 & 0 \\ 0 & 1 & 0 & 0 \\ 0 & 0 & 1 & 0 \\ 0 & 0 & 0 & 1 \end{bmatrix} \tag{4.11a}$$

$$\mathbf{G} = \begin{bmatrix} 1 & 0 & 0 & 0 \\ 0 & -1 & 0 & 0 \\ 0 & 0 & -1 & 0 \\ 0 & 0 & 0 & -1 \end{bmatrix} \tag{4.11b}$$

So, $1-p^2$ maps the square of the Kennaugh matrix after taking out the magnitude, so the depolarization response plot has (9-1) = 8 degrees of freedom. It is not known if the above map can be inverted, namely to yield a one-to-one correspondence with the Kennaugh (covariance) matrix.

Ultimately, it is important to understand the strategy to follow for information extraction. The minimal degree of polarization, even though similar to entropy, is not necessarily the most interesting or the only quantity to consider. Indeed, as shortly introduced in the first paragraph, some degrees of polarization can be sensitive to a number of target features, whereas other degrees of polarization can be sensitive only to a subset of these features. So, there are cases where interesting physics is highlighted by the maximal degree of polarization (in our case the discrimination between rain and non-rain) or by the difference between two degrees of polarization. For example, with reference to the concept of canting parameter CP, in the study of canting angles (p_C-p_{45}) could be an interesting quantity to look at.

4.3 The Depolarization Response: Applications.

In the following, we analyze the depolarization response for two cases of interest for weather radar applications: isotropic targets (differential reflectivity close to 0 dB, examples might be graupel, hail or dry snow) and anisotropic targets (positive differential reflectivity, like rain or rain/small hail mixtures).

4.3.1 Anisotropic weather targets

The Kennaugh matrix that can qualitatively illustrate the depolarization response pattern for rain can be constructed as a cloud of spheres plus a cloud of oblate, horizontally oriented spheroids. The two Kennaugh matrices that come in the sum can be computed from the respective scattering matrices with the help of (4.8).
As an example, from the following scattering matrices,

$$\mathbf{S}_{\text{sphere}} = \begin{bmatrix} 1 & 0 \\ 0 & 1 \end{bmatrix} \qquad \mathbf{S}_{\text{oblate}} = \begin{bmatrix} 1 & 0 \\ 0 & 0.5 \end{bmatrix} \tag{4.12}$$

the plot shown in Fig. 4.1 H can be obtained.
The depolarization response of this bimodal distribution has a different pattern than the isotropic case: the degree of polarization attains its minimal values on the circular/slant circle of the Poincaré sphere (the great circle containing the poles and +/-45° linear polarization), and its maximal values (one) at horizontal and vertical linear transmit (Fig. 4.1 H). In the case of rain or rain/hail mixtures, the degree of polarization at horizontal or vertical transmit is the least sensitive to depolarization effects.

For the case of rain, values of entropy, copolar correlation coefficient and minimal degree of polarization were evaluated also for a more realistic case, namely for a Marshall-Palmer Drop Size Distribution.
The covariance matrix (containing equivalent information to the Kennaugh matrix) was computed for a cloud of non canted raindrops using the Rayleigh approximation. The formulae needed to evaluate the matrix elements can be found in [1, 4, 5].

$$[\mathbf{C}] = \begin{bmatrix} \int |S_{hh}|^2 N(D) dD & 0 & \int S_{hh}(D) \cdot S_{vv}^*(D) N(D) dD \\ 0 & 0 & 0 \\ \int S_{vv}(D) \cdot S_{hh}^*(D) N(D) dD & 0 & \int |S_{vv}|^2 N(D) dD \end{bmatrix} \tag{4.13}$$

The Marshall-Palmer Drop Size Distribution is an exponential distribution of the form

$$N(D) = N_0 \cdot e^{-\Lambda D}$$

$$N_0 = 8000\ m^{-3} mm^{-1}$$

$$\Lambda = 4.1 \cdot R^{-0.21} \tag{4.14}$$

where R is the rain rate in mm/hr.

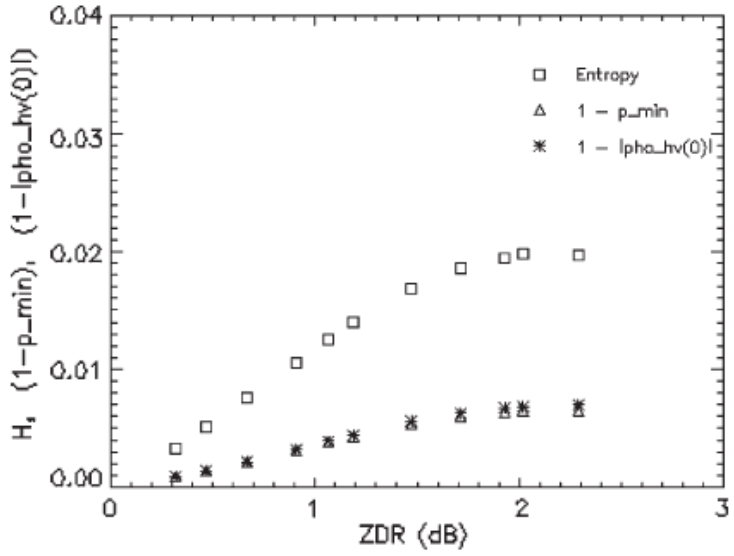

Figure 4.2 **Simulation results for a cloud of non-canted raindrops with exponential Drop Size Distribution (Marshall-Palmer). The plots reported in the graph correspond to entropy (squares), one minus the minimal degree of polarization (triangles) and one minus the copolar correlation coefficient (asterisks). The covariance matrix used for the simulation is shown in (4.12). Note the almost identical values assumed by p_{MIN} and $|\rho_{hv}(0)|$.**

After the evaluation of the copolar correlation coefficient, the covariance matrix was either diagonalized to evaluate the scattering entropy or rotated to circular polarization to evaluate the minimal degree of polarization. The simulation yields numerical values for H, $(1-p_{MIN})$ and $(1-|\rho_{hv}(0)|)$ and shows how these quantities are affected by raindrop oblateness dispersion. Note that, even though not included in the model, Mie scattering also relevantly contributes to the numerical value of the variables in question and, as will be proven in Chapter 5, is responsible for the deviations of the experimental values from the simulation results presented in Fig. 4.2.
On the other hand, p_H and p_V are identically 0 for a cloud of non-canted raindrops and, as a consequence, these variables are expected to enhance the contrast between rain and non-rain targets in a way that is unique.
Ultimately, it is helpful to remind some theoretical relationships between the minimal degree of polarization and the copolar correlation coefficient [17].
Under the assumption of a diagonal scattering matrix (oblate, non-canted raindrop) acting on slant polarization,

$$\begin{bmatrix} S_{hh} \\ S_{vv} \end{bmatrix} = \begin{bmatrix} S_{hh} & 0 \\ 0 & S_{vv} \end{bmatrix} \begin{bmatrix} 1 \\ 1 \end{bmatrix} \tag{4.15}$$

simple algebra leads to the following relationship between the degree of polarization at slant send and the copolar correlation coefficient (see 3.37).

$$(1 - p_{45}^2) = \frac{4 \cdot Z_{DR}^{hy}}{\left[1 + Z_{DR}^{hy}\right]^2} \left(1 - \left|\rho_{hv}^{hy}\right|^2\right) \tag{4.16}$$

Almost identical algebra yields the same result for the degree of polarization at circular send (p_C).
All these considerations suggest a similar behavior for p_{45}, p_C, and $|\rho_{hv}(0)|$ when rain is illuminated and, indeed, the experimental results substantiate these results accurately. So, when non-canted rain is illuminated, the information carried by p_{45}, p_C, and $|\rho_{hv}(0)|$ can be considered practically identical.
There is however an important case, not yet substantiated by experimental data, where differences among these variables might arise. Contrary to p_C, that is canting independent, both quantities appearing in round brackets in (4.16) show a linear dependency on canting angle.
Ultimately, we note how differential propagation phase does not affect the measurement of the degree of polarization at circular/slant transmit when anisotropic targets are illuminated. This is due to the fact that, even though the polarization state of the transmitted wave migrates along the circular/slant circle upon forward propagation, the depolarization response of rain presents a constant (minimal) value along this path. This circumstance does not however hold for isotropic weather targets, analyzed in the next paragraph.

4.3.2 Isotropic weather targets

A simple model for isotropic weather targets can be thought of as a cloud of randomly oriented spheroids. Considering Huynen parameters, a simple way to compute the degree of polarization as a function of the transmitted polarization state is obtained by means of the following Kennaugh matrix.

$$\mathbf{K}_{\mathrm{iso}} = \begin{bmatrix} 1+\mathrm{B}_0 & 0 & 0 & 0 \\ 0 & 1 & 0 & 0 \\ 0 & 0 & 1 & 0 \\ 0 & 0 & 0 & -1+\mathrm{B}_0 \end{bmatrix} \tag{4.17}$$

B_0 ranges between 0 and 1, depending if the spheroids are spheres (B_0=0) or dipoles (B_0=1). Simple algebra yields the following expression for the depolarization response for a cloud of randomly oriented spheroids:

$$\mathrm{p}(\chi) = \frac{\sqrt{\cos^2(2\chi) + (1-\mathrm{B}_0)^2 \sin^2(2\chi)}}{1+\mathrm{B}_0} \tag{4.18}$$

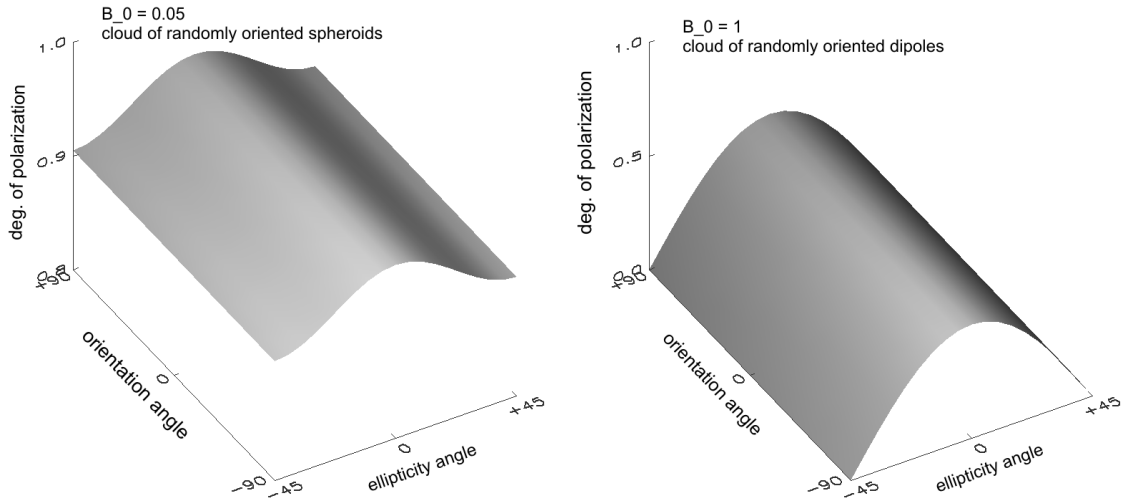

Figure 4.3 **Left: depolarization response for a cloud of randomly oriented, slightly oblate, spheroids (B_0=0.05). Right: depolarization response for a cloud of randomly oriented dipoles (B_0=1). Note the different scale on z axis, [0.8 – 1.0] for the spheroids and [0.0 - 1.0] for the dipoles. For a cloud of spheres (B_0=0.0) the depolarization response is constant and equal to 1.**

Here, χ is the ellipticity angle and B_0 is the generator of target structure. The above expression shows that, for an isotropic target, the degree of polarization attains its minimal values at the poles of the Poincaré sphere (circular polarization transmit) and the maximal values at the equator (linear polarization transmit) (Fig. 4.3).

Further, if we consider the quantity 1-p, the relation between the minimum and the maximum is a simple 3 dB difference.

$$1 - p_{MIN} = \frac{2B_0}{1 + B_0} \qquad 1 - p_{MAX} = \frac{B_0}{1 + B_0} \tag{4.19}$$

The depolarization response of an isotropic target shows a number of symmetries, namely invariance with respect to orientation angle and handedness of the transmitted polarization state.
It is worth noting that the depolarization response corresponding to B_0=0 and B_0=2 are constant and equal to 1 and 1/3 respectively. The first case could be realized by a cloud of spheres whereas the second could be obtained by an admixture of randomly oriented dipoles and a suitable balance of right and left helices [3].
Fig. 4.4 shows that, contrary to the case of anisotropic weather targets (rain), p_C, p_{45} and $|\rho_{hv}(0)|$ can take on different values. This is to be expected, since these variables are in general independent. With regards to Fig. 4.4, a couple of comments highlighting pros and cons of these three variables are helpful.

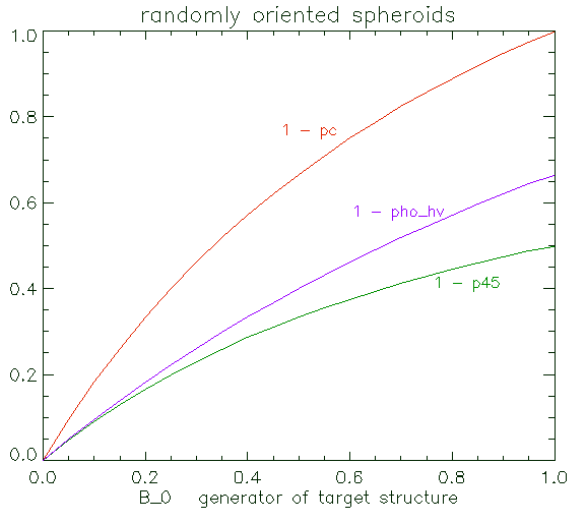

Figure 4.4 **Values of (1-p_C), (1-p_{45}) and (1-$|\rho_{hv}(0)|$) for a cloud of randomly oriented spheroids as a function of axis-ratio (B_0 is the generator of target structure). B_0=0 corresponds to a cloud of spheres, B_0=1 corresponds to a cloud of dipoles.**

Firstly, the degree of polarization at circular transmit has a larger dynamic range than the copolar correlation coefficient and might offer the possibility to better discriminate between target classes. This possibility should be investigated.
Secondly, when simultaneous transmission is used (as with operational weather radars) and isotropic, depolarizing targets are illuminated (examples could be graupel, small hail and hail) the value of the copolar correlation coefficient is biased by cross-talk upon backscattering.

$$\rho_{hv}^{hy} = \frac{\langle (S_{hh} + S_{hv})(S_{vv} + S_{vh})^* \rangle}{\sqrt{|S_{hh} + S_{hv}|^2 \cdot |S_{vv} + S_{vh}|^2}} \tag{4.20}$$

Contrary to the copolar correlation coefficient, the degree of polarization at circular/slant send is not affected by cross-talk on backscatter.

A drawback for the use of the degree of polarization with simultaneous transmission when isotropic targets are illuminated is that, in this special case (and only in this case), the value of the degree of polarization is affected by differential propagation phase.
Indeed, if the transmit state lies on the circular/slant circle of the Poincaré sphere, (as in the case of simultaneous transmission) differential propagation phase (Φ_{DP}) occurring from the antenna to the target is responsible for a migration of the polarization state of the forward propagating wave along this circle. If the illuminated targets are anisotropic (rain) no bias occurs as the Φ_{DP} induced migration displaces the polarization state of the propagating wave along a minimal circle. If the illuminated targets are isotropic, the degree of polarization is dependent upon the one-way differential phase shift (from the antenna to the target). As shown in (4.18), the bias can be up to 3 dB but, since differential propagation phase can be measured independently, it is possible to correct for this effect by means of (4.17). Ultimately, with the help of (4.20), the generator of target structure of isotropic targets can be estimated.

$$p = \frac{\sqrt{\cos^2 \Phi_{DP} + (1 - B_0)^2 \sin^2 \Phi_{DP}}}{1 + B_0} \tag{4.21}$$

4.4 Propagation effects

In this paragraph we review the effects of propagation on target entropy and on the degree of polarization (for every transmit state).

4.4.1 Degree of polarization – propagation effects

Regardless of the polarization state of the transmitted wave, the degree of polarization is independent from polarization-independent attenuation, as this simply appears as a scalar factor multiplying Wolf's coherency matrix.

If the transmit state lies on the circular/slant circle of the Poincaré sphere, differential propagation phase (Φ_{DP}) occurring from the antenna to the target is responsible for a migration of the polarization state of the forward propagating wave along this circle (the circular/slant circle goes through the right hand circular, left hand circular and slant linear polarization states). If the illuminated targets are anisotropic (rain), no bias occurs, as the Φ_{DP} induced migration displaces the polarization state of the propagating wave along a minimal circle. If the illuminated targets are isotropic, the degree of polarization is dependent upon the one-way differential phase shift (from the antenna to the target). As shown in the previous paragraph, the bias for (1-p) can be up to 3 dB but, since differential propagation phase can be measured independently, it is possible to correct for this effect and provide an estimate of the generator of target structure of the illuminated isotropic target.

At H or V send, differential propagation phase does not change the polarization state of the forward propagating wave and as a consequence the degrees of polarization corresponding to these transmit states are to a first order Φ_{DP} independent.
Differential phase shifts occurring after the scattering, namely from the target to the antenna, do not further affect the degree of polarization of the backscattered wave. This fact is again encapsulated in equation (4.5) as non-attenuating propagation effects in the atmosphere map to unitary transformations.

4.4.2 Entropy – propagation effects

Propagation through a medium can be described by a matrix T acting on a covariance matrix C (cross indicates adjoint) [6].

$$\mathbf{C}' = \mathbf{T}\mathbf{C}\mathbf{T}^{+} \tag{4.22}$$

In the case of T being unitary, (4.21) reduces to a similarity transformation. Such a transformation set contains (in the strict sense) the set of polarization basis change, which, in turn, contains the set of rotations around the radar line of sight [16]. Since the eigenvalue problem is intrinsically invariant under unitary transformations, two observations can be made. The first is that, because of roll-invariance, whenever an anisotropic cloud of hydrometeors is illuminated, entropy is not dependent on the mean canting angle (insofar as only a rotation of the symmetry axis of the target occurs and the orientation distribution keeps unaltered). The second is that, since unitarity corresponds to energy conservation, propagation phenomena associated with non attenuating media with different electrical lengths at different polarizations do not affect entropy (in particular, entropy is not affected by differential propagation phase). More specifically, the matrix T modelling propagation through a non-attenuating medium is an element of a representation of the rotation group SO(3), which is a subgroup of U(3). Non-attenuating propagation effects in the atmosphere map to SL(2,C) over SU(2) and the corresponding group representation is SO(3,C) which is isomorphic to the Lorentz group SO(3,1). Non-

attenuating propagation effects map to a smaller set than U(3) because the latter contains power-preserving transformations that cannot physically occur in the atmosphere.
Further, since entropy is explicitly normalized with respect to power, it is unaffected by polarization independent attenuation (but it is affected by differential attenuation). Entropy is an amplitude invariant scalar like Z_{DR} and LDR, but, unlike the latter, it has the property of being canting independent.

References Chapter 4

[1] V. N. Bringi and V. Chandrasekhar, Polarimetric Doppler Weather Radar. principles and applications, Cambridge University Press, 2001.

[2] R. J. Doviak and D. S. Zrnic, Doppler Radar and Weather Observations, 2nd ed. San Diego, CA: Academic Press, 1993.

[3] M. Galletti, D. H. O. Bebbington, M. Chandra, T. Boerner, "Fully polarimetric analysis of weather radar signatures" Proc. 2008 IEEE Radar Conference, Rome, Italy, May 2008.

[4] H. R. Pruppacher and J. D. Klett, Microphysics of Clouds and Precipitation, Kluwer Academic Publishers, 1997.

[5] P. S. Ray, "Broadband complex refractive indices of ice and water," Appl. Opt., 11, pp. 1836-1844, 1972.

[6] D. H. O. Bebbington, "Degree of polarization as a radar parameter and its susceptibility to coherent propagation effects," URSI Commission F Symposium on Wave Propagation and Remote Sensing, Ravenscar, N. Yorkshire, UK, pp. 431-436, June 1992.

[7] D. H. O. Bebbington, R. McGuinness and A. R. Holt, "Correction of propagation effects in S-band circular polarization-diversity radars," Proc. IEE, 134H, pp. 431-437, 1987.

[8] G. Brussaard, "Rain-induced crosspolarizaton and raindrop canting," Electron. Lett., vol. 10, pp. 411-412, 1974.

[9] M. Chandra, Y. M. Jain and P. A. Watson, "Assessment of the influence of drop oscillations on dual polarization radar measurements," Preprints, ICAP, Norwich, U.K., IEE Publ. No219, pp. 34-39, 1983.

[10] J. R. Saylor and B. K. Jones, "The existence of vortices in the wakes of simulated raindrops," Physics of Fluids, 17, 031706, 2005.

[11] Ryzhkov, A. V., 2001: Interpretation of polarimetric radar covariance matrix for meteorological scatterers: Theoretical analysis. J. Atmos. Oceanic Technol., 18, 315-328.

[12] Ryzhkov, A. V., D. S. Zrnic, 1996: Assessment of rainfall measurement that uses specific differential phase. J. Appl. Meteor., 35, 2080-2090.

[13] Caylor, I. J., and V. Chandrasekhar, 1996: Time varying ice crystal orientation in thunderstorms observed with multiparameter radar. IEEE Trans. Geosci. Remote Sens., 34, 847-858.

[14] Beard, K. V., and A. R. Jameson, 1983: Raindrop canting. J. Atmos. Sci., 40, 448-454.

[15] Krehbiel, P., T. Chen, S. McCray, W. Rison, G. Gray, and M. Brook, 1996: The use of dual-channel circular polarization radar observations for remotely sensing storm electrification.

[16] S. R. Cloude and E. Pottier, "A Review of Target Decomposition Theorems in Radar Polarimetry," IEEE Transactions on Geoscience and Remote Sensing, vol. 34, no. 2, pp. 498-518, March 1996.

[17] M. Born and E. Wolf, Principles of Optics: Electromagnetic Theory of Propagation, Interference and Diffraction of Light, 7th ed. Cambridge University Press, 1999.

5. Experimental Results

5.1 Overview

The data presented in this chapter were collected with DLR C-band polarization diversity weather radar (POLDIRAD). The radar was operated in fully polarimetric mode, transmitting alternating horizontal and vertical polarization states and receiving the co and cross polar components of the backscattered signal, thus allowing estimation of complete scattering matrices at H/V polarization basis. The two RHIs relative to the convective event (June) were taken at 16.00 local time with pulse repetition frequency PRF=1200 Hz and pulse width τ =1μs. The stratiform event (November) was taken at 13.05 local time and 272° azimuth with PRF=800 Hz and τ =1μs. Besides being fully polarimetric, these datasets have the desirable advantage of RHI (Range Height Indicator) scan mode. RHIs are obtained by scanning in elevation for a fixed azimuth direction, and the resulting image appears as a vertical section of the illuminated event, allowing analysis of rayplots in context.

5.2 Case study 1: Convective event

The first case study presents a convective event characterized by two cores located approximately 24 and 26 km away from the radar. Φ_{DP} and Z_{DR} signatures guarantee a major presence of rain in the lowest 2 – 2.5 km. In correspondence of the centre of the first core (24 km) a mixture of rain and frozen, irregularly-shaped, hydrometeors is probably responsible for higher values of Z_H, H and 1-p. Accordingly, Z_{DR} assumes smaller values around 0.5 dB.
After the evaluation of standard radar meteorological variables, a ray passing through the core of the storm (highlighted in black in Fig. 5.1) was chosen for the rayplots shown in Fig. 5.2. This case study focuses on anisotropic weather targets (rain or rain/small-hail mixture) and aims at

- confronting the sensitivity to depolarization from rain of the following variables: entropy (H), degree of polarization at horizontal send (p_H), degree of polarization at vertical send (p_V), degree of polarization at circular send (p_C), degree of polarization at slant send (p_{45}) and copolar correlation coefficient ($|\rho_{hv}(0)|$).

- identifying the scattering phenomena responsible for depolarization from rain and their impact on the variables under consideration.

- evaluate the dependence of the degree of polarization at horizontal send (p_H) with respect to antenna cross-channel coupling.

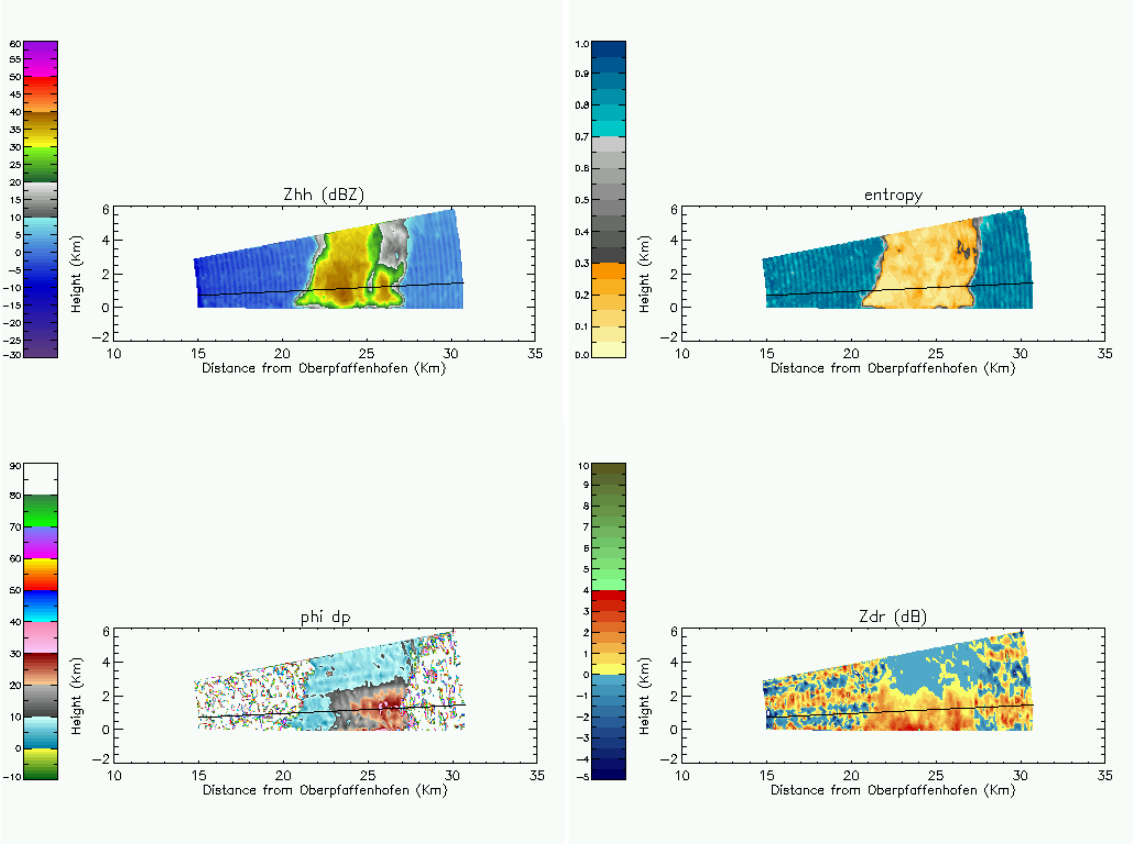

Figure 5.1 **Convective event, RHI images. Upper left: reflectivity (Z_H, in dBZ), upper right: entropy (H), lower left: copolar phase (Φ_{DP}, doppler shift corrected), lower right: differential reflectivity (Z_{DR}, in dB). The black ray is chosen for the analysis of entropy, degree of polarization and copolar correlation coefficient when anisotropic targets (rain or rain/small-hail mixtures) are illuminated. The corresponding rayplots are shown in Fig. 5.2**

As shown in Fig. 5.2, the degree of polarization at horizontal send (p_H) behaves very similarly to the degree of polarization at vertical send (p_V). The same happens for the pair p_{+45} and p_{-45}, and for the pair p_{RHC} and p_{LHC} (graphs not reported for compactness).
Further, p_{45} behaves very similarly to p_C, and both variables take on smaller values than p_H or p_V. These observations are in qualitative accordance with the theoretical description provided by the depolarization response for anisotropic weather targets provided in Section III.
The condition for a cloud of horizontally oriented spheroids to show a minimal depolarization response on the circular/slant circle is to have an axis-ratio distribution. In the limit, a simple incoherent target showing such a behavior can be constructed as a cloud of spheres plus a cloud of same axis-ratio, horizontally oriented spheroids, namely, the bimodal distribution used in chapter 4. The dispersion in axis-ratios corresponds to a variability in scattering mechanisms that is naturally perceived by entropy, but not necessarily by the degree of polarization. Indeed, if the transmit polarization is

horizontal, every scatterer (regardless of its axis-ratio) responds with a horizontally polarized wave, producing no depolarization on backscatter. For slant transmit on the other hand, (but in theory this holds for any transmit polarization state other than horizontal or vertical) every scatterer responds with a polarization state that is dependent on its axis ratio, thus producing depolarization on backscatter.

The observations above suggest that, among all possible degrees of polarization, the minimal is the most effective in capturing depolarization effects and, as a consequence, its performance is expected to be comparable to entropy. The graphs in Fig. 5.2 confirm that H and p_{MIN} (although assuming different numerical values) have similar patterns. Fig. 5.2 also shows that, as expected from the theoretical results of chapter 4, the copolar correlation coefficient and the minimal degree of polarization take on almost identical values. The maximal degrees of polarization (p_H and p_V) show on the other hand decreased sensitivity to depolarization from rain.

Regardless the different sensitivities, all these variables (p_{MIN}, p_{MAX}, $|\rho_{hv}(0)|$ and H) are capable of distinguishing between rain (22-23 km) and mixtures of rain and small-hail (24 km).

As far as propagation is concerned, theory and experimental data are in agreement and confirm that H, p_H and p_V are not sensitively affected by differential propagation phase which, in the far range, attains values of 30°.

At 22-23 km distance, radar cells are presumably filled with rain and the signatures are not affected by differential propagation phase. Degree of polarization at horizontal or vertical send should be identically zero for every rain rate, and in this case experimental data do agree with the theory rather satisfactorily (p_H and p_V take on low values, less than 0.01). A discrepancy occurs when confronting experimental and simulated values of H, p_C, p_{45} and $|\rho_{hv}(0)|$. In the area under consideration, where differential reflectivity takes on values of 1 – 2 dB, measured values for p_C and $|\rho_{hv}(0)|$ are around 0.03, while simulated values are around 0.005.

In the present study it is possible to compare parameters normally associated with different transmission states through the ability to synthesize full scattering matrices. This allows us to rule out some of the possible mechanisms of depolarization which can be expected to occur to a similar degree in either mode. As the polarization basis transformations involved in the processing are linear, noise should in principle affect equally p_H or p_V and p_C or p_{45}. The effect of noise on the degree of polarization at horizontal or vertical send is small and, as a consequence, it does not seem reasonable to indicate it as the responsible for the observed discrepancy between experimental and simulated results for p_C, p_{45}, $|\rho_{hv}(0)|$ and H.

Besides a variability of axis ratio induced by the drop size distribution (modeled in the simulation), factors that affect differentially p_{MAX} on one side and $|\rho_{hv}(0)|$ and p_{MIN} on the other, are drop oscillations and Mie scattering.

Our simulation considers an axis-ratio variability given by raindrops in their equilibrium shape. However, what is actually perceived by the radar variables is the ‘instantaneous’ axis-ratio distribution. Axisymmetric drop oscillations are responsible for the enhancement of ‘instantaneous’ axis-ratio variability and might be a factor contributing to the discrepancy between data and numerical results.

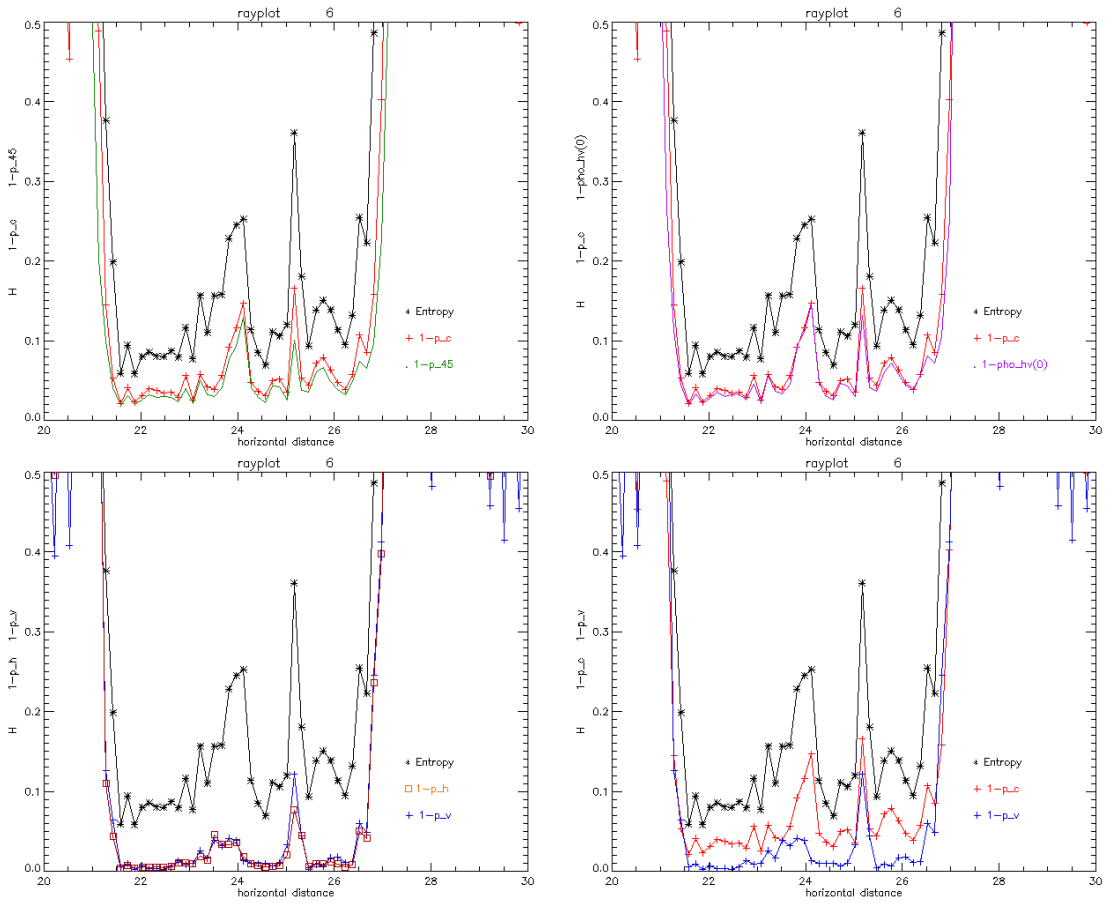

Figure 5.2 **Rayplots corresponding to the ray in black in Fig. 5.1. The top plot on all of the four graphs is the entropy (H, in black). In the upper left graph are two minimal degrees of polarization, namely at circular transmit (p_C in red) and at 45° linear transmit (p_{45} in green). In the lower left graph are the two maximal degrees of polarization, at horizontal transmit (p_H in orange) and vertical transmit (p_V in blue). In the upper right graph are the minimal degree of polarization (at circular transmit, p_C in red) and the copolar correlation coefficient (in violet). In the lower right graph are the minimal degree of polarization (at circular transmit, p_C in red) and the maximal degree of polarization (at vertical transmit, p_V in blue). The images show the different sensitivity of the minimal and maximal degree of polarization to the depolarizing properties of rain. The copolar correlation coefficient performs very similarly to the minimal degree of polarization and their sensitivity appears comparable to entropy. The maximal degree of polarization (at horizontal or vertical transmit) shows decreased sensitivity to depolarization effects from anisotropic targets.**

At C-band, scattering from large raindrops can deviate from the Rayleigh model assumed in the simulation. According to Mie theory, every spheroid responds with a backscatter differential phase that is dependent on its size. If the transmit polarization lies on the circular/slant circle (p_C or p_{45}), this phenomenon might be responsible for a further dispersion in the polarization states backscattered by the target. In this case $|\rho_{hv}(0)|$ is also affected. A simulation for $|\rho_{hv}(0)|$ at C-band considering Mie scattering and a Gaussian distribution of canting angles with a mean of 0° and a standard deviation of 7° is reported in the literature [5]. For Z_{DR} around 1 – 2 dB, it yields values for $1-|\rho_{hv}(0)|$ around 0.02. Inclusion of Mie scattering appears to provide numerical results that match more satisfactorily with the experimental data (0.03).
The analysis of this case study suggests that drop size distribution, drop oscillations and Mie scattering do not affect p_H and p_V but have an impact on the numerical values of H, p_{45}, p_C and $|\rho_{hv}(0)|$. Further, in presence of all these scattering phenomena, the numerical values of p_{45}, p_C and $|\rho_{hv}(0)|$ are almost identical. Differences between these variables, (p_C-p_{45}) or $(p_C - |\rho_{hv}(0)|)$ might be indicators of canting effects. Further work should be addressed at the experimental and theoretical investigation of these differences because they could be available to weather radars operating in hybrid mode.
Some of the experimental results from this case study can be summarized as follows:
When non-canted rain is illuminated,

- Antipodal polarization states on the Poincare sphere present the same scattering behavior, namely, p_{+45} behaves like p_{-45}, p_{RHC} behaves like p_{LHC}, p_H behaves like p_V.

- The analyzed variables can be grouped into two sets, depending on their sensitivity to geophysical properties of backscattering from rain:

    - $|\rho_{hv}(0)|$, p_C, p_{45}, H
      these variables are sensitive to axis ratio distribution (drop size distribution plus axisymmetric drop oscillations), finite width of a 0-mean canting angle distribution, backscatter differential phase dispersion within the resolution volume (Mie scattering). Ultimately, if isotropic targets are also considered, these variables are sensitive to irregular hydrometeor shape.

    - p_H, p_V
      these variables are sensitive only to a finite width of a 0-mean canting angle distribution. Ultimately, when also isotropic targets are considered, these variables are sensitive to irregular hydrometeor shape.

The first conclusion is that, when observing rain, H, p_C, p_{45} do not appear to provide additional information with respect to $|\rho_{hv}(0)|$. The only case where a difference might arise is in presence of a non-zero mean canting angle. In this case H and p_C are strictly canting independent whereas $|\rho_{hv}(0)|$ and p_{45} are not. There is not yet experimental evidence of this effect.

The second conclusion is that p_H and p_V perform better than $|\rho_{hv}(0)|$ for the discrimination between rain and non-rain. This occurs because, for p_H and p_V, the only cause of deviation from unity is given by the finite width of a 0-mean canting angle distribution, and not by the other above-listed factors that, on the other hand, decrease the value of $|\rho_{hv}(0)|$ in rain and, consequently, decrease the polarimetric contrast between rain and other targets (the latter generally characterized by lower copolar correlation coefficient values). The next case study aims at substantiating this observation, namely that p_H and p_V perform noticeably better than $|\rho_{hv}(0)|$ for rain non-rain discrimination. When rain is illuminated, since p_H and p_V are only affected by a finite width of a 0-mean canting angle distribution, the backscattering behavior of these variables is identical to the linear depolarization ratio. The next case study also compares p_H and LDR in order to understand if the first variable brings additional information with respect to the second.

For clarity, we anticipate the result:
p_H, p_V and LDR have the same backscattering properties when rain is illuminated (are sensitive to the same geophysical features of the target).
The polarimetric contrast with other targets present in weather radar signatures is optimized with respect to variables like $|\rho_{hv}(0)|$, p_C, p_{45} and H.

The last issue concerning the present case study is a first assessment of the dependence of the degree of polarization at horizontal send with respect to antenna cross-channel coupling. With reference to Fig. 5.2 areas of rain were selected (22 – 23 km), for which the degree of polarization was evaluated at horizontal transmit and (after a polarization basis transformation) at slant transmit. Since the degree of polarization is not dependent on the polarimetric receive channels but only on the transmit polarization state, the above-mentioned measurement can be utilized, under the assumption of illuminating non-canted rain, to simulate electromagnetic power leaking coherently into the cross-channel upon transmission.

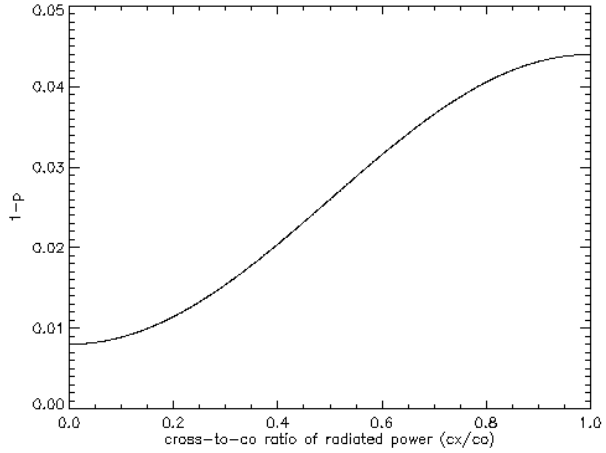

Figure 5.3 Degree of polarization versus antenna cross-channel coupling (both expressed in linear scale).

If we consider an antenna with -15 dB cross channel isolation, namely, an antenna with rather poor isolation, we have

$$-15\ \mathrm{dB} = 10\log_{10}\left(\frac{\mathrm{cx}}{\mathrm{co}}\right) \qquad \rightarrow \qquad \left(\frac{\mathrm{cx}}{\mathrm{co}}\right) = 0.032 \tag{5.1}$$

where cx is the power present in the cross-polar channel and co is the power in the copolar channel. On the abscissa of Fig. 5.3, is the ratio of cross-to-co polar power. Ideally, a value of 0 corresponds to transmission of pure horizontal polarization, whereas a value of 1 corresponds to pure slant polarization transmit. On the y axis is plotted an interpolation of the corresponding values of the degree of polarization as measured by the POLDIRAD system.
If we linearize the function represented in Fig. 5.3 a rough estimate for the bias induced in the value of the degree of polarization by an antenna with -15 dB cross channel isolation is

$$\Delta p_H = 0.0012 \tag{5.2}$$

This value appears to be low, probably less than the standard deviation associated with the degree of polarization when rain is illuminated. As a consequence, this first rough estimate suggests that the degree of polarization is relatively robust to antenna cross-channel coupling.

5.3 Case study 2: convective event

5.3.1 Observation of rain

The experimental results exposed in the previous paragraph indicate, in accordance with the theory, that the considered variables can be divided into two groups, depending on the sensitivity to the physical features of the rain medium:

- $|\rho_{hv}(0)|$, p_C, p_{45}, H
- LDR, p_H, p_V

The use of these variables in radar meteorology is for hydrometeor classification and, in particular, these variables are expected to differentiate low entropy weather targets (drizzle, rain, dry snow) from higher entropy targets (graupel, small hail, clutter contaminated cells, etc.). Also, it appears that the degree of polarization at horizontal send is robust with respect to antenna cross channel coupling.
The aim of the present case study is to further reinforce the above illustrated ideas, namely:

- Demonstrate that LDR, p_H and p_V provide a finer discrimination between rain and non-rain targets than $|\rho_{hv}(0)|$ and H.

- Demonstrate that, contrary to LDR, p_H and p_V are not relevantly affected by antenna cross-channel coupling.

In Fig. 5.4 are reported 6 RHIs corresponding to different polarimetric variables for the same convective event.
The variables are reflectivity at horizontal polarization (Z_H), target entropy (H), differential phase (Φ_{DP}), differential reflectivity (Z_{DR}), orientation parameter (ORTT), and linear depolarization ratio (LDR).
In this case study we aim at studying the behavior of p_H, p_V, LDR, H and $|\rho_{hv}(0)|$, and rayplots for the analysis of these variables are reported in Fig. 5.5.

The RHIs of Z_H, Φ_{DP}, Z_{DR} and ORTT are used to get an understanding, after a visual analysis, of the presence of anisotropic and isotropic weather targets along the ray chosen for the rayplots, indicated in black in Fig. 5.3. The reflectivity at horizontal polarization shows values within 40 dBZ at the center of the storm, and the pattern of the differential phase, that in the far range attains values of 30°, suggests the presence of rain along the path. In order to get an a priori knowledge (before the analysis of LDR, p_H, p_V, H, and $|\rho_{hv}(0)|$) of the exact location of anisotropic (raindrops) and isotropic (graupel, small hail) weather scatterers, differential reflectivity and the orientation parameter are analyzed. Both variables agree in indicating a transition from isotropic targets to rain at 25 km distance from the radar. Indeed, differential reflectivity assumes values close to 0 between 23 and 25 km, and higher positive values before and after this core of isotropic hydrometeors, namely between 25 and 26 km and between 22 and 23 km. The same pattern is displayed by the orientation parameter, with lower (grey) values between 23 and 25 km and higher (red) values before and after the core.
After this preliminary analysis, we turn to the study of the behavior of LDR, p_H, p_V, H, and $|\rho_{hv}(0)|$, with the rayplots reported in Fig. 5.4.
The first observation is that LDR, $(1-p_H)$ and $(1-p_V)$ feature an abrupt transition from higher to lower values at 25 km distance, thus confirming the pattern qualitatively suggested by Z_{DR} and ORTT.
However, at 25 km, the transition from small hail to graupel is not clearly detected by entropy and the copolar correlation coefficient.
In the case of entropy, despite progressively decreasing values for ranges between 23.5 and 26.5, numerical values do not clearly drop at 25 km, thus failing to clearly highlight a transition between rain and non rain targets.
As far as the copolar correlation coefficient is concerned, its discrimination capabilities appear to perform rather poorly in this case, since no transition or even progressively decreasing values are featured by the corresponding rayplot.
As explained above, the decreased polarimetric contrast shown by entropy and copolar correlation coefficient is probably due to the sensitivity to Mie scattering effects when rain is illuminated at C band.

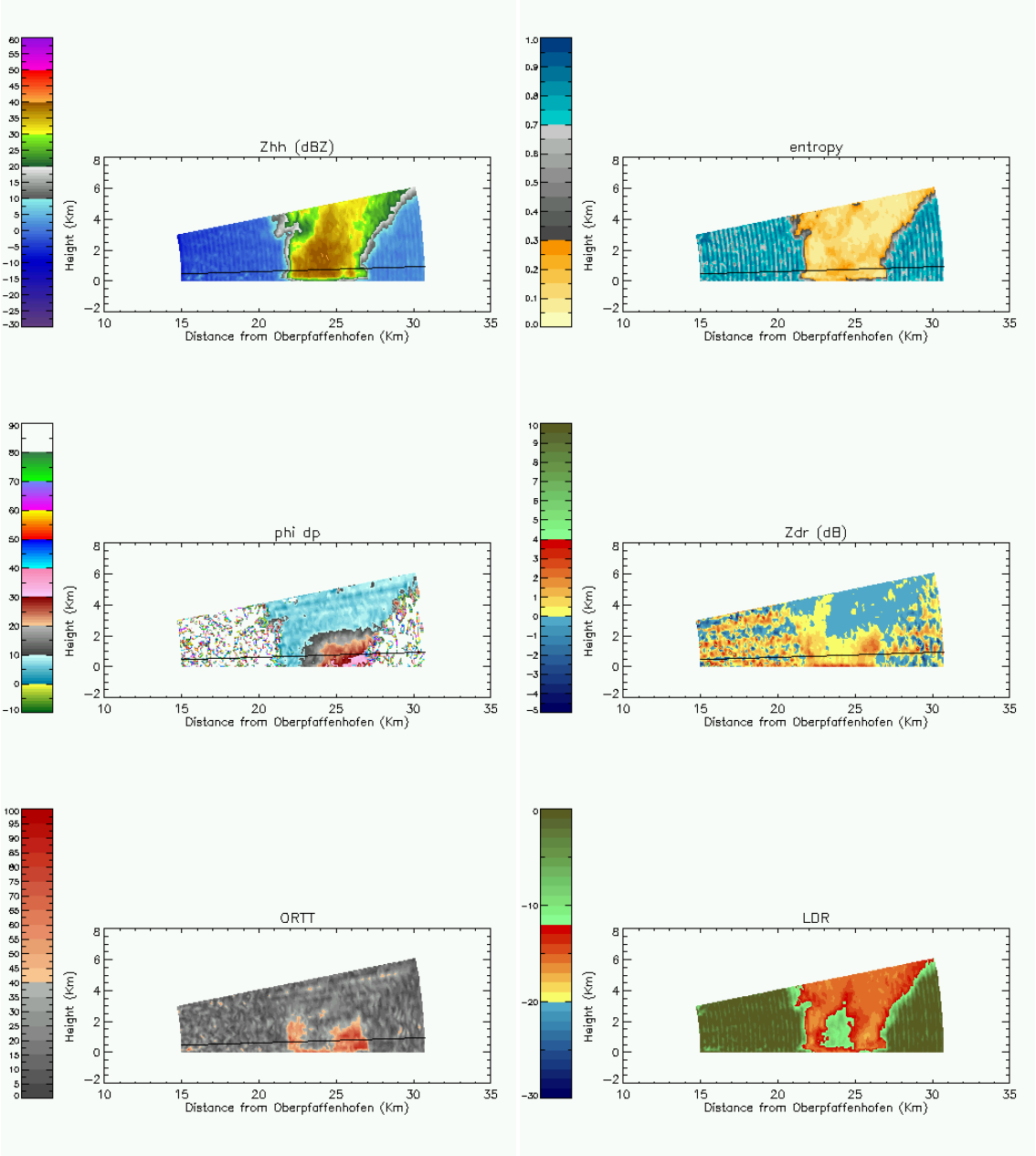

Figure 5.4 **Convective event, RHI images. Upper left: reflectivity (Z_H, in dBZ), upper right: entropy (H), middle left: copolar phase (Φ_{DP}, doppler shift corrected), middle right: differential reflectivity (Z_{DR}, in dB), lower left (ORTT), lower right (LDR, in dB).**
Ray number 3 (in black in the RHIs above) is chosen for the comparison of the capabilities to discriminate between rain and non-rain. For ray number 3, Fig. 5.4 shows comparative rayplots for H, p_H, p_V and $|\rho_{hv}(0)|$.
Ray number 4 is chosen for the comparison of p_C, p_{45} and $|\rho_{hv}(0)|$ when isotropic weather targets are illuminated. Corresponding rayplots are shown in fig. 5.5

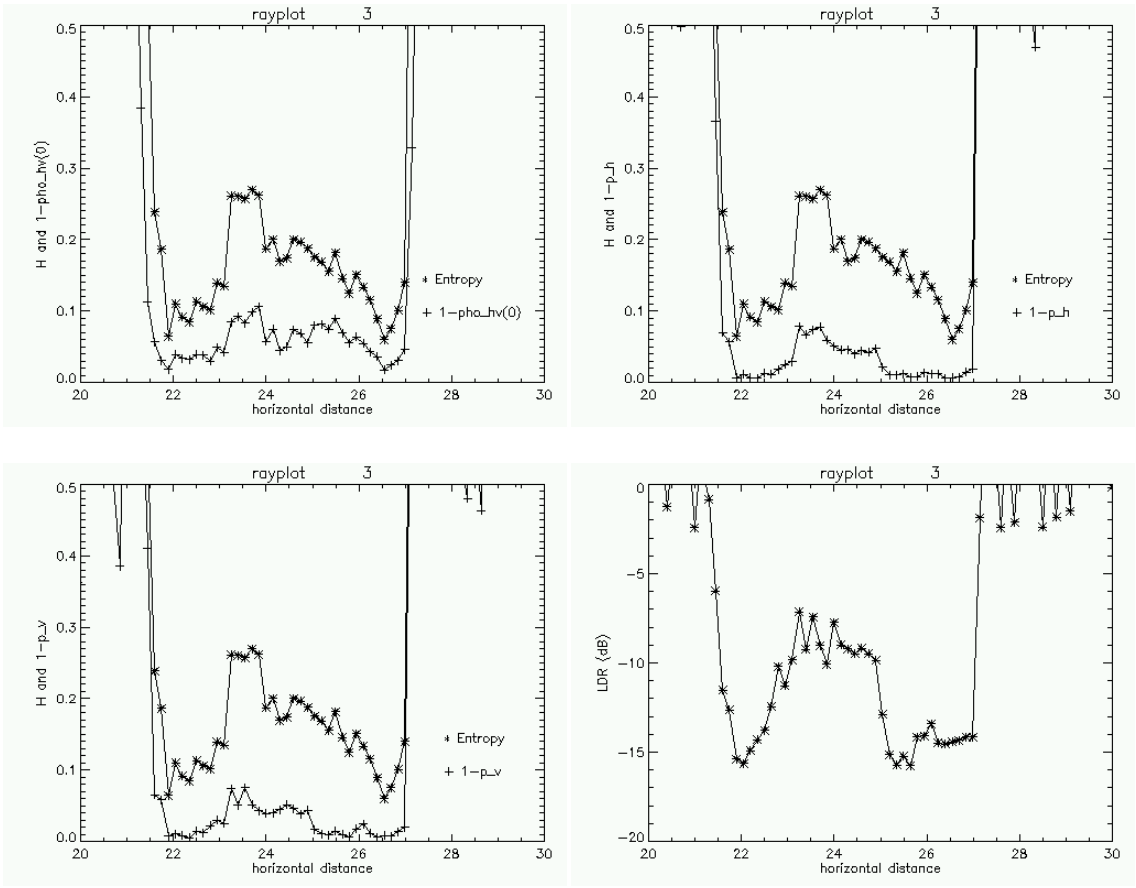

Figure 5.5 Rayplots corresponding to ray number 3 (in black in fig. 5.4). Upper left is H versus (1- $|\rho_{hv}(0)|$), upper right is H versus (1-p_H), lower left is H versus (1-p_V), lower right is LDR (in dB). At 25 km occurs the transition between rain (25-27 km) and more depolarizing hydrometeors (22.5-25 km). The transition from frozen, irregularly shaped hydrometeors is neatly detected by p_H, p_V and LDR, but not by H and $|\rho_{hv}(0)|$.

After confirming the first thesis, namely that LDR, p_H and p_V perform better than H and $|\rho_{hv}(0)|$ for rain non-rain discrimination, we turn to the analysis of the differences between LDR, p_H and p_V.

These three variables are capable of neatly detecting the transition between rain and non-rain as shown by the analysis of their rayplot patterns. However, when we turn our attention to the absolute values assumed by these variables we find that p_H and p_V take on very low values (around 0.01), whereas LDR shows values between -16 dB and -14 dB for what was supposed to be rain. If the values for the degree of polarization are well reasonable for rain, LDR values are indeed extremely high. Typically, LDR values for drizzle or light rain (20-25 dBZ) should be in the range -30 -28 dB. Even though we are observing light to moderate rain (horizontal reflectivity indicates values between 30 and

35 dBZ, corresponding rain-rate is 2-5 mm/hr) the observed LDR values are still high and do not match with the values expected for this hydrometeor class.
The reason for this discrepancy is known and is due to the relatively poor cross-channel isolation of the radar system at the time the measurements were taken.
In the case of POLDIRAD, cross-channel coupling is due to a number of different factors:

- Suboptimal performance of ferrite phase-shifters in the polarization network
- Feed-horn misalignment
- Cross-channel coupling inherent in the physical limitations of the circular waveguide connecting the OMT and the feed horn
- Cross-channel coupling inherent in the physical limitations of the OMT
- Imperfections in the reflector surface
- Imperfections due to the spatial extension of the parabolic reflector
- Scattering effects due to the presence of the supporting boom (this occurs for both center-fed and Cassegrain systems)

A couple of comments on the above factors are due.

Firstly, we distinguished between imperfections in the reflector surface from imperfections due to the spatial extension of the parabolic reflector because, if the first can be considered as deviations of a real metal surface from an ideal parabolic surface, the second effect occurs also when considering an ideal parabolic surface. Namely, not only the direction of every ray radiated by the horn and reflected by the parabolic surface must be collimated, but also its polarization state. If an ideal parabolic reflector collimates the rays coming from the horn into one single spatial direction, the same does not exactly happen for the polarization state, with an overall degradation of the polarimetric purity of the radiated beam. This effect cannot be overcome.

Secondly, we note that, if the first of the items listed above only occurs with the POLDIRAD system (since it uses ferrite phase shifters in the polarization network) all other items are also common to conventional dual-polarization radar systems, and require accurate polarimetric calibration in order to avoid effects like those encountered in the case study presented above, with unduly high LDR values.

Thirdly, we note that all the effects responsible for cross-channel coupling occur, reasonably to the same extent, for every radiated pulse that comes in the formation of the Wolf's coherency matrix measured by the system.
This observation has an important consequence.

Namely, if LDR is heavily affected by cross-channel coupling, p_H and p_V are not, at least to a first order approximation.

Indeed, the above-itemized effects are mainly responsible for the transmission of a polarization state that is different from the intended one, but this non-ideal polarization

state will be common to every pulse radiated by the system and does not actually contribute to the randomness of Wolf's coherency matrix.

The effects of suboptimal polarimetric calibration on LDR and p_H can be illustrated by the following example. Let us imagine we are illuminating a 0 entropy target, a cloud of spheres can be an example. If, instead of pure horizontal polarization, a fully polarized wave with a small vertical component is radiated (namely, a polarization state lying in the vicinity of horizontal polarization on the Poincare sphere), the backscattered wave would still be completely polarized, with the same polarization state except for reversed handedness.
In this case, LDR would be adversely affected by the presence of the small amount of power (indeed radiated by the system itself) in the cross polar (vertical) channel, even though the backscattered wave is fully polarized.
The degree of polarization measured by the system would, on the other hand, keep constant, and equal to 1 (the backscattered wave is, indeed, fully polarized).

We can complexify the example above by considering backscattering from rain.
The amount of cross polar power returned to the system will be dependent on the amount of cross polar power transmitted by the system (due to suboptimal polarimetric calibration) and to the cross-polarization properties of the target, namely, for rain, the finite width of a 0-mean canting angle distribution or, in other words, any non axisymmetric oscillation mode that makes the drop shape deviate from spheroids aligned with the principal axes of the polarization plane.

LDR is sensitive to both effects: the suboptimal polarimetric calibration is responsible for a constant bias in its numerical value, the weather target is responsible for the additional pattern superimposed to the calibration induced bias. This is the reason why in the case study presented above LDR still nicely detects the transition between rain and non-rain, even though its numerical values do differ from those expected for a well-calibrated system.

On the other hand, p_H is only affected by the fluctuations in the returned polarization state produced by the non-axisymmetric oscillations of the drops. Indeed, its values are only influenced by the backscattering physics of the target, but not by suboptimal polarimetric calibration of the system. This circumstance is substantiated by the data presented in the previous case study, where the degree of polarization at horizontal transmit takes on very low values when rain is illuminated, even though the cross-channel coupling of the radar system in use (POLDIRAD) is rather poor. Also, these values for rain of the degree of polarization at horizontal transmit are comparable to those reported in [1], a radar system (DARR, Delft Atmospheric Research Radar) with good cross-channel isolation (-27 dB).

More precisely, p_H is also affected if some power leaks in the cross-polar channel upon transmission, but this effect is in practice negligible. The theoretical reason for this is that, in case of suboptimal polarimetric calibration, instead of measuring p_H, the system is measuring $p_{H+\varepsilon}$ namely, the degree of polarization corresponding to a transmit polarization state that is slightly displaced from the horizontal (intended) polarization

state. With reference to the depolarization response for anisotropic weather targets, we note that the lobe on the maximal axis is indeed wide, and the power leaking in the vertical channel upon transmission is not, in general, capable of displacing the transmitted polarization state to regions of the depolarization response whose values are sensitively different from those for the intended polarization state. Of course, the effects on the degree of polarization will appear if slant polarization is transmitted instead of horizontal, but in this case the amount of power on the horizontal and vertical channels is the same and we assume that this is the result of an intention of the operator rather than the result of a badly calibrated system trying to radiate horizontal polarization.

In synthesis, the difference between LDR, p_H and p_V can be summarized as follows: if suboptimal polarimetric calibration is responsible for the transmission of a polarization state that is slightly different from the intended one, the effect on LDR is relevant, whereas the effect on p_H is in practice negligible.

We remind once again that this result is important also for the operational weather radar community, since horizontal transmission and simultaneous coherent reception of the horizontal and vertical channels is an operating mode implemented in today's dual-polarization operational weather radars. Indeed, this mode allows the simultaneous measurement of LDR and p_H, and a joint use of these two variables might lead to more robust products, especially in terms of sensitivity to suboptimal polarimetric calibration of the system.

5.3.2 Observation of isotropic weather targets (frozen hydrometeors)

The objective of the present section is to investigate the differences between $|\rho_{hv}(0)|$, p_C and p_{45} when isotropic weather targets are illuminated. The experimental and analytical results outlined in the previous sections indicate that these variables have an identical behavior if rain is illuminated and, until now, there is no evidence of the capability of p_C and p_{45} to bring additional information with respect to $|\rho_{hv}(0)|$.
When rain is illuminated, the only case where these variables might differ is in presence of canted raindrops. This case could not however be substantiated by experimental evidence.
As far as isotropic weather targets are concerned, we remind to the reader the results achieved in the previous sections. The depolarization response plot for isotropic weather targets shows a minimal axis along the north/south poles of the Poincare sphere, and a maximal circle along the equator. This means that, for isotropic targets, p_C is minimal and p_{45} is maximal. The case study presented in this section provides experimental evidence of the correctness of the depolarization response for isotropic targets.
Also, since isotropic weather targets are typically embedded in rain, differential propagation phase occurring from the antenna to the isotropic target (and due to the presence of rain in between) affects the values of p_C and p_{45}. This is due to the fact that, in presence of differential propagation phase, the polarization state of the forward propagating wave migrates along the circular/slant circle of the Poincare sphere and, consequently, migrates through the two minima and two maxima of the depolarization

response of isotropic targets (and not, like in the case of anisotropic targets, along a constant (minimal) circle).
In the present case study, the core of isotropic weather targets is located at approximately 24 km from the radar, where Φ_{DP} attains values of 20°.
Since differential propagation phase can be measured independently, this bias can be removed, as explained in [1].
In the following, the correction for differential propagation phase is not applied to the data presented in the rayplots because of two reasons.
The first is that 20° is not too large a value and its effects are not so relevant to prevent the qualitative experimental observation of the minimal and maximal degree of polarization of isotropic weather targets.
The second is that the data presented in the following are obtained after performing a polarization basis rotation. The transformation of scattering matrices affected by propagation effects to different polarization bases involves theoretical problems that go beyond the scope of the present paper. As a consequence, it is simply assumed that a differential phase of 20° has a limited impact on the observed pattern, the data are rotated to circular polarization, and no further correction is implemented.
The procedure outlined in [1] remains however perfectly applicable when data are collected at hybrid mode (simultaneous transmission, horizontal and vertical coherent reception), the primary operating mode of operational dual-polarization weather radar.
In Fig. 5.5 two graphs are reported for variables evaluated from ray number 4 of the second convective case study. Corresponding RHIs are reported in Fig. 5.3 where the ray in black is ray number 3.

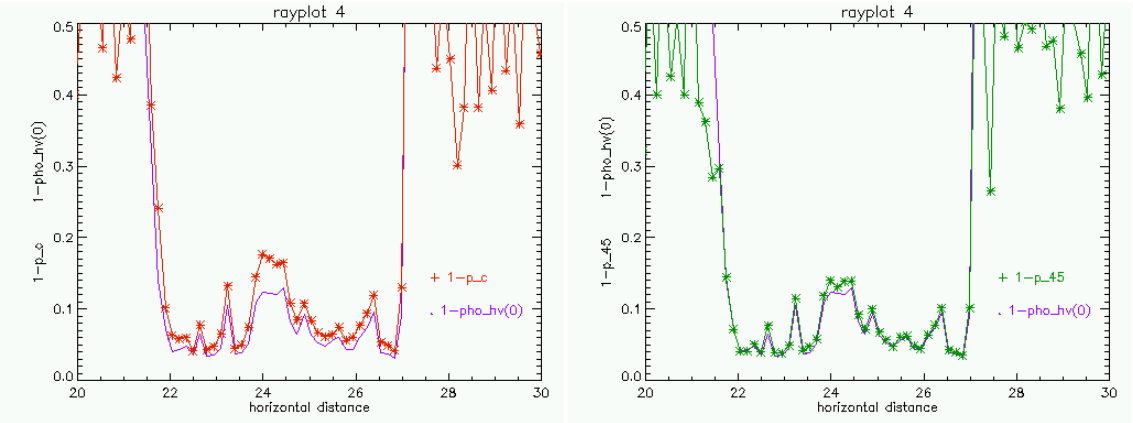

Figure 5.6 **Rayplots corresponding to ray number 4 (ray number 3 is traced in black in fig. 5.3).**
Left, 1-$|\rho_{hv}(0)|$ (in violet) versus 1-p_C (in red).
Right, 1-$|\rho_{hv}(0)|$ (in violet) versus 1-p_{45} (in green).
Note the different behavior of p_C and p_{45} in presence of isotropic weather targets, in accordance with the depolarization response presented in [].

In fig 5.5, the graph on the left features 1-p_C (in red) versus 1-$|\rho_{hv}(0)|$ (in violet). The graph on the right features 1-p_{45} (in green) versus 1-$|\rho_{hv}(0)|$ (in violet).
The important result from these plots is that, in accordance with the theory, these variables assume different values in correspondence of the core of isotropic weather targets, located at approximately 24 km from the radar. This is indeed to be expected since, in general, p_C, p_{45} and $|\rho_{hv}(0)|$ are independent, and do not necessarily assume the same values as in the special case of rain.

These results must be considered in the context of the capabilities of operational, dual-polarization weather radars. The latter radiate a polarization state that lies on the circular/slant circle of the Poincare sphere. In this operating mode, when isotropic targets are illuminated, a couple of remarks are useful.

Firstly, the measured copolar correlation coefficient ($|\rho_{hv}(0)|$), even though not biased by non-simultaneous measurement acquisitions, is biased by cross-talk upon backscattering, and, ultimately, the measured quantity is

$$\rho_{hv}^{hy} = \frac{|\langle (S_{hh} + S_{hv})(S_{vv} + S_{vh})^* \rangle|}{\sqrt{\langle |S_{hh} + S_{hv}|^2 \rangle \langle |S_{vv} + S_{vh}|^2 \rangle}} \tag{5.3}$$

The degree of polarization measured by operational weather radars is dependent on two factors, the first is the initial phase difference (at the antenna) between the horizontal and the vertical simultaneously transmitted components, the second is the differential propagation phase that the beam undergoes along its path to the isotropic targets (one way). Both factors are responsible in determining the polarization state with which the radiated wave impacts the isotropic target. The polarization state of the radiated wave at the location of the target, in the case of isotropic hydrometeors, determines whether the measured degree of polarization is minimal or maximal or in between the two.

Since at hybrid only one degree of polarization is available (with polarization state on the circular/slant circle), if a choice can be made, the degree of polarization at circular transmit provides a larger dynamic range than the degree of polarization at slant linear transmit and would probably be preferable.
Jointly with the copolar correlation coefficient, the degree of polarization could serve as a second constraint for models of depolarizing isotropic weather targets, perhaps allowing a more precise inversion/classification.
Further study should be addressed at this issue.

5.4 Case study 3: Stratiform Event

The third dataset relates to a stratiform event with a clearly visible melting band 1 km above the ground (Fig.5.6). Besides standard radar meteorological variables, H, p_H and p_V

were evaluated to conduct a phenomenological analysis of their behavior in presence of stratiform precipitation and ground clutter. Even though worked out from experimental data, the numerical values given in the following are indicative and are not meant to fully characterize the hydrometeor classes they refer to. Further work is needed, for example, to evaluate membership functions for implementation in hydrometeor classification algorithms.

A visual analysis of the images reported in Fig. 5.6 suggests the presence of rain and dry snow below and above the melting band respectively. H and p can detect wet snow (melting band) with values that can exceed 0.3 whereas rain and dry snow appear to be characterized by lower values. Typical values for rain are less than 0.1 for H and less than 0.01 for p_H, p_V.

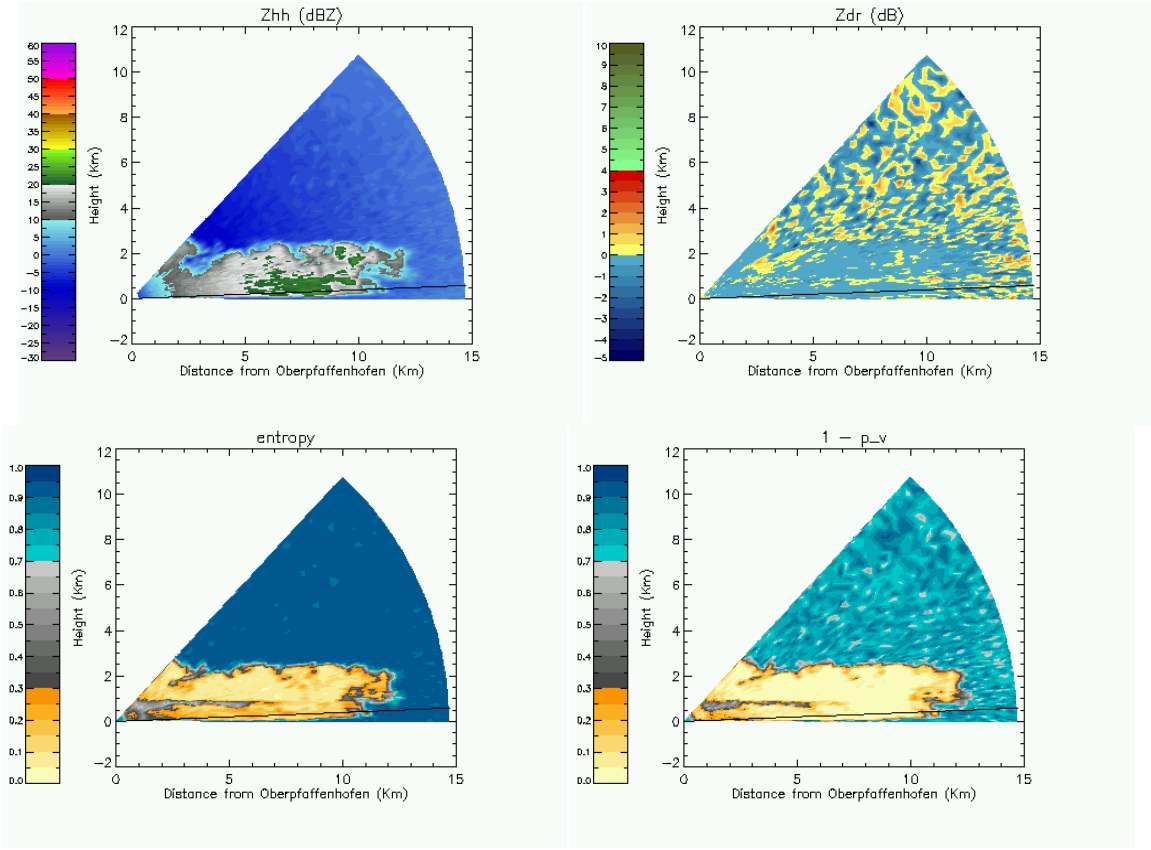

Figure 5.7 **Stratiform event, RHI images. Upper left image is reflectivity (Z_H, in dBZ), upper right is differential reflectivity (Z_{DR}, in dB), lower left is entropy and lower right is the degree of polarization at vertical transmit ($1-p_v$). Entropy and degree of polarization are capable of detecting the melting band, clearly visible in the images with values that can exceed 0.3 for both variables. Ray in black is number 8, the corresponding elevation is 2.26°.**

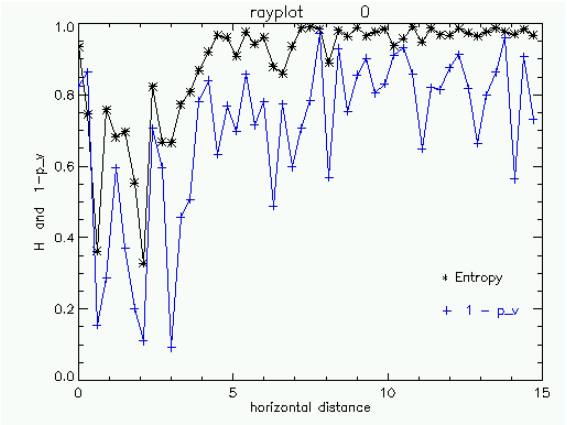
rayplot 0
H and 1-p_v
horizontal distance
Entropy
1 - p_v

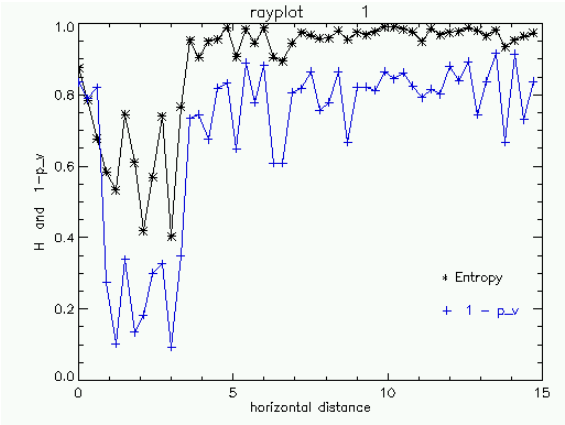
rayplot 1
H and 1-p_v
horizontal distance
Entropy
1 - p_v

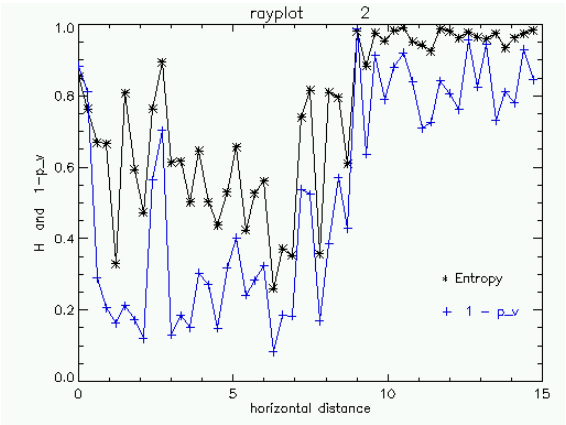
rayplot 2
H and 1-p_v
horizontal distance
Entropy
1 - p_v

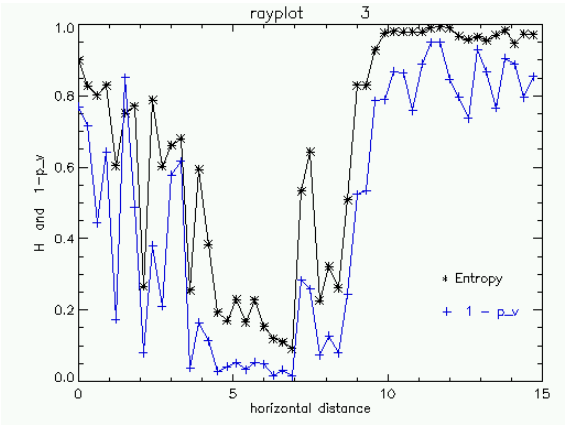
rayplot 3
H and 1-p_v
horizontal distance
Entropy
1 - p_v

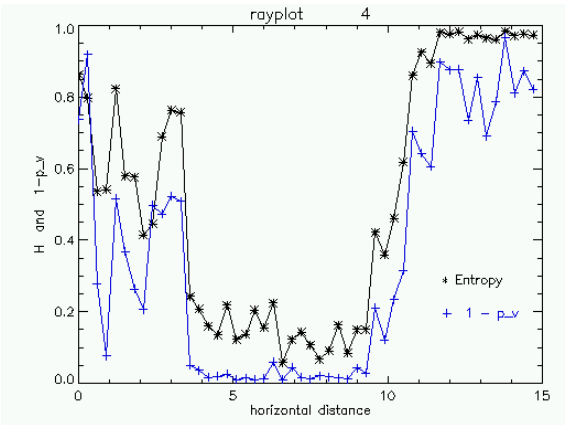
rayplot 4
H and 1-p_v
horizontal distance
Entropy
1 - p_v

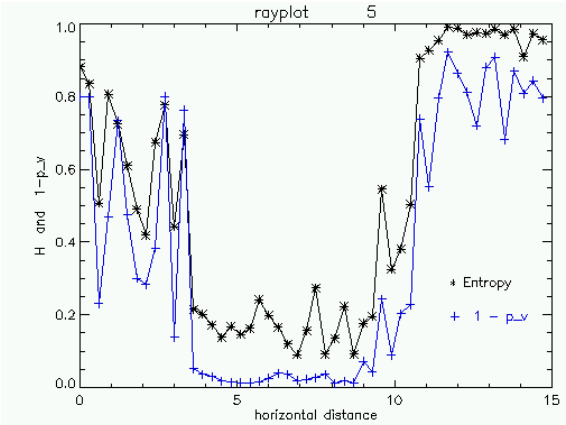
rayplot 5
H and 1-p_v
horizontal distance
Entropy
1 - p_v

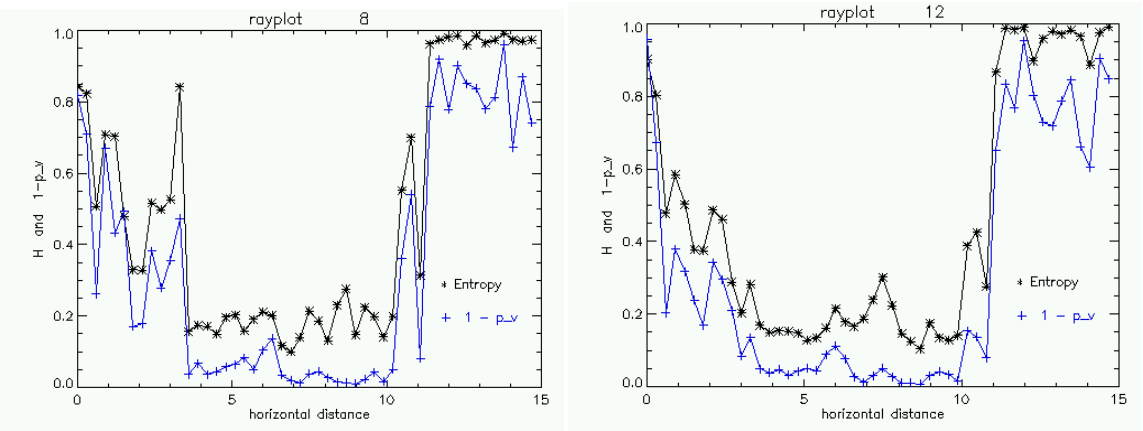

Figure 5.8 **The rayplots show the different contribution of clutter for progressively increasing elevations. Rayplots are labeled with the number in the RHI dataset ranging from the lowest ray (rayplot 0, elevation angle -0.30°) to higher rays (rayplot 12, elevation: 3.04°). Rayplot 8 corresponds to the ray in black in Fig. 5.3. Entropy and the degree of polarization are sensitive indicators of the presence of clutter.**

Besides enabling detection of the melting band, the relatively low depolarizing properties of rain and dry snow prompt the use of H and p for clutter detection, being the latter characterized by relevant cross-polarization on backscatter. In particular, when rain is present in the lower sections of the atmosphere, p_H or p_V enhance the contrast with clutter and should therefore perform better than H, p_C, p_{45} or $|\rho_{hv}(0)|$. However, as the depolarizing properties of clutter are relevantly larger than rain, the use of more sensitive variables is not strictly excluded for this application.

In order to test sensitivity to ground clutter, a series of eight rays were chosen with the following elevation angles: -0.30°, -0.11°, 0.29°, 0.46°, 0.96°, 1.01°, 2.26°, 3.04°. The corresponding rayplots are shown in Fig. 5.7 with the labels 0, 1, 2, 3, 4, 5, 8, 12. The labels correspond to the ray number in the RHI dataset, rays 6, 7, 9, 10, 11 are not shown for compactness. Ray 0 corresponds to the lowest elevation angle (-0.30°), ray 8 (elevation 2.26°) is plotted in black in Fig. 5.6.
In the first 3 km of every rayplot the relatively high values of H and p suggest that the received signatures are dominated by switch leakage and side-lobe clutter.
Between 3 and 10 km from the radar, the graphs feature an interesting transition from high to low entropy patterns as the ray elevation increases. This phenomenon is clearly due to the gradually changing contribution of high entropy clutter and low entropy weather targets to the backscattered signal. For this case study, the low entropy weather target is constituted by rain, but clutter detection should be feasible also when dry snow occupies the lowest layers of the atmosphere. It has to be noted that even for ray 12 (elevation 3.04°) the values of H and p are higher than those normally expected for rain, indicating that the signatures are probably still contaminated with clutter. The presence of

the latter becomes more relevant with decreasing elevation, as larger sections of the beam intercept the ground. In the limit, for rayplots 0 and 1 (corresponding to negative elevations of -0.30° and -0.11° respectively) H and p assume values close to 1, indicating that returns from the ground neatly dominate the signal.
Between 10 and 15 km the main beam no longer impinges on weather targets and no backscattered energy flows into the receiver. In this section of the rayplots, only hardware and external noise is detected and, due to the random nature of noise, H and p assume values close to 1.

References Chapter 5

[1] D. Moisseev, C. Unal, H. Russchenberg, L. Ligthart, "A New Method to Separate Ground Clutter and Atmospheric Reflections in the Case of Similar Doppler Velocities" TGRS, Vol. 40 n.2, February 2002

[2] R. B. Da Silveira and A. R. Holt, "A neural network application to discriminate between clutter and precipitation using polarization information as feature space" Proc. 28th Conf. Radar Meteorology, Austin, TX, Sept. 7-12, 1997, pp.57-58.

[3] D. H. O. Bebbington, "Degree of polarization as a radar parameter and its susceptibility to coherent propagation effects," URSI Commission F Symposium on Wave Propagation and Remote Sensing, Ravenscar, N. Yorkshire, UK, pp. 431-436, June 1992.

[4] M. Galletti, D. H. O. Bebbington, M. Chandra, T. Boerner, "Measurement and Characterization of Entropy and Degree of Polarization of Weather Radar Targets" TGRS, Vol. 46 n.10, October 2008

[5] M. Galletti, D. H. O. Bebbington, M. Chandra, T. Boerner, "Fully polarimetric analysis of weather radar signatures" Proc. 2008 IEEE Radar Conference, Rome, Italy, May 2008

6. Conclusions (Thesen)

The main results of the present doctoral thesis can be itemized as follows:

1. With the primary operating mode of dual-polarization operational weather radars, (simultaneous transmission/simultaneous reception) the degree of polarization corresponding to a transmit state on the circular/slant circle of the Poincare sphere can be evaluated. If non-canted rain is illuminated, this variable behaves like the copolar correlation coefficient and, consequently, does not appear to add significant information. When more depolarizing isotropic weather targets are illuminated, it was theoretically and experimentally shown that the degree of polarization and the copolar correlation coefficient can in general differ, and the first might therefore add significant information. In this latter case, the degree of polarization will be affected by differential propagation phase, (due to the presence of rain between the antenna and the target) and a correction procedure was developed. Ultimately, the degree of polarization might help in the classification of weather targets.

2. The most important result of the present thesis is the characterization of the degree of polarization at horizontal transmit, available from the secondary operating mode of dual-polarization operational weather radars. Upon backscattering from rain, the degree of polarization at horizontal transmit behaves like the linear depolarization ratio, and is therefore optimal for the discrimination between rain and non-rain targets. With respect to the linear depolarization ratio, the degree of polarization has the distinctive advantage that it is not affected by antenna cross-channel coupling. These features prompt its integration in hydrometeor classification algorithms, especially to counter the effects of suboptimal polarimetric calibration.

3. The concept of depolarization response was introduced to characterize incoherent targets. For a given incoherent target, the depolarization response maps the state of polarization of the transmitted wave onto the degree of polarization of the backscattered wave. These plots are capable of shedding light on the multidimensional nature of the concept that is generally and ambiguously referred to as depolarization. A satisfactory analytical characterization of these plots is however still needed. Open issues are the analytical characterization of its extrema, and formulae to approximate target entropy by means of these extrema.